2016

STUDIES TO IMPROVE EXHAUST SYSTEM ACOUSTIC PERFORMANCE BY DETERMINATION AND ASSESSMENT OF THE SOURCE CHARACTERISTICS AND IMPEDANCE OPTIMIZATION

Yitian Zhang
University of Kentucky, olezyt@gmail.com
Digital Object Identifier: http://dx.doi.org/10.13023/ETD.2016.141

STUDENT AGREEMENT:

I represent that my thesis or dissertation and abstract are my original work. Proper attribution has been given to all outside sources. I understand that I am solely responsible for obtaining any needed copyright permissions. I have obtained needed written permission statement(s) from the owner(s) of each third-party copyrighted matter to be included in my work, allowing electronic distribution (if such use is not permitted by the fair use doctrine) which will be submitted to UKnowledge as Additional File.

I hereby grant to The University of Kentucky and its agents the irrevocable, non-exclusive, and royalty-free license to archive and make accessible my work in whole or in part in all forms of media, now or hereafter known. I agree that the document mentioned above may be made available immediately for worldwide access unless an embargo applies.

I retain all other ownership rights to the copyright of my work. I also retain the right to use in future works (such as articles or books) all or part of my work. I understand that I am free to register the copyright to my work.

REVIEW, APPROVAL AND ACCEPTANCE

The document mentioned above has been reviewed and accepted by the student's advisor, on behalf of the advisory committee, and by the Director of Graduate Studies (DGS), on behalf of the program; we verify that this is the final, approved version of the student's thesis including all changes required by the advisory committee. The undersigned agree to abide by the statements above.

Yitian Zhang, Student

Dr. David W. Herrin, Major Professor

Dr. Haluk E. Karaca, Director of Graduate Studies

STUDIES TO IMPROVE EXHAUST SYSTEM ACOUSTIC PERFORMANCE BY DETERMINATION AND ASSESSMENT OF THE SOURCE CHARACTERISTICS AND IMPEDANCE OPTIMIZATION

DISSERTATION

A dissertation submitted in partial fulfillment of the requirements for the degree of Doctor of Philosophy in the College of Engineering at the University of Kentucky

By

Yitian Zhang

Lexington, Kentucky

Director: Dr. David W. Herrin, Professor of Mechanical Engineering

Lexington, Kentucky

2016

ABSTRACT OF DISSERTATION

STUDIES TO IMPROVE EXHAUST SYSTEM ACOUSTIC PERFORMANCE BY DETERMINATION AND ASSESSMENT OF THE SOURCE CHARACTERISTICS AND IMPEDANCE OPTIMIZATION

It is shown that the relationship between an impedance change and the dynamic response of a linear system is in the form of the Moebius transformation. The Moebius transformation is a conformal complex transformation that maps straight lines and circles in one complex plane into straight lines and circles in another complex plane. The center and radius of the mapped circle can be predicted provided that all the complex coefficients are known. This feature enables rapid determination of the optimal impedance change to achieve desired performance.

This dissertation is primarily focused on the application of the Moebius transformation to enhance vibro-acoustic performance of exhaust systems and expedite the assessment due to modifications. It is shown that an optimal acoustic impedance change can be made to improve both structural and acoustic performance, without increasing the overall dimension and mass of the exhaust system. Application examples include mufflers and enclosures. In addition, it is demonstrated that the approach can be used to assess vibration isolators. In many instances, the source properties (source strength and source impedance) will also greatly influence exhaust system performance through sound reflections and resonances. Thus it is of interest to acoustically characterize the sources and assess the sensitivity of performance towards source impedance. In this dissertation, the experimental characterization of source properties is demonstrated for a diesel engine. Moreover, the same approach can be utilized to characterize other sources like refrigeration systems. It is also shown that the range of variation of performance can be effectively determined given the range of source impedance using the Moebius transformation.

This optimization approach is first applied on conventional single-inlet single-outlet exhaust systems and is later applied to multi-inlet multi-outlet (MIMO) systems as well, with proper adjustment. The analytic model for MIMO systems is explained in details and validated experimentally. The sensitivity of MIMO system performance due to source properties is also investigated using the Moebius transformation.

KEYWORDS: transmission loss, insertion loss, 2-load measurement, Moebius transformation, source properties, multi-inlet multi-outlet

Yitian Zhang
Student's Signature

April 23rd, 2016
Date

STUDIES TO IMPROVE EXHAUST SYSTEM ACOUSTIC PERFORMANCE BY DETERMINATION AND ASSESSMENT OF THE SOURCE CHARACTERISTICS AND IMPEDANCE OPTIMIZATION

By

Yitian Zhang

David W. Herrin

Director of Dissertation

Haluk Karaca

Director of Graduate Studies

April 23rd, 2016

Date

Acknowledgements

I would like to first express my deepest gratitude to Professor David W. Herrin for being my advisor for my Ph.D. study. His suggestions and guidance have made these five years the most enriched and productive period of my student life. I am thankful to the numerous opportunities provided to me, which help me improve as a student, engineer and person.

I would also like to thank Professor Tingwen Wu, for his guidance and comments both in learning and living. I would also thank Professor John Baker and Professor Jun Zhang for being my committee and providing valuable suggestions.

I want to thank my colleagues, Huangxing Chen, Keyu Chen, Gong Cheng, Rui He, Shujian He, Aihua Huang, Xin Hua, Quentin Hunsucker, Caoyang Li, Jundong Li, Jiazhu Li, Wanlu Li, Weiyun Liu, Jiawei Liu, Srinivasan Ramalingam, Kangping Ruan, Yucong Sang, Shishuo Sun, Wei Sun, Peng Wang, Weichen Wang, Robert Wick, Ruimeng Wu, Nan Zhang, Limin Zhou and Wentao Zhuo. I will always remember their discussions and friendship that help me confront the difficulties and frustrations. Also I want to thank my friends Tao Chen and Yan Jin for the fun that we have in soccer, basketball, hotpot and kebab.

TABLE OF CONTENTS

LIST OF TABLES

LIST OF FIGURES

Chapter 1 INTRODUCTION

1.1 Background

People are constantly subjected to undesirable noise and vibration. Humans are influenced to different extents and that influence is manifested by a number of physiological effects including contraction of blood vessels, pupil dilation, and effects on breathing. Noise reduces attention and can therefore degrade work performance. Hearing loss is prevalent in our society and vibration can lead to motion sickness, reduced comfort and diminished work performance. In addition, vibration is detrimental to the durability of machinery.

One of the most prevalent sources of noise is internal combustion engines. This includes noise from trucks, automobiles, heavy equipment, turf and lawn equipment, snow removal equipment, and generator sets. The most effective and commonly used measure for reducing internal combustion engine noise is the use of a muffler or silencer. Sometimes exhaust systems combine noise and emission controls into a single element. For example, diesel particulate filters (DPF) are primarily used to remove the particles generated in the exhaust due to incomplete combustion. At the same time, DPFs also provide broadband noise attenuation and may sometimes provide sufficient noise attenuation independently of other muffler elements. Catalytic converters (CC) are more commonly used in automobiles. A CC converts toxic pollutants in exhaust gas to less toxic pollutants by catalyzing a redox reaction (oxidation or reduction). Catalytic converters also attenuate noise improving the noise performance of the exhaust system. Regardless of the exhaust system layout or whether emission

devices are included, there is a need to predict and measure the noise performance of an exhaust system prior to installation on an engine.

Herrin et al. (2014) suggested a design process for development and prototyping of mufflers and silencers. The steps are laid out in Table 1.1. The first step is a clarification of task stage where noise targets and important parameters are identified and catalogued. This is followed by a conceptual design stage where design rules and plane wave modeling are used to develop a muffler which should meet performance and packaging specifications. Detailed design follows and may be considered as a virtual prototyping stage. Detailed CAD models of the muffler or silencer can be developed and analyzed. This is followed by a prototyping stage where transmission loss can be measured in the lab. Transmission loss is a metric that can be used for judging muffler performance prior to installing the muffler into the system. The final step is to make an in situ measurement of the muffler on the actual source.

Table 1.1 Design process of mufflers and silencers (Herrin et al., 2014).

1	Clarification of Task
	Establish targets (SPL at receiver, transmission and insertion loss, pressure drop, breakout transmission loss) Maintain a database (source properties, flow rate, temperatures, insertion loss of prior designs)
2	Conceptual Design
	Design rules (i.e. cross-flow mufflers are generally effective, perforates are effective with flow, avoid sharp edges in flow) Virtual design (plane wave modeling, 1-D CFD modeling, handbook equations)
3	Detailed Design
	CAD modeling Virtual prototyping (acoustic BEM and FEM)
4	Prototyping
	Measure transmission loss in the lab to confirm modeling approach Measure insertion loss with the muffler in situ

In each of the aforementioned steps, improvements need to be made to enhance muffler design and performance. This thesis will examine a number of improvements that can be made to improve the overall process and muffler

design in general. The needs and corresponding objectives are expanded in the following.

1. There is no standard process for measurement of transmission loss of mufflers. The two primary methods for determining transmission loss are the two-load and two-source methods. Although a two-load measurement standard is available for absorptive materials (ASTM, 2009), measurement of transmission loss of mufflers may be difficult particularly if accurate and smooth results are desired. It is demonstrated that the selections of number of channels, location of reference and processing techniques will influence the quality of the transmission loss measurement. **Objective 1** is to establish the best practices that ensure high quality measurement of transmission loss for different types of mufflers.

2. As sound attenuation is related to the interaction between the muffler system and the source, exhaust system and the termination, the properties of the source may strongly influence the acoustic performance. To predict the actual performance of a given exhaust system, the source strength and source impedance must be known. However, due to the complexity, it is difficult to model an internal combustion engine and determine the source properties. Experimental methods are preferred. **Objective 2** is to demonstrate experimental procedures to measure the source strength and impedance on a diesel engine. A new wave decomposition approach is used to measure the source impedance and source strength. Results are compared against the more established multi-load electrical analogy approach.

3. There is increasing pressure in industry to decrease muffler and silencer size while boosting the performance. It is found that the impedance modification can be related to the dynamic response using the Moebius transformation (Needham, 1998). Taking advantage of the properties of Moebius transformation, the optimal solution can be found analytically, and the acoustic and structural performance can be substantially improved without increasing the overall size of the exhaust system. **Objective 3** is to solve for the optimal impedance modification using the Moebius transformation. Though the primary focus is on muffler systems, it is demonstrated that the vibro-acoustic performance can be optimized by enclosures, and isolator systems using the approach.

4. Transmission loss is a measure of the muffler performance that does not take into account system installation effects such as lengths of inlet pipes, and source and termination characteristics. Though termination characteristics are easily accounted for, the effect of the source is difficult to include in a model a priori. Consequently, only a general range of source impedance can be estimated in many cases. Beginning with a feasible range for the source impedance, the possible range of exhaust system performance can be predicted using the Moebius transformation. **Objective 4** is to investigate the sensitivity of muffler performance due to source impedance using the Moebius transformation.

5. Most prior muffler research has been dedicated to the single-inlet and single-outlet (SISO) muffler case. However, often multi-inlet and multi-outlet (MIMO) configurations are used in practice but have been paid less attention to. Mode-matching and impedance matrix methods have been applied to investigate MIMO

mufflers. However, both methods have limitations in terms of flexibility. **Objective 5** is to develop the method using a superposition method for the MIMO case. The multiple inlet single outlet (MISO) has been considered by Hua et al. (Hua et al., 2014). In this work, the approach is extended to include multiple outlets. After the model is validated experimentally, a similar analysis to that used to accomplish Objective 4 is then applied to determine the exhaust system response range given a feasible range of source impedance.

1.2 Organization

The dissertation is organized as follows.

Chapter 2 first gives the basic background of muffler performance evaluation. Special attention is paid to transmission loss measurements as they are most widely used during the design stage. Current standard practice is detailed. Following this, possible errors in the current standard are highlighted and countermeasures are provided.

Chapter 3 details the experimental characterization of source impedance. The approach is then applied to a diesel engine. Both the circuit analogy and wave decomposition approaches are detailed and then applied to a diesel engine. Both circuit analogy model and wave decomposition model are introduced and corresponding processing techniques have been applied on a diesel engine. Practical aspects such as experimental setup and signal processing techniques are discussed and recommendations are made.

Chapter 4 discusses the usage of the Moebius transformation to determine optimal point impedance changes to improve performance of mufflers, enclosures, and isolators. The sensitivity of vibro-acoustic performance to source properties is examined using the Moebius transformation in Chapter 5.

Chapter 6 includes the analysis on multi-inlet multi-outlet mufflers. It is shown that the transfer matrix method on conventional single-inlet single-outlet muffler is transferable to multi-inlet multi-outlet mufflers with slight adjustment. The sensitivity of acoustic performance to source properties is also investigated using the Moebius transformation.

Summary, conclusions and suggestions for future work are presented in Chapter 7.

1.3 Acoustic impedance and exhaust system

In the design of exhaust system, acoustic impedance is an important concept to understand the sound attenuation mechanism. Different types of acoustic impedance will be given in following section. After the introduction of acoustic impedance, some basic background about muffler and silencers will be given.

Sound is a propagating displacement of fluid medium particles from their equilibrium positions, and can be considered as the interaction between the volumetric strain and pressures generated by elastic reaction (Fahy, 2001). There are two important physical variables when characterizing sound field: sound pressure p and particle velocity v. Alternatively, volume or mass velocity,

defined as the respective volume or mass the particles sweep per unite time, can be used in the place of particle velocity (Munjal, 1987).

Acoustic impedance is defined as the ratio of sound pressure to particle velocity and can be expressed as

$$z = \frac{p}{v} \tag{1.1}$$

Acoustic impedance is the ratio of the effort and flow variables. In this case, it is the sound pressure (effort variable) generated for a given unit particle velocity (flow variable). The reciprocal of impedance is an indicator of the hardness/softness of an object, which is, how much particle vibration a unit sound pressure can excite on an object. Several different types of acoustic impedance will be defined in the discussion which follows. In addition, the measurement procedure for each of the impedance types is detailed.

1.3.1 Surface impedance

Surface impedance is defined as the ratio between sound pressure and particle velocity in the defined direction of impedance, usually at the surface of an interface between different media. It is used to characterize acoustic absorption material, and the direction of impedance is usually defined normal to the surface of absorber.

Surface impedance is directly related to the reflection of sound, and is measured by placing the sample in an impedance tube (ASTM, 1998 and Seybert, 1977). A specially prepared material sample is mounted at one end of the tube and a

loudspeaker is positioned and used as the source at the other end. Plane wave propagation may be assumed if the tube diameter is much smaller than an acoustic wavelength which is equal to the speed of sound divided by frequency (i.e., $\lambda = c/f$). If that is the case, the pressure and particle velocity will be uniform for any cross-section. The upper limit for this assumption to be valid is determined by the diameter of impedance tube. For a conventional impedance tube specialized for impedance measurement with inner diameter of d, the upper limit can be determined as $f_u = c/1.8d$ (Wallin et al., 2012) for measurement in normal room condition.

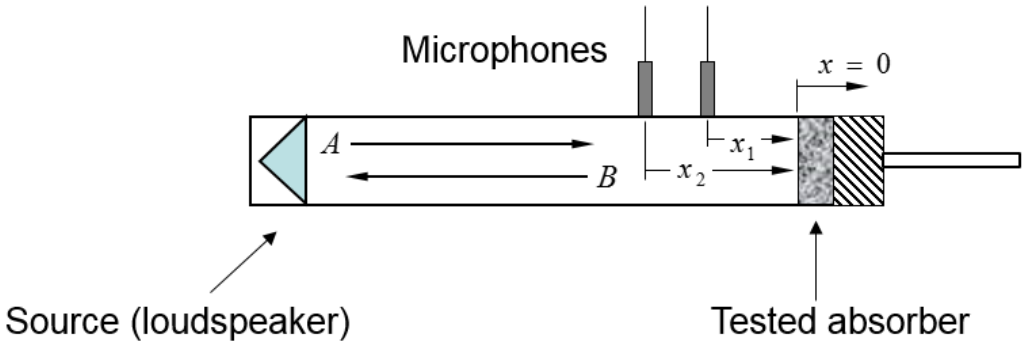

Figure 1.1 Experimental setup for surface impedance measurement.

Under this assumption, the sound field inside the impedance tube can be decomposed into two wave amplitudes: an incident wave amplitude A and a reflected wave amplitude B. The sound pressure and particle velocity at location x can be expressed as

$$p(x) = Ae^{-ikx} + Be^{ikx} \tag{1.2}$$

and

$$v(x) = \frac{1}{\rho_0 c}(Ae^{-ikx} - Be^{ikx}) \tag{1.3}$$

where k is the wavenumber, ρ_0 is the density and c is the speed of sound of air. The surface impedance of the sample ($x = 0$) can then be calculated as

$$z(0) = \rho_0 c \frac{A + B}{A - B} = \rho_0 c \frac{1 + R}{1 - R} \tag{1.4}$$

where R is the coefficient of reflection and is defined as

$$R = \frac{B}{A} \tag{1.5}$$

Notice that the reflection coefficient is complex. It is customary to characterize sound absorbing materials by defining an absorption coefficient which can be expressed in terms of the reflection coefficient as

$$\alpha = 1 - R^2 \tag{1.6}$$

The absorption coefficient is the ratio of the absorbed to incident sound powers.

1.3.2 Transfer impedance

A transfer impedance is used to model thin foils and perforates. It is perhaps best explained by introducing the transfer matrix concept. Transfer matrices can be used to represent most simple muffler components and can also be applied to layered materials. If plane wave propagation is assumed at both sides of an acoustic component, the sound pressures and particle velocities can be related to one another using the transfer matrix equation

$$\begin{Bmatrix} p_1 \\ v_1 \end{Bmatrix} = \begin{bmatrix} T_{11} & T_{12} \\ T_{21} & T_{22} \end{bmatrix} \begin{Bmatrix} p_2 \\ v_2 \end{Bmatrix} \tag{1.7}$$

where p_1 and v_1 and p_2 and v_2 are the sound pressures and particle velocities on sides 1 and 2 respectively as shown in Figure 1.2.

Figure 1.2 Definition of transfer matrix.

For thin components like membranes or foils, it can be assumed that the particle velocity across the structure remain the same, and the difference in sound pressures across the structure is proportional to the particle velocity. Under this assumption, the transfer matrix for the structure can be simplified as

$$\begin{Bmatrix} p_1 \\ v_1 \end{Bmatrix} = \begin{bmatrix} 1 & z_{tr} \\ 0 & 1 \end{bmatrix} \begin{Bmatrix} p_2 \\ v_2 \end{Bmatrix} \tag{1.8}$$

and the T_{12} entry in transfer matrix is then defined as the transfer impedance. Note that the transfer impedance is the ratio between the difference in sound pressures and the particle velocity and can be written as

$$z_{tr} = \frac{p_1 - p_2}{v_1} \tag{1.9}$$

For many common membrane or perforate materials, the transfer impedance can be calculated assuming certain physical parameters are known (Ver and Beranek, 2006 and Maa, 1998).

For a straight tube, the transfer matrix can be derived as (Munjal, 1987)

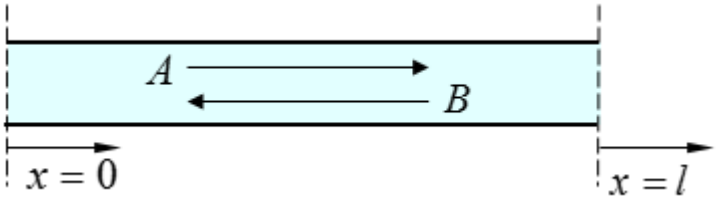

Figure 1.3 Transfer matrix of a straight tube.

$$\begin{Bmatrix} p_1 \\ v_1 \end{Bmatrix} = \begin{bmatrix} \cos(kl) & i\rho_0 c\sin(kl) \\ \dfrac{i\sin(kl)}{\rho_0 c} & \cos(kl) \end{bmatrix} \begin{Bmatrix} p_2 \\ v_2 \end{Bmatrix} \tag{1.10}$$

Where l is the length of the tube and k is the wavenumber. When l is sufficiently short compared to the wavelength of sound, the transfer matrix can be simplified as

$$\begin{Bmatrix} p_1 \\ v_1 \end{Bmatrix} = \begin{bmatrix} 1 & i\rho_0 ckl \\ 0 & 1 \end{bmatrix} \begin{Bmatrix} p_2 \\ v_2 \end{Bmatrix} \tag{1.11}$$

and is in the form of transfer impedance.

1.3.3 Source impedance

Acoustic sources are commonly modeled as a source strength coupled with a source impedance. The source impedance is essentially a special type of transfer impedance. It can be developed using either a circuit analogy (Munjal, 1987, Prasad and Crocker, 1983, Prasad and Crocker, 1983, Prasad 1987) or

wave decomposition (Bodén and Åbom, 1995, Rämmal and Åbom, 2007, and Liu and Herrin, 2008) approach. For the circuit analogy, the source impedance is compared to an internal resistor, which is helpful in understanding the energy loss within the sound source. For the wave decomposition model, the source impedance is more closely related to the sound reflection at the source, which affects the resonances in the intake or exhaust system. It should be noted that both circuit analogy model and wave decomposition model are developed under the assumption that for the source properties, both the strength and the impedance, remain constant with varied loads. More sophisticated models are available to take nonlinearity and interaction between both sides of the source into consideration, however, in many cases, linear models prove to be satisfactorily accurate. More details about these two models will be provided in Chapter 3. In addition, procedures to measure the source impedance are described in detail.

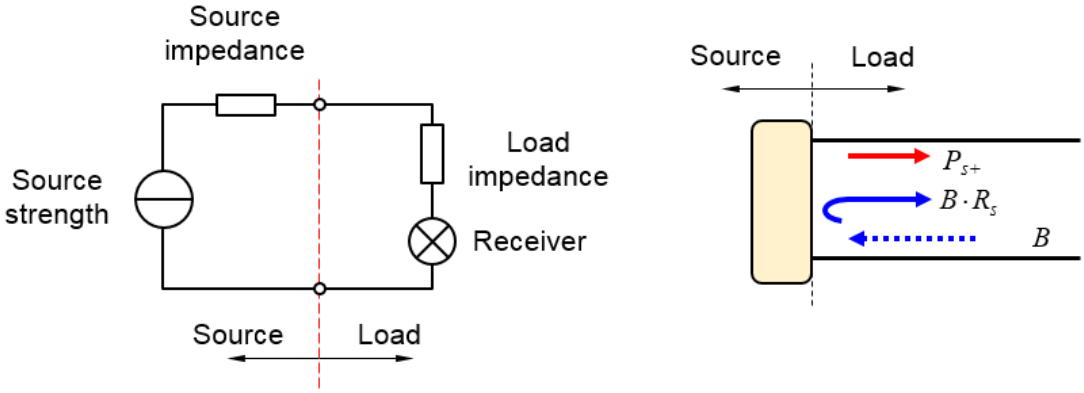

Figure 1.4 Circuit analogy model and wave decomposition model.

1.3.4 Exhaust system

Generally, there are two strategies to realize sound attenuation in exhaust systems. The first way is through sound reflection and cancellation introduced by impedance mismatches at areas changes or volume expansions. An example of a reactive muffler is shown in Figure 1.4.

Figure 1.5 Reactive sound attenuation design at the discharge of a compressor.

Other mufflers attenuate sound by using sound absorptive material or perforates within the muffler. As the absorption material is usually effective in higher frequency range, the typical attenuation curve of a dissipative type of muffler is often poor in the low frequency range and increases with frequency. A dissipative muffler and associated attenuation curve is shown in Figure 1.6.

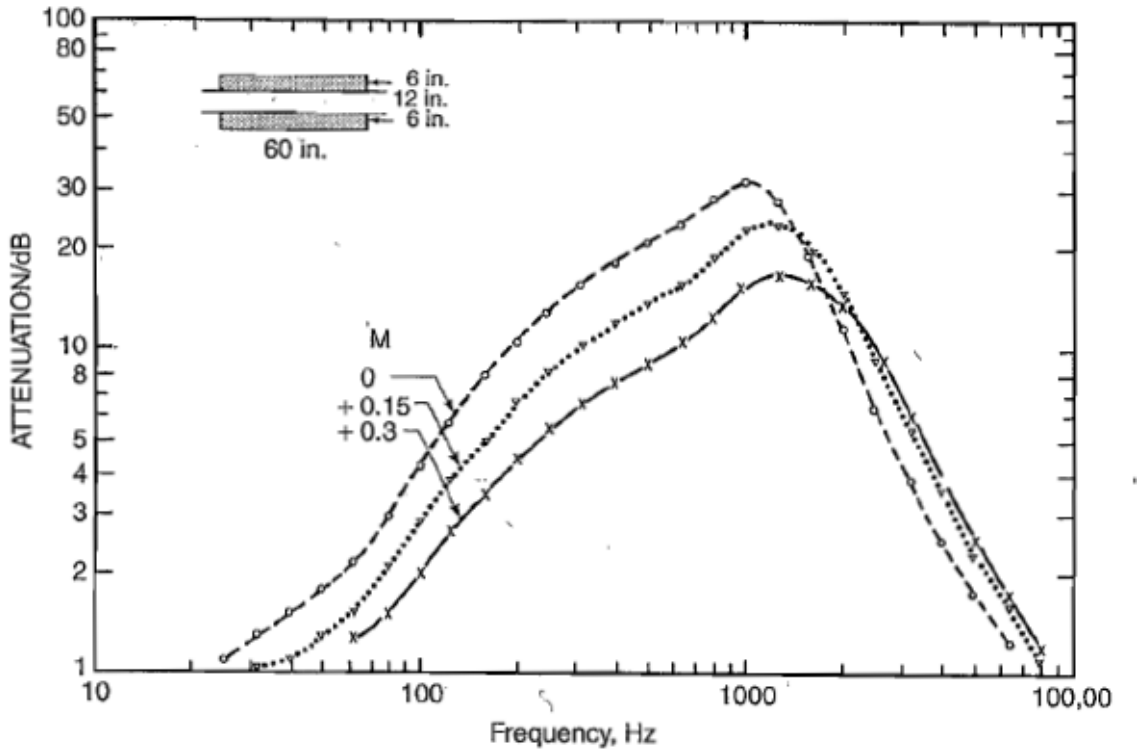

Figure 1.6 Typical dissipative muffler and its attenuation curve (Ver and Beranek, 2006).

Generally, the sound propagation from source to receiver can be related to the interaction between source impedance, impedances defined by the design of exhaust system, and the radiation impedance at the outlet of exhaust system. If the source impedance is bridged to the radiation impedance through a series of smooth impedance changes, the sound energy of the source is very effectively radiated to exterior. A good example is the design of loud speaker. The impedance of the sound source of a small volume is smoothly connected to the impedance of the exterior using a gradual expansion. To make the transition even smoother, modern loud speakers adopt folded paths to increase the length of expansion.

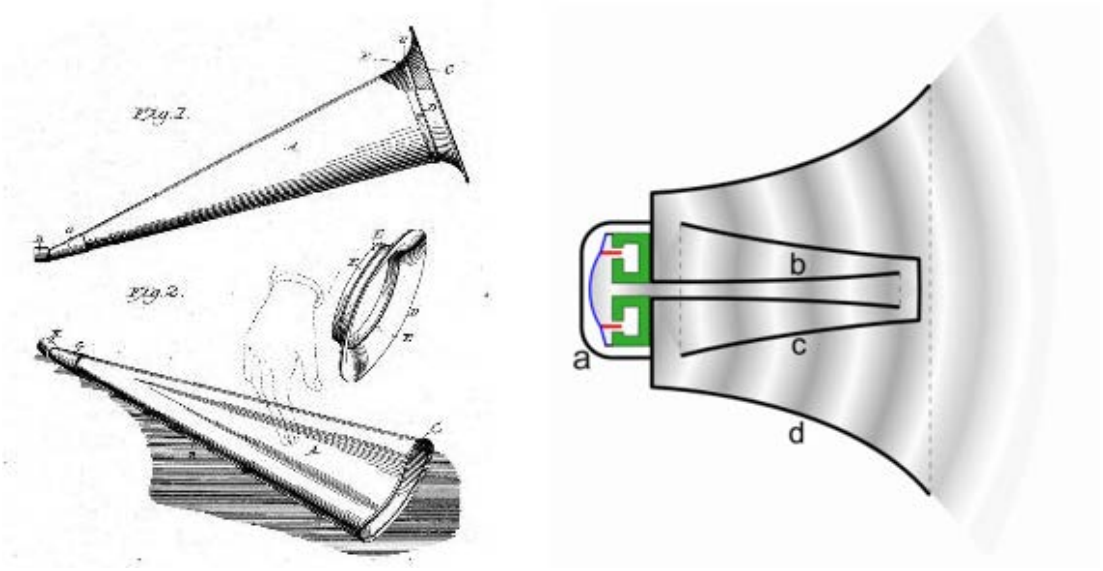

Figure 1.7 Horn in 19th century and a modern loud speaker (https://en.wikipedia.org/wiki/Horn_loudspeaker).

Chapter 2 THE MEASUREMENT OF MUFFLERS PERFORMANCE

2.1 Introduction

In industry, insertion loss (IL) and transmission loss (TL) are often used to assess muffler performance. Insertion loss is defined as the difference in sound pressure at a position downstream of the termination with and without a muffler installed. Insertion loss is determined by the design of the muffler, the source and termination impedances, and the lengths of the inlet and outlet ducts. Hence, insertion loss is a measure of the attenuation of a muffler when installed on a particular source.

Transmission loss is defined as the ratio between incident sound power and transmitted sound power, under the assumption that both source and termination are anechoic. As transmission loss eliminates the influence of source and termination properties, transmission loss is often used in the design stage, when source and termination impedances are unavailable.

Since mufflers can be easily inserted into many systems, insertion loss is often straightforward to measure. However, it is impossible to directly measure transmission loss due to the lack of an ideal anechoic source and termination. Methods have been developed to indirectly measure transmission loss. The two commonly used techniques are the two-load (To and Doige, 1979, To and Doige, 1979, and Lung and Doige, 1983) and two-source (Munjal and Doige, 1990) methods. In measurements where an impedance tube are used, it is more convenient to change the termination rather than the location of the source. Accordingly, the two-load method is emphasized in the discussion which follows

because it is more commonly used for assessing the transmission loss of mufflers. However, the conclusions made are likely transferable to the two-source method as well.

The routine to make a transmission loss measurement on a muffler has been standardized in ASTM E2611-09 (ASTM, 2009). Although this standard is geared towards determining the transmission loss through a sound absorbing material, the algorithm and methodology can be applied directly to the measurement of muffler transmission loss. In this standard, the transfer matrix of a muffler is first measured, then the transmission loss is calculated based on the measured transfer matrix.

Alternatively, a less commonly used scattering matrix algorithm developed by Åbom (Åbom, 1991) may be used. Instead of sound pressure and particle velocities, the scattering matrix relates the traveling wave amplitudes on both sides of a muffler. If this algorithm is used, the scattering matrix is measured before the calculation of transmission loss.

In this chapter, both methods based on the transfer and scattering matrix are reviewed and their performances are compared in experiments. The transfer matrix approach can be performed with either 2 or 4 microphones. It is observed that when 2 microphones are used, the reference microphone should be placed downstream of the muffler or error will occur at certain frequencies. Error analysis is performed to find the cause of the error and provide solutions to avoid it. The scattering matrix method requires more complex processing algorithms which are currently commercially unavailable, but is theoretically less influenced

by measurement error. In this work, it is shown that both the transfer and scattering matrix algorithms yield excellent results when performed following the suggested protocol.

2.2 Transfer and scattering matrix approach: theory and results

2.2.1 Transfer matrix approach

Figure 2.1 shows the two-load measurement setup using an impedance tube on each side of the muffler. There are two microphone mounting locations on both the upstream and downstream sides of the muffler. Changing the termination varies the acoustic load. The two acoustical loads must be sufficiently different throughout the frequency range in order to make accurate measurements (Munjal and Doige, 1990, and Åbom, 1992). In the current work where flow is not considered, one reactive (open termination) and one absorbing (closed with thick foam) load is selected.

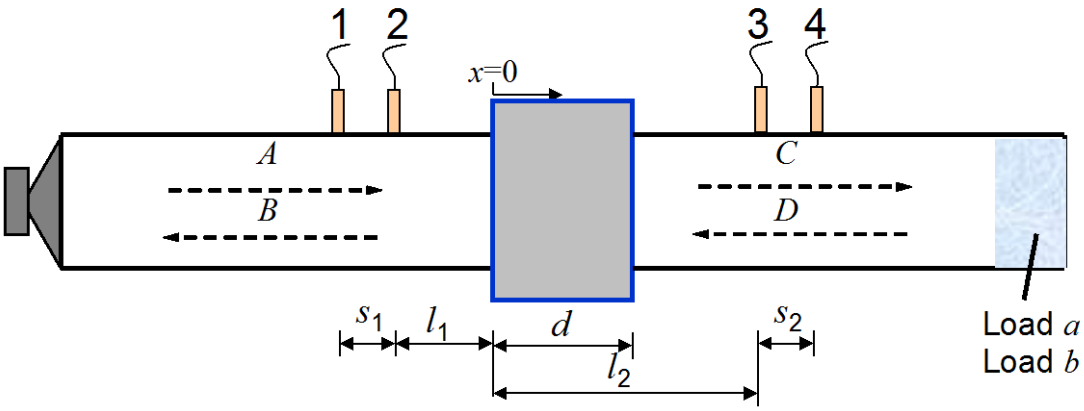

Figure 2.1 Schematic setup for transmission loss measurement.

For the transfer matrix approach (ASTM E2611-09), the transfer matrix of the muffler is determined as a preliminary step to determining the transmission loss.

The excitation signal for the source (i.e. loudspeaker) or the response from one of the microphones is chosen as a reference. Then the transfer functions between the sound pressures measured at the microphone locations and the reference channel are measured. Appling wave decomposition, the relative complex wave amplitudes A, B, C, and D can be determined as

$$A = j\frac{H_{R1}e^{-jkl_1} - H_{R2}e^{-jk(l_1+s_1)}}{2\sin(ks_1)} \tag{2.1a}$$

$$B = j\frac{H_{R2}e^{jk(l_1+s_1)} - H_{R1}e^{jkl_1}}{2\sin(ks_1)} \tag{2.1b}$$

$$C = j\frac{H_{R3}e^{jk(l_2+s_2)} - H_{R4}e^{jkl_2}}{2\sin(ks_2)} \tag{2.1c}$$

$$D = j\frac{H_{R4}e^{-jkl_2} - H_{R3}e^{-jk(l_2+s_2)}}{2\sin(ks_2)} \tag{2.1d}$$

where H_{Ri} denotes the transfer function between microphone i and reference R, and k is the wavenumber. l_1, l_2, s_1 and s_2 are identified in Figure 2.1. For each acoustic load, sound pressure and particle velocity at the inlet ($x = 0$) and outlet of the muffler ($x = d$) can be expressed as

$$p_0 = A + B \tag{2.2a}$$

$$u_0 = (A - B)/\rho_0 c \tag{2.2b}$$

$$p_d = Ce^{-jkd} + De^{jkd} \tag{2.2c}$$

$$u_d = \left(Ce^{-jkd} - De^{jkd}\right)/\rho_0 c \tag{2.2d}$$

where ρ_0 is the air density and c is the speed of sound. The transfer matrix can then be written as

$$T = \begin{bmatrix} \dfrac{p_{0,a}u_{d,b} - p_{0,b}u_{d,a}}{p_{d,a}u_{d,b} - p_{d,b}u_{d,a}} & \dfrac{p_{0,b}p_{d,a} - p_{0,a}p_{d,b}}{p_{d,a}u_{d,b} - p_{d,b}u_{d,a}} \\ \dfrac{u_{0,a}u_{d,b} - u_{0,b}u_{d,a}}{p_{d,a}u_{d,b} - p_{d,b}u_{d,a}} & \dfrac{p_{d,a}u_{0,b} - p_{d,b}u_{0,a}}{p_{d,a}u_{d,b} - p_{d,b}u_{d,a}} \end{bmatrix} \tag{2.3}$$

where the subscripts a and b denote the two different loads. In the case where the inlet and outlet cross-sectional area are equal, transmission loss is expressed as

$$TL_T = 20\log_{10}\left|\frac{1}{2}\left(T_{11} + \frac{T_{12}}{\rho c} + \rho c T_{21} + T_{22}\right)\right| \tag{2.4}$$

One noteworthy feature of the transfer matrix approach is that the transfer functions may be measured simultaneously or sequentially. Hence, either a four or two channel data acquisition system may be used. One advantage of measuring the transfer functions sequentially is that the microphones do not need to be phase calibrated. However, measurements can generally be made faster using four microphones once calibrated.

2.2.2 Scattering matrix approach

An alternative approach is the scattering matrix approach suggested by Åbom (Åbom, 1991) where the scattering matrix is first determined as an interim step to finding transmission loss. The scattering matrix relates the complex wave

amplitudes in the upstream (A and B) and complex wave amplitudes in the downstream (C and D) as

$$\begin{Bmatrix} B \\ C \end{Bmatrix} = \begin{bmatrix} S_{11} & S_{12} \\ S_{21} & S_{22} \end{bmatrix} \begin{Bmatrix} A \\ D \end{Bmatrix} \tag{2.5}$$

One of the complex wave amplitudes is used as a reference. The scattering matrix can be expressed in terms of the transfer functions between complex wave amplitudes as

$$S_{11} = \frac{H_{RB,a}H_{RD,b} - H_{RB,b}H_{RD,a}}{H_{RA,a}H_{RD,b} - H_{RA,b}H_{RD,a}} \tag{2.6a}$$

$$S_{12} = \frac{H_{RB,b}H_{RA,a} - H_{RB,a}H_{RA,b}}{H_{RA,a}H_{RD,b} - H_{RA,b}H_{RD,a}} \tag{2.6b}$$

$$S_{21} = \frac{H_{RC,a}H_{RD,b} - H_{RC,b}H_{RD,a}}{H_{RA,a}H_{RD,b} - H_{RA,b}H_{RD,a}} \tag{2.6c}$$

$$S_{22} = \frac{H_{RC,b}H_{RA,a} - H_{RC,a}H_{RA,b}}{H_{RA,a}H_{RD,b} - H_{RA,b}H_{RD,a}} \tag{2.6d}$$

where H_{Ri} denotes the transfer function between complex wave amplitude i and reference amplitude R, and the subscripts a and b denote the two different loads. If there is no flow and the inlet and outlet have the same cross-sectional area, the transmission loss can be expressed as

$$TL_S = 20\log_{10}\left|\frac{1}{S_{21}}\right| \tag{2.7}$$

The advantage of the scattering matrix approach is that a complex wave amplitude is used as a reference instead of the sound pressure at a position. Theoretically, it is less impacted if a microphone position corresponds with a standing wave node. This advantage is examined hereinafter.

2.2.3 Experimental results

The transfer and scattering matrix approaches were compared using a simple cylindrical expansion chamber. The muffler was constructed out of 11.5 mm thick polycarbonate plastic. The length was 200 mm and the inner diameter was 150 mm. The inlet and outlet diameter was 34.8 mm, which exactly matched the impedance tube. Although this muffler was geometrically symmetric so that only one load was required, the two-load method was employed. The transmission loss can be calculated theoretically (Åbom,1990) as shown in Figure 2.2.

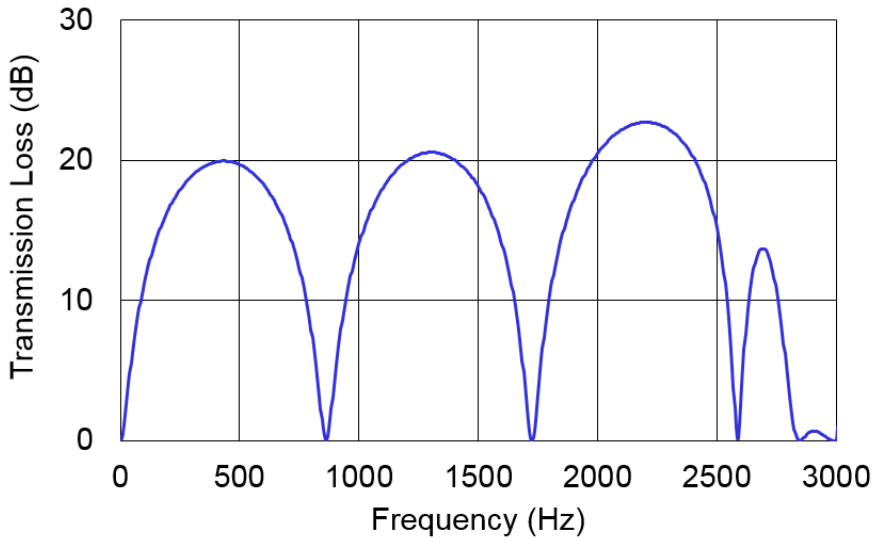

Figure 2.2 The theoretical transmission loss curve for the simplex expansion chamber.

The transmission loss was measured using the transfer matrix approach with 2 microphones and 4 microphones. When 2 microphones are used, different microphone locations are selected as reference and transmission loss results are compared in Figure 2.3. Though the four results generally agree, there is noticeable noise at both 100 and 400 Hz if microphone 1 or 2 is selected as a reference whereas the measurement is smooth using reference 3 or 4 for the entire frequency range.

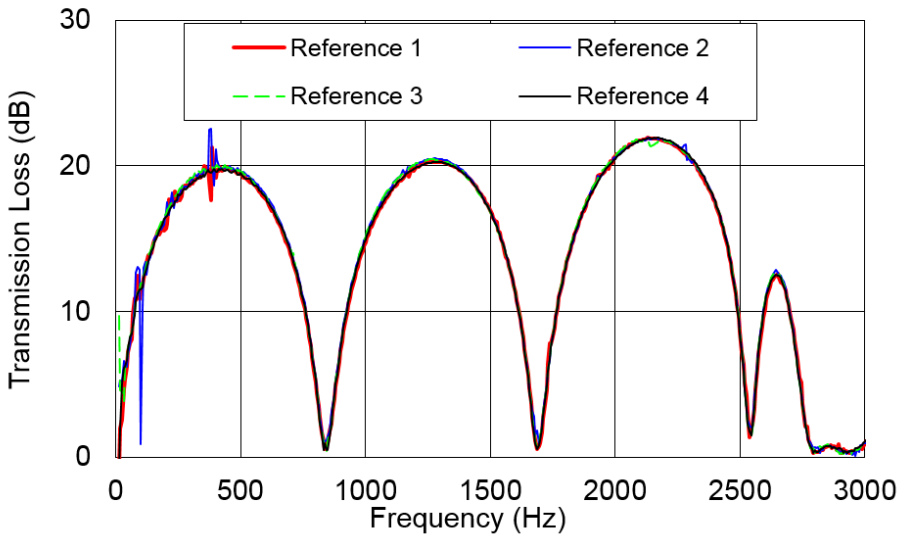

Figure 2.3 Measured transmission loss with transfer matrix approach using two microphones.

The measured TL curves using 4 microphones are plotted in Figure 2.4. If 4 microphones are used, the transmission loss results compare well over the entire frequency range regardless of the reference selected. This suggests that the errors noted in Figure 2.3 can be mitigated by measuring transfer functions simultaneously.

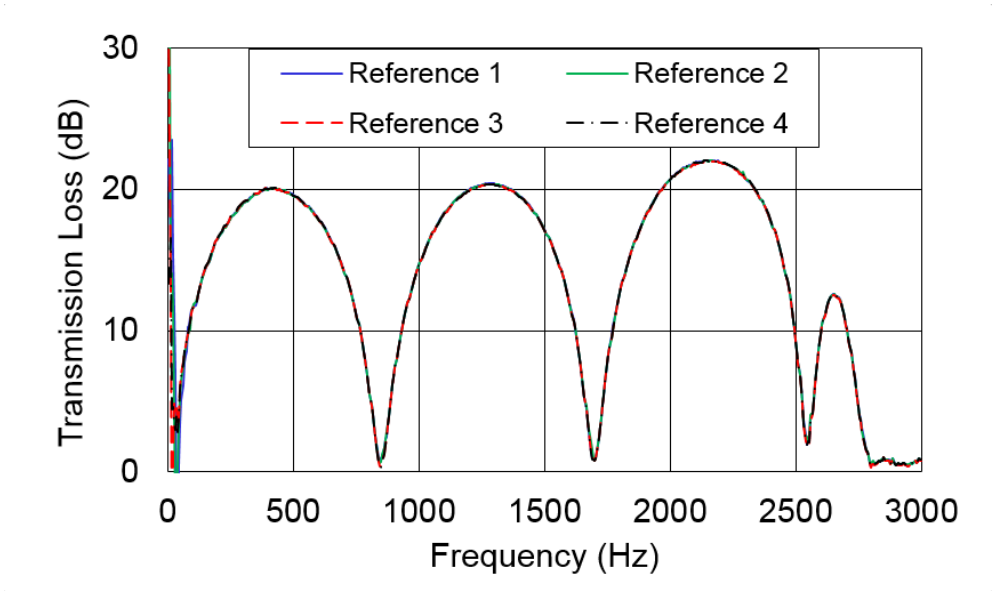

Figure 2.4 Measured transmission loss with transfer matrix approach using four microphones.

Figure 2.5 shows results for the scattering matrix approach. As required by the algorithm, 4 microphones are used simultaneously and each of the different complex wave amplitudes are used as a reference. For this example, measured transmission loss results are smooth regardless of the reference wave amplitude selected though there is some discrepancy at 2550 Hz if the upstream reflected complex wave amplitude is selected. Also in the lower frequency range (below 100 Hz), large discrepancies are observed if either of the upstream complex amplitudes is selected as reference.

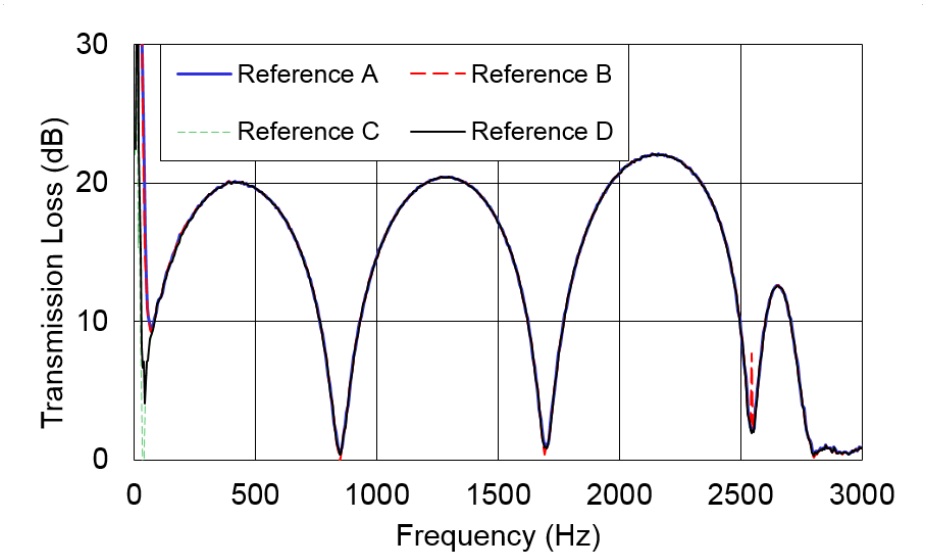

Figure 2.5 Measured transmission loss with scattering matrix.

For comparison purposes, the transmission loss curves obtained using each approach are compared in Figure 2.6. Except for the previously noted noise at 100 Hz and 400 Hz if the two-microphone transfer matrix approach is used, the transmission loss curves compare well with one another.

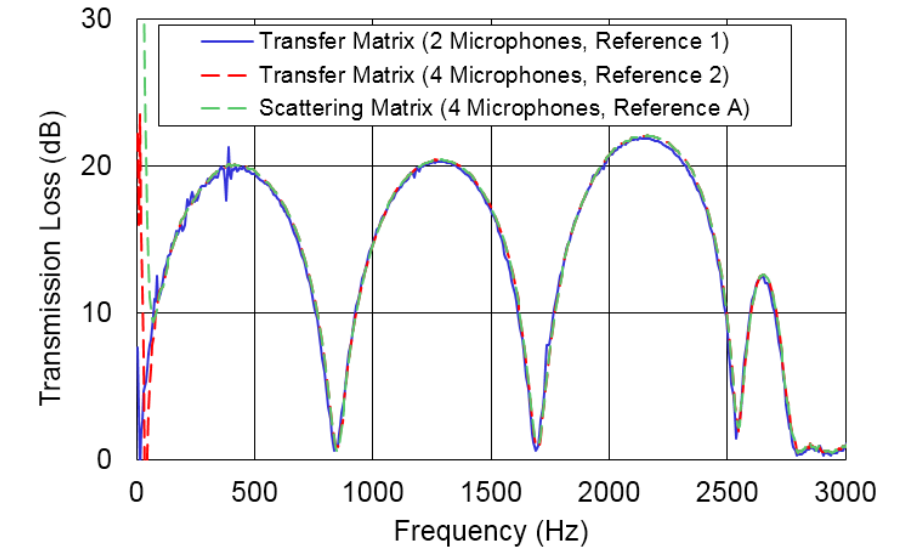

Figure 2.6 Comparison between transmission loss curves obtained using different approaches.

From these results, several observation can be made:

1. When the two-microphone transfer matrix approach is used, noisy peaks will occur at the frequencies of 100 and 400 Hz, if an upstream microphone is selected as reference. When a downstream microphone is selected as reference, the transmission loss curve is smooth throughout the frequency range.
2. When the four-microphone transfer matrix approach is used, the transmission loss curve is always smooth, regardless of the selection of reference.
3. The scattering matrix approach, which requires 4 microphones, gives smooth and good results except for the lower frequency range (below 100 Hz).

In the following discussion, the reason for the difference between 2-microphone and 4-microphone transfer matrix approaches is investigated. This investigation also provides suggestions as to which microphone should be used as reference to get best results. After that, the comparison between transfer matrix and scattering matrix approaches will be made. observed for the scattering matrix approach is also studied.

2.3 Transfer matrix approach analysis

2.3.1 Coherence problem

Figure 2.3 showed that the transmission loss measured using 2 microphones was noisy at 100 and 400 Hz if an upstream reference was selected. However,

the transmission loss measurement using 4 microphones was smooth over the entire frequency range regardless of the choice of reference. This discrepancy is significant because measurements are often made using 2 microphones if impedance tubes are adapted for the measurement of transmission loss.

If the transfer matrix approach is used, four transfer functions are measured for each load, which are H_{R1}, H_{R2}, H_{R3}, and H_{R4}. For convenience, one of the four microphones is often selected as the reference signal. Hence, the number of the transfer functions measured is reduced to three for each load because one of the four transfer functions is unity.

Elnady (Elnady, 2007) developed a transmission loss measurement system that included flow and selected the source voltage as a reference. Song and Bolton (Song and Bolton, 2000), whose work is the basis for ASTM E2611 (ASTM, 2009), used the source as a reference as well. Tao and Seybert (Tao and Seybert, 2003) used an upstream microphone. However, ASTM E2611 does not recommend a specific reference.

A few comments regarding the selection of a reference can be made. First, one of the transfer functions is by design unity, with no error, if one of the microphones is selected as a reference. Accordingly, selecting one of the microphones as a reference should be preferred if it can be assumed that measurement errors are similar regardless of the choice of reference. Secondly, measurement errors will be lessened if there are no strong resonances in the tubes. This is more likely to be the case if the muffler or silencer is dissipative instead of reactive. Such measurement errors can also be minimized if the

coherence is improved. This is sometimes accomplished by using a sinusoidal or stepped sine excitation (Elnady, 2007). However, to speed up the data acquisition process, random excitation is used in most commercial testing systems. The coherence will be lower if a reflective load like an open or closed tube is used. If an absorbing termination is used, there will be less interference at the nodes due to the damping and the coherence being greatly improved. However, as both Munjal and Doige (Munjal and Doige, 1990) and Åbom (Åbom, 1992) pointed out, a potential challenge of the two-load method is to find two loads that are different enough from one another at all frequencies of interest. If the acoustic loads have similar impedances at a particular frequency, the determined transmission loss is prone to error due to a potential singularity in solving Equation 2.3. As a result, one reflective termination is nonetheless recommended in the two-load measurement.

Figure 2.7 shows the coherence for an open termination, using the upstream and downstream microphones as reference respectively. Coherence is low because of the modal behavior of the muffler and upstream and downstream piping. The results indicate that the coherence is low at a greater number of frequencies for transfer functions between microphones separated by the muffler (i.e. H_{13} and H_{31}). The coherence for transfer functions between microphones on the same side of the muffler (i.e., H_{12} and H_{34}) will be lower at a smaller number of frequencies.

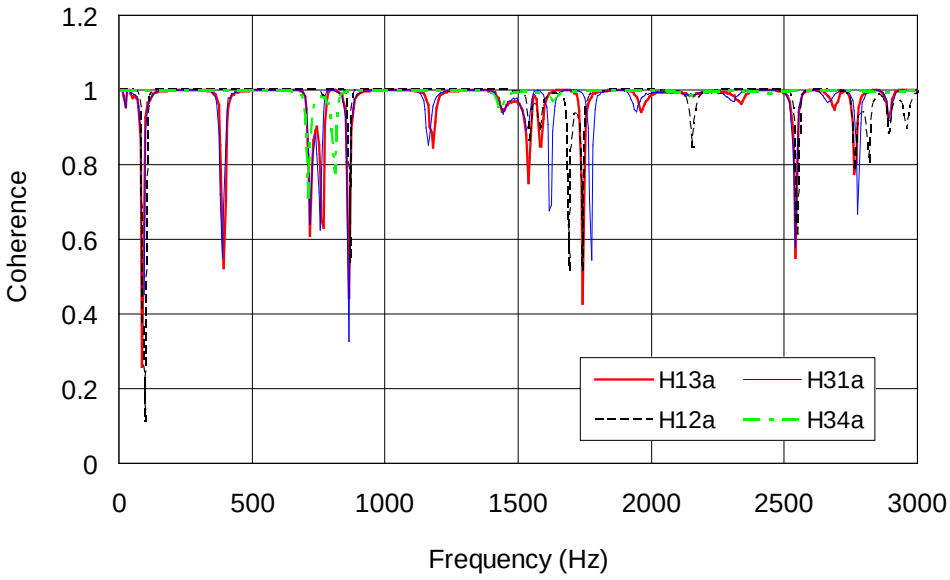

Figure 2.7 Measured coherence of transfer function H_{13a}, H_{12a}, H_{31a} and H_{34a}.

Coherence is particularly low when the reference microphone corresponds to a standing wave node (regions of greatest interference). Accordingly, a shorter length of tube will reduce the number of standing wave nodes. For the particular system used, the length of the upstream tube is greater than that of the downstream. Hence, it is not surprising that the coherence is better if a downstream microphone is used as reference, as shown in Figure 2.7.

Figures 2.8 and 2.9 compare the measured four-pole parameters using the 2-microphone approach, with microphone 1 and 3 as reference respectively. Alternatively, microphone 2 or 4 could be selected as a reference but the conclusions are the same. The curve for T_{21} and T_{22} with microphone 1 used as reference is noisy at approximately 400 Hz. However, the results are smooth if microphone 3 is chosen.

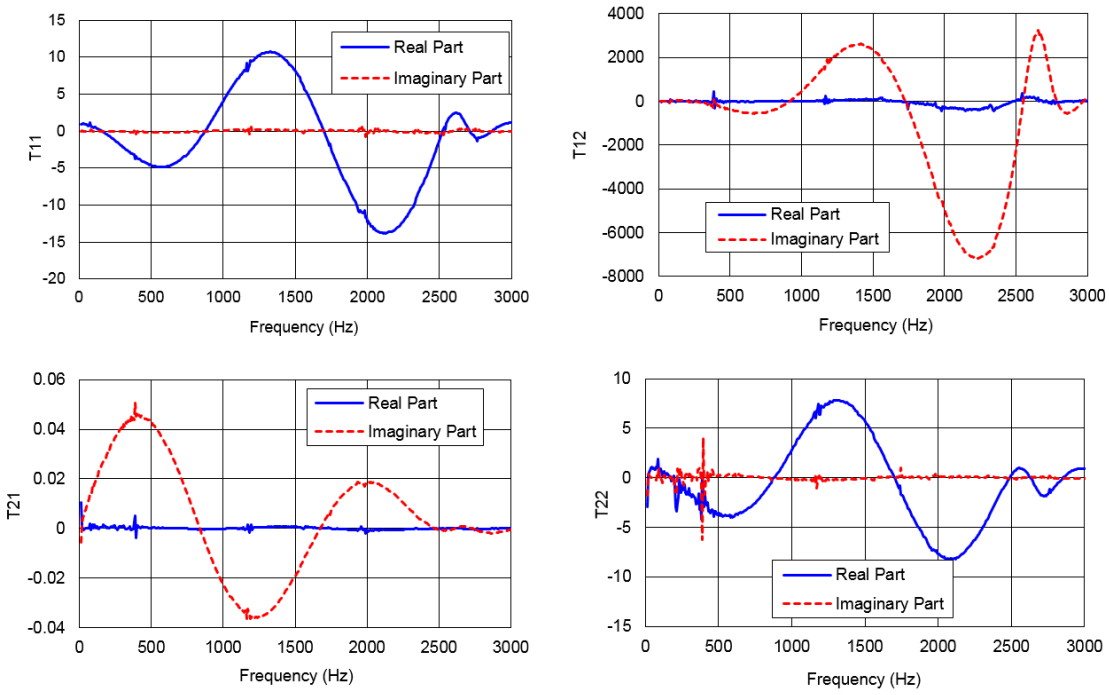

Figure 2.8 Measured four-pole parameters of the simple expansion chamber with Reference 1.

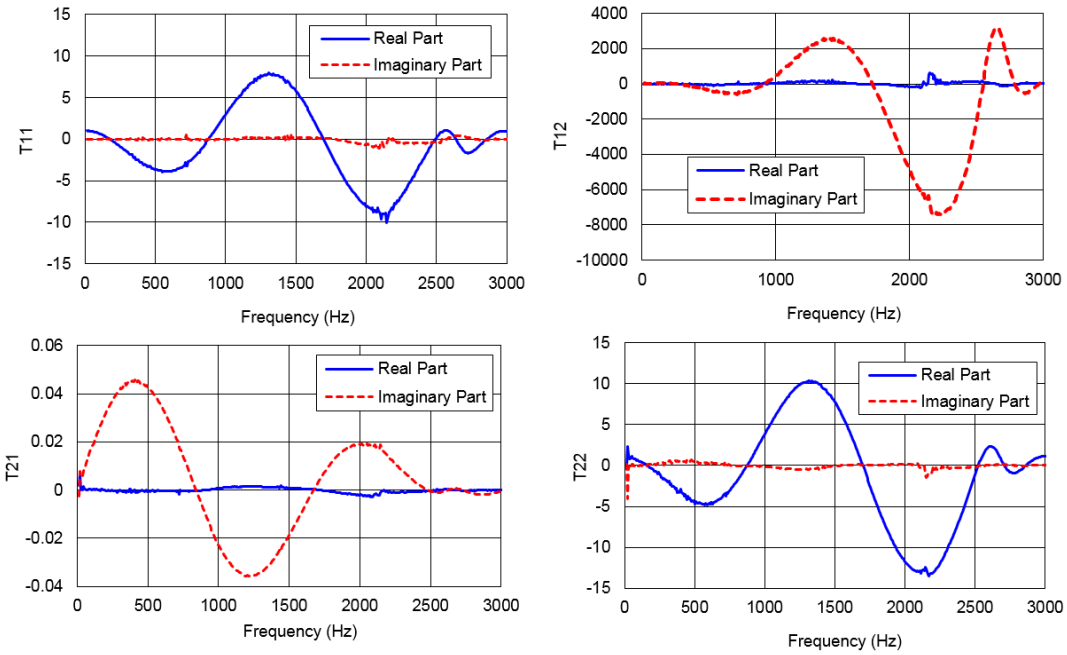

Figure 2.9 Measured four-pole parameters of the simple expansion chamber with Reference 3.

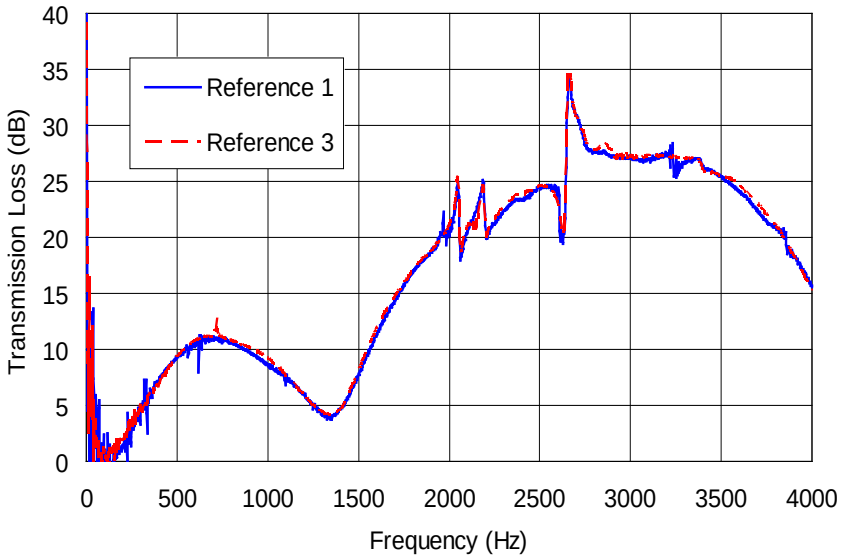

Figure 2.10 Measured transmission loss of a reactive muffler with different reference signals.

This phenomenon is evident not only for the simple expansion chamber, but is also present for other reactive mufflers. The transmission loss of one such muffler is measured using 2 microphones and shown in Figure 2.10. When microphone 1 is selected as reference, the measured transmission loss is noisy at 225 Hz, 330 Hz, 620 Hz and so forth. The quality of the measurement is similar if the source is selected as a reference. When microphone 3 is selected as reference, the transmission loss is very smooth for the entire frequency range with 700 Hz being the lone exception.

While the measurement is subject to inevitable errors and interference, an analytical approach can be used to reproduce the ideal situation. Analytical four-poles of the simple expansion chamber were obtained via plane wave muffler theory using the Sidlab software (Munjal, 1987 and SIDLAB, 2011). The

termination impedances Z_t for each of the two different loads were measured. Then, the transfer function between the ith microphone and the termination pressure can be calculated using

$$H_{it} = \frac{p_i}{p_t} = T_{11}^{it} + \frac{T_{12}^{it}}{Z_t} \tag{2.8}$$

where p_i and p_t are sound pressures at the ith microphone and the termination respectively. T_{11}^{it} and T_{12}^{it} are corresponding transfer matrix elements from microphone i to the termination. The transfer functions between microphone i and microphone j were further determined by $H_{ij} = H_{jt}/H_{it}$ and can be expressed as

$$H_{ij} = \frac{T_{11}^{jt} Z_t + T_{12}^{jt}}{T_{11}^{it} Z_t + T_{12}^{it}} \tag{2.9}$$

Figure 2.11 shows the comparison between measured and analytically constructed transfer functions H_{13a}. A phase jump occurs at both 100 and 400 Hz, where a standing wave node coincides with microphone 1. The coincidence of microphone location and standing wave node is the reason for noise at these particular frequencies (Seybert and Sornarko, 1981).

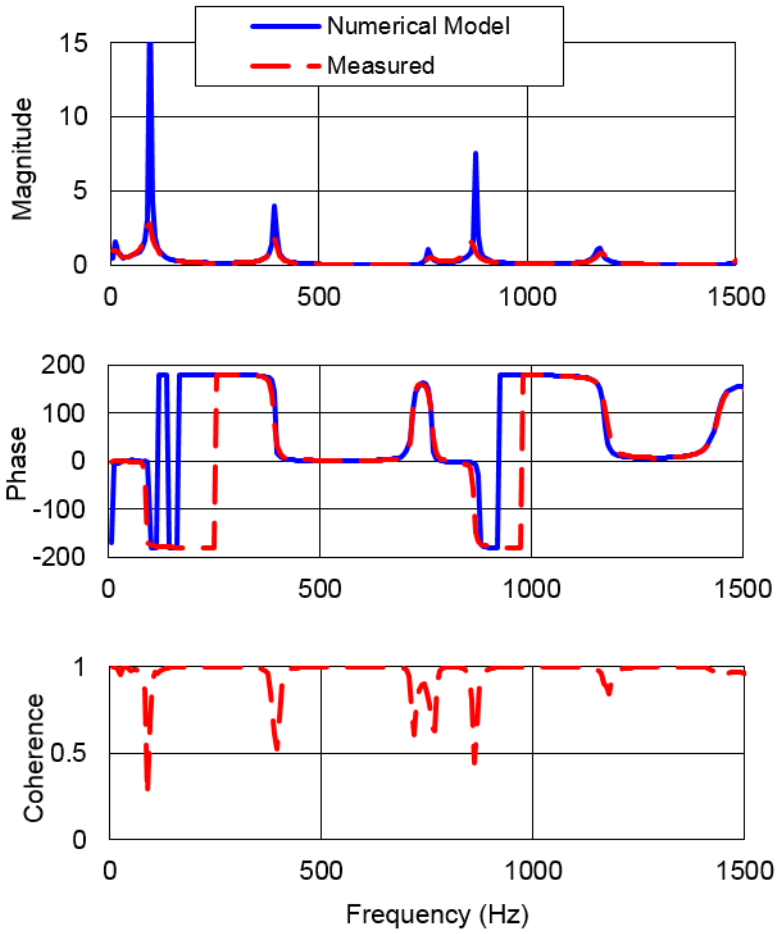

Figure 2.11 Measured and simulated transfer function H_{13a} of the simple expansion chamber.

2.3.2 Difference between 2-microphone and 4-microphone approach

Even though the theory and processing technique are identical, there are no noticeable peaks at 100 and 400 Hz if the 4-microphone approach is used. Accordingly, it does not seem reasonable to expect the 2 microphone method to have greater error. However, it should be borne in mind that the measurements are not made simultaneously if 2 microphones are used. It is assumed that transfer functions are time invariant. To investigate the soundness of this

assumption, the following measurement was conducted. The setup was the same as the transmission loss measurement for the expansion chamber described earlier with an open termination. Then, the transfer functions H_{12}, H_{13}, and H_{14} were measured for 5 times. A deviation ratio (DR) was defined as

$$DR_i = \left| \frac{\sigma(H_{1i}^1, H_{1i}^2, \dots, H_{1i}^5)}{\text{mean}(H_{1i}^1, H_{1i}^2, \dots, H_{1i}^5)} \right| \tag{2.10}$$

where σ stands for standard deviation and the superscript stands for the sequence of measurement. The deviation ratios for H_{12}, H_{13} and H_{14} are plotted in Figure 2.12. It is shown that at frequencies of 100 and 400 Hz, the deviation ratio is high, which indicates that the assumption of time invariance fails at those particular frequencies. However, by measuring the transfer function at the same time, the deviation will not influence the results.

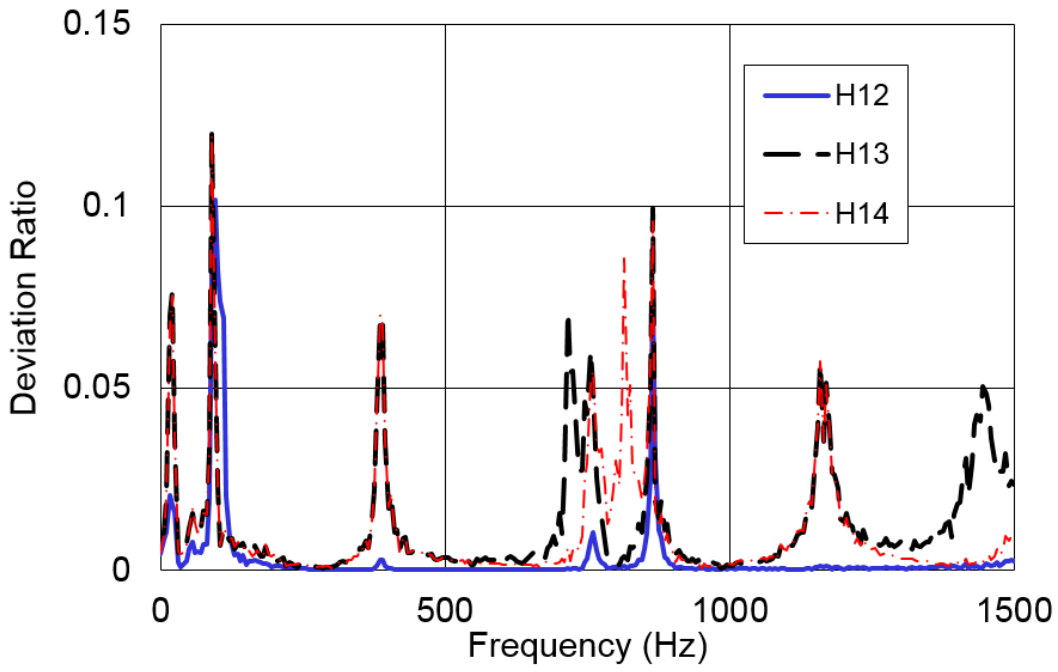

Figure 2.12 Deviation ratios of measured transfer functions H_{12}, H_{13} and H_{14}.

2.3.3 Error Analysis of the Transfer Matrix Approach

It was observed that the noise can be reduced by using a downstream microphone as reference if the two-microphone transfer matrix approach is used. This can be explained by looking at the algorithm for the transfer matrix approach. First, note that p_d and u_d occur in the denominator of each term in the transfer matrix (Equation 2.3). Note that p_d and u_d are determined from C and D which depend solely on H_{R3} or H_{R4}. If a downstream reference is selected, one of these two transfer functions will be unity and the coherence should be good for the other since the two microphones are adjacent to one another. If a downstream microphone is used as reference, it is reasonable to assume that most of the error will be confined to the numerator of Equation 2.3 whereas error will be introduced into both the numerator and denominator if an upstream microphone or the source is selected as a reference.

Note that microphones that are adjacent to one another on the same side of the muffler normally have good coherence and minimal error. If the microphones are separated by the muffler, the coherence is normally poor at certain frequencies. Accordingly, it is reasonable to assume that H_{12} or H_{34} will have negligible error and higher errors are anticipated for H_{13}, H_{14}, H_{31}, and H_{32}.

By examining Equation 2.1, it can be seen that errors will accumulate on C and D if an upstream microphone is chosen as a reference and on A and B if a downstream microphone is chosen.

In order to compare the errors with microphone 1 and 3, some assumptions are made in order to simplify the error analysis. First, errors occur only on the

transfer functions H_{13a} and H_{31a} with the reactive load. Secondly, error levels on H_{13a} and H_{31a} are the same. Other transfer functions are assumed to have no error. If errors on H_{14a} and H_{32a} were included, errors in A, B, C, and D will be increased by a constant factor but the conclusions will remain the same.

2.3.3.1 Numerical error study

A 10% magnitude error and a 10° phase error are artificially applied onto the transfer function H_{13a} and H_{31a} over the entire frequency range. Figure 2.13 shows the error in transmission loss versus frequency. It can be seen that errors will be higher for reference 1 at approximately 60% of the frequencies. Additionally, the error standard deviation is 1.4 dB for reference 1 compared to 0.9 dB for reference 3. Note that the relative errors predicted in Figure 2.13 manifest themselves in the transmission loss measurement shown in Figure 2.3. There are high errors if microphone 1 is chosen at both 100 and 400 Hz. Also, note that the errors are higher for reference 3 at 2175 Hz.

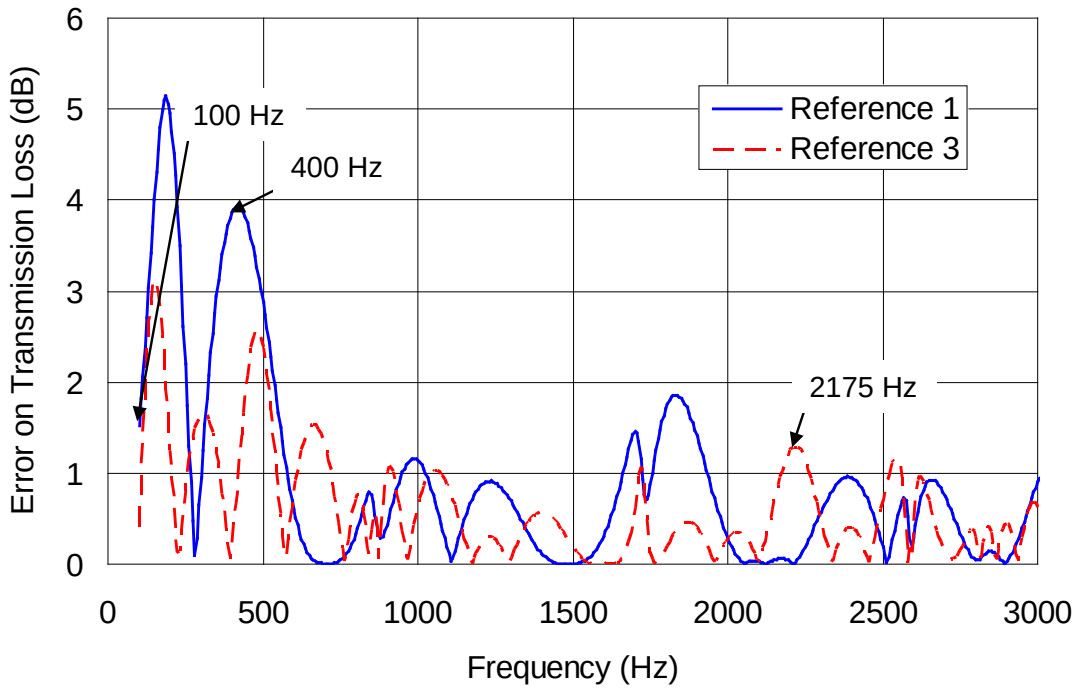

Figure 2.13 Error on transmission loss of the simple expansion chamber with 10% and 10° measured error on transfer function H_{13a} or H_{31a} respectively.

The numerical error analysis above is for a simple expansion chamber, which is typical of reactive mufflers. For dissipative mufflers, the effect of selecting a reference is not as important. Four-pole parameters of a 50 mm acoustic foam with 15000 rayls/m flow resistivity are obtained using Wu's model (Wu, 1988). Using the method discussed above, a node is found at 594 Hz. Figure 2.14 shows the error in transmission loss versus frequency. It is evident that the errors on transmission loss are minimal whichever microphone is used as reference.

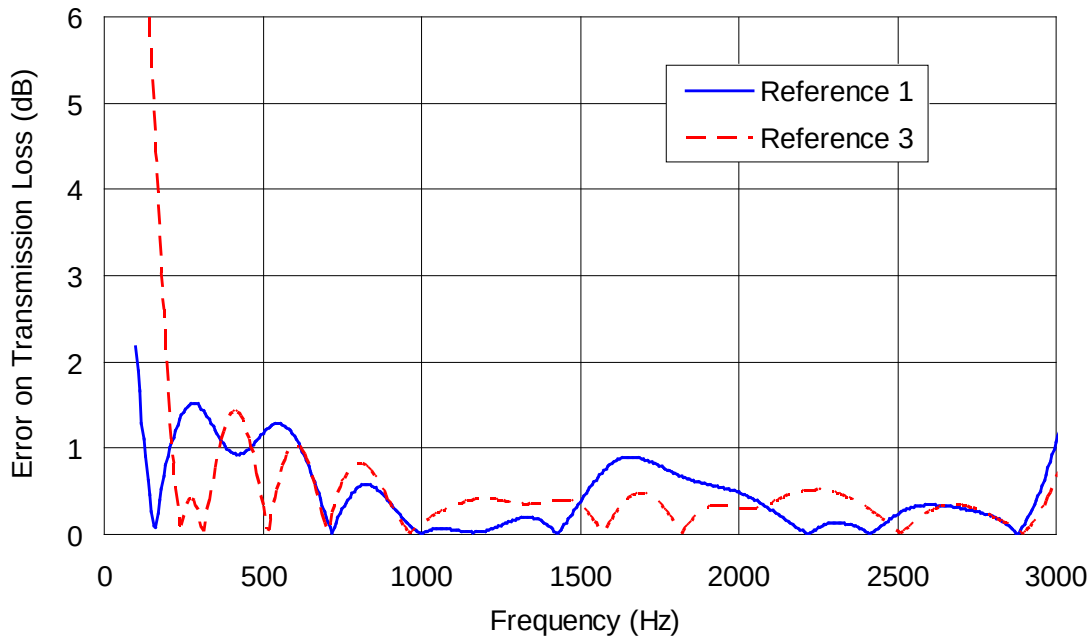

Figure 2.14 Error on transmission loss of the acoustic foam with 10% and 10° measured error on transfer function H_{13a} or H_{31a} respectively.

2.3.3.2 Analytical error study

Although the direct numerical simulation above is straightforward, a sensitivity analysis using a Taylor expansion is more suitable for drawing general conclusions. In this section, the sensitivities of errors on H_{13a} and H_{31a} to each four-pole parameter are determined.

Errors on the measured transfer function will first accumulate on the incident and reflected wave amplitudes (A, B, C, and D) and then propagate to each of the four-pole parameters. If microphone 1 is the reference, the errors of the transfer function between microphones 1 and 3 occur on H_{13a}, then accumulate to C_a and D_a, and finally propagate to each of the four-pole parameters. If microphone 3 is

the reference, the errors of the transfer function between microphones 1 and 3 occur on H_{31a}, and then propagate to the four-pole parameters via A_a and B_a.

When microphone 1 is the reference, the sensitivities of C_a and D_a to the H_{13a} error can be calculated from Equation 2.1 using

$$\frac{\partial C_a}{\partial H_{13a}} = \frac{je^{jk(l_2+s_2)}}{2\sin(ks_2)} \tag{2.11a}$$

$$\frac{\partial D_a}{\partial H_{13a}} = \frac{-je^{-jk(l_2+s_2)}}{2\sin(ks_2)} \tag{2.11b}$$

It follows that the sensitivities of the four-pole parameter T_{11} to C_a and D_a errors can be calculated using

$$\frac{\partial T_{11}}{\partial C_a} = \frac{-p_{0,b}/\rho c}{p_{d,a}u_{d,b} - p_{d,b}u_{d,a}} - \frac{\left(p_{0,a}u_{d,b} - p_{0,b}u_{d,a}\right)\left(u_{d,b} - p_{d,b}/\rho c\right)}{\left(p_{d,a}u_{d,b} - p_{d,b}u_{d,a}\right)^2} \tag{2.12a}$$

$$\frac{\partial T_{11}}{\partial D_a} = \frac{p_{0,b}/\rho c}{p_{d,a}u_{d,b} - p_{d,b}u_{d,a}} - \frac{\left(p_{0,a}u_{d,b} - p_{0,b}u_{d,a}\right)\left(u_{d,b} + p_{d,b}/\rho c\right)}{\left(p_{d,a}u_{d,b} - p_{d,b}u_{d,a}\right)^2} \tag{2.12b}$$

Then, the sensitivities of T_{11} to H_{13a} errors can be calculated using

$$\frac{\partial T_{11}}{\partial H_{13a}} = \frac{\partial T_{11}}{\partial C_a}\frac{\partial C_a}{\partial H_{13a}} + \frac{\partial T_{11}}{\partial D_a}\frac{\partial D_a}{\partial H_{13a}} \tag{2.13}$$

Similarly, when microphone 3 is the reference, the sensitivities of A_a and B_a to H_{31a} error can be calculated using

$$\frac{\partial A_a}{\partial H_{31a}} = \frac{je^{-jkl_1}}{2\sin(ks_1)} \tag{2.14a}$$

$$\frac{\partial B_a}{\partial H_{31a}} = \frac{-je^{jkl_1}}{2\sin(ks_1)} \tag{2.14b}$$

The sensitivities of the four-pole parameter T_{11} to A_a and B_a error can be calculated using

$$\frac{\partial T_{11}}{\partial A_a} = \frac{u_{d,b}}{p_{d,a}u_{d,b} - p_{d,b}u_{d,a}} \tag{2.15a}$$

$$\frac{\partial T_{11}}{\partial B_a} = \frac{u_{d,b}}{p_{d,a}u_{d,b} - p_{d,b}u_{d,a}} \tag{2.15b}$$

In a similar manner, the sensitivities of T_{11} to H_{31a} error can be calculated via

$$\frac{\partial T_{11}}{\partial H_{31a}} = \frac{\partial T_{11}}{\partial A_a}\frac{\partial A_a}{\partial H_{31a}} + \frac{\partial T_{11}}{\partial B_a}\frac{\partial B_a}{\partial H_{31a}} \tag{2.16}$$

The sensitivities of other four-pole parameters T_{12}, T_{21} and T_{22} to H_{13a} and H_{31a} error can be analyzed using the same approach. For an upstream reference

$$\frac{\partial T_{ij}}{\partial H_{13a}} = \frac{\partial T_{ij}}{\partial C_a}\frac{\partial C_a}{\partial H_{13a}} + \frac{\partial T_{ij}}{\partial D_a}\frac{\partial D_a}{\partial H_{13a}} \tag{2.17}$$

For a downstream reference

$$\frac{\partial T_{ij}}{\partial H_{31a}} = \frac{\partial T_{ij}}{\partial A_a}\frac{\partial A_a}{\partial H_{31a}} + \frac{\partial T_{ij}}{\partial B_a}\frac{\partial B_a}{\partial H_{31a}} \tag{2.18}$$

For the reactive muffler case discussed before, the sensitivities of each four-pole parameter to the H_{13a} and H_{31a} errors are shown in Figures 2.15 and 2.16 respectively. It is apparent that the sensitivities with microphone 1 as reference are more significant than with microphone 3 as reference. Moreover, with

microphone 1 as reference, the sensitivities on T_{21} and T_{22} are more significant than those on T_{11} and T_{12} for most of the frequency range, especially at around 400 Hz, where a phase jump occurs. This is consistent with the numerical simulation result and the observed result of the real measurement. For the dissipative muffler case discussed before, the sensitivities of the H_{13a} error and H_{31a} error to each four-pole parameter are shown in Figures 2.17 and 2.18 respectively. It can be observed that the sensitivities are much lower.

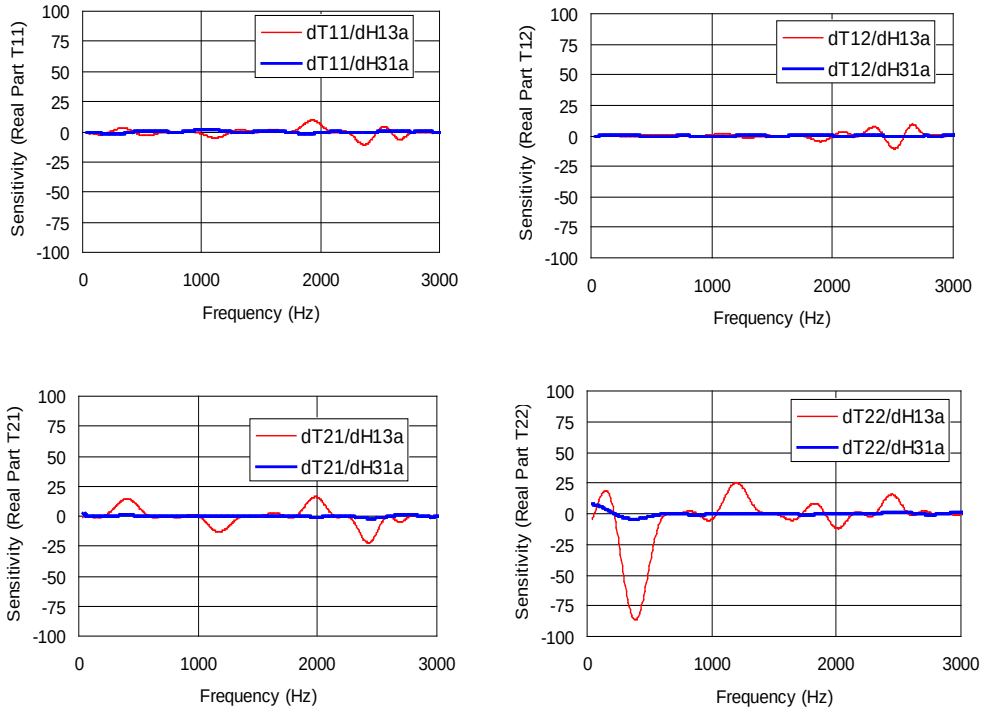

Figure 2.15 The sensitivities of each four-pole parameter (real part) of the simple expansion chamber to the H_{13a} and H_{31a} error.

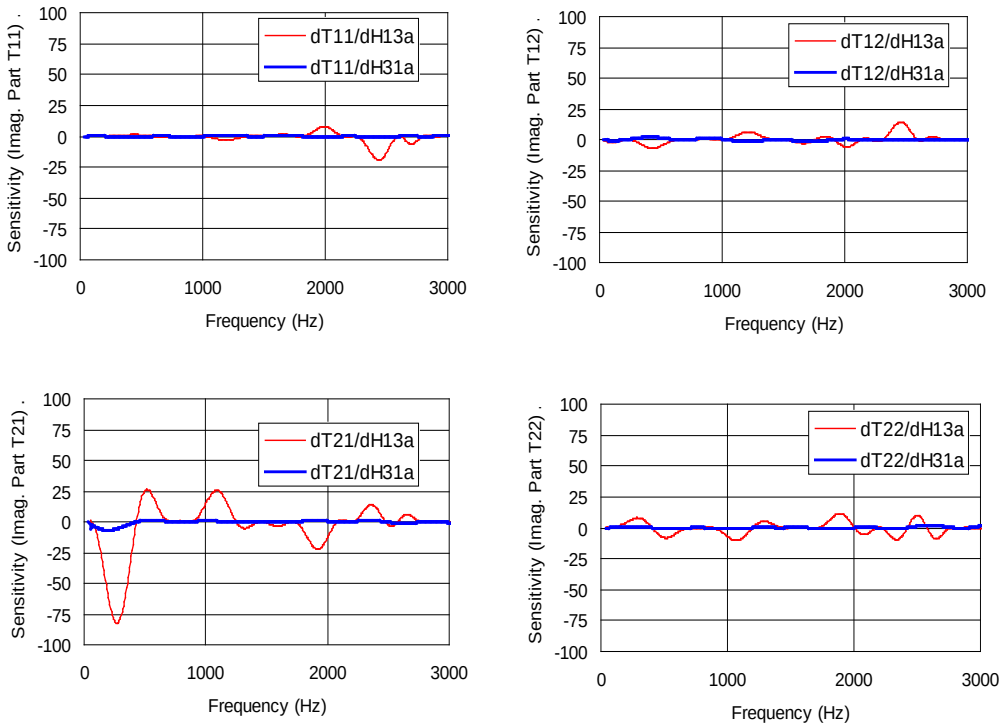

Figure 2.16 The sensitivities of each four-pole parameter (imaginary part) of the simple expansion chamber to the H_{13a} and H_{31a} error.

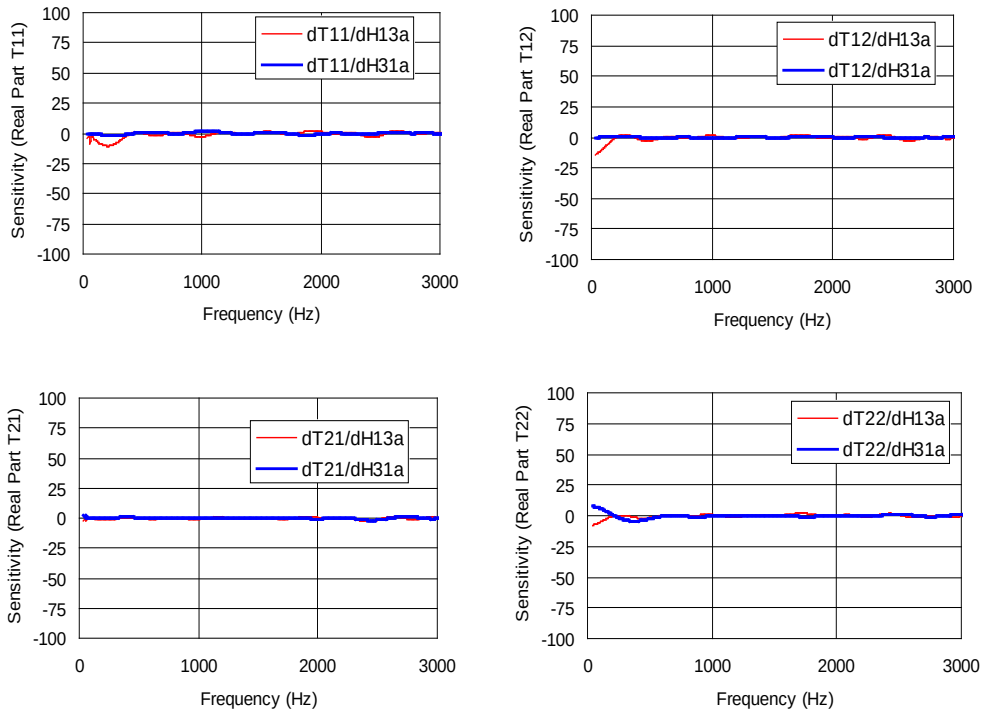

Figure 2.17 The sensitivities of the each four-pole parameter (real part) of the 50 mm foam to the H_{13a} and H_{31a} error.

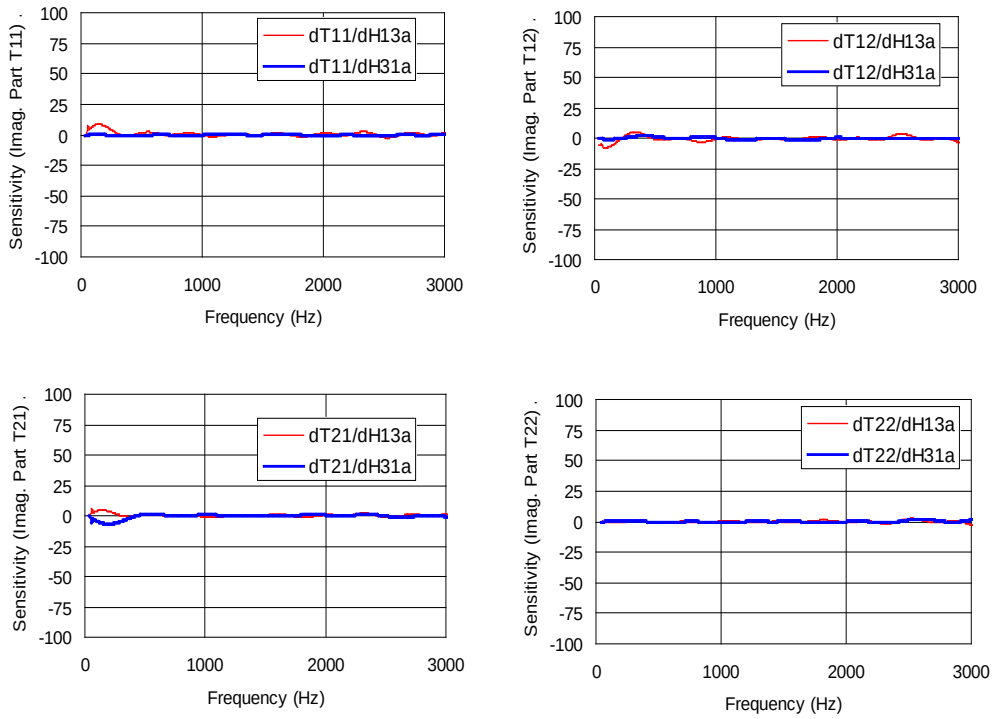

Figure 2.18 The sensitivities of the each four-pole parameter (imaginary part) of the 50 mm foam to the H_{13a} and H_{31a} error.

2.4 Advantages of scattering matrix approach

Assuming the H1 estimator is used when measuring the transfer functions,

$$H_{RX} = \frac{G_{RX}}{G_{RR}} = \frac{E[R^* X]}{E[R^* R]} \tag{2.19}$$

where E stands for average over a number of time records and R and X are the discrete Fourier transforms of the reference and response, respectively. For transfer matrix approaches, the transfer functions between sound pressures at microphone locations are measured and used for calculation. If the reference microphone location coincides with a standing wave node, the denominator in

Equation 2.19 goes to zero, and large errors are expected. Identical issues are anticipated if the other estimators are used.

In the case of the scattering matrix approach, the complex wave amplitude is used as reference. For instance, if the incident wave amplitude in upstream (A) is used as reference, the denominator in the transfer function calculation will be

$$G_{AA} = \frac{1}{4\sin^2(ks)}[G_{11} - G_{12}e^{-iks} - G_{21}e^{iks} + G_{22}] \tag{2.20}$$

where for the number subscripts, G_{ij} denotes the auto- or cross-spectrum of ith and jth microphone. With the sound pressure written in polar form, $P_1 = |P_1|e^{i\varphi_1}$ and $P_2 = |P_2|e^{i\varphi_2}$,

$$G_{AA} = \frac{1}{4\sin^2(ks)}E[|P_1|^2 - 2|P_1||P_2|\cos(\varphi_1 - \varphi_2 + ks) + |P_2|^2] \tag{2.21}$$

By observation, G_{AA} only goes to zero when $|P_1| = |P_2|$ and $\varphi_1 - \varphi_2 + ks = 2n\pi, n = 0,1,2,$ .... It can be concluded that if the complex wave amplitude is used as a reference, it is improbable that the auto-spectrum of reference signal will be zero. Note that we do see errors at very low frequencies using the scattering matrix approach in Figure 2.5. These are perhaps because $|P_1| \approx |P_2|$ since the wavelength is approximately two orders of magnitude larger than the microphone spacing.

To verify this explanation, the scattering matrix measurement was repeated with longer microphone spacings upstream of the muffler. Spacings of 7.6 cm and 54.3 cm were selected, and the complex wave amplitude A was selected as a

reference in each measurement. The results are shown in Figure 2.19. It can be seen that the transmission loss results are more accurate at lower frequencies if a larger microphone spacing is used. Figure 2.19 also shows that the calculation will fail at around 200 Hz for the 54.29 cm microphone spacing. These results agree well with the observations of Åbom (Åbom, 1991).

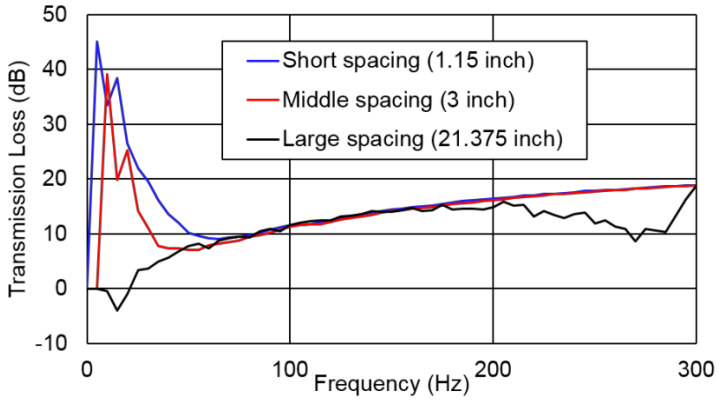

Figure 2.19 Measured transmission loss with different microphone spacing.

Compared to the transmission loss calculation based on the transfer matrix approach, the scattering matrix approach inherently avoids the problem induced by coincidence of microphone locations and standing wave nodes. However, the measurement results in this paper demonstrate that the transfer matrix approach will produce smooth curves if four microphones are used or if a downstream reference is used with two microphones.

2.5 Summary

Several aspects of using the two-load method to determine the transmission loss have been examined in this chapter.

The choice of reference has been investigated experimentally, numerically and analytically, for both the transfer and scattering matrix approaches. For measuring reactive mufflers with a reflective termination, transfer functions between upstream and downstream microphones will have errors, especially at those frequencies where a standing wave node coincides with the reference microphone. While such errors do not noticeably influence the smoothness of the transmission loss curves measured by the four-microphone transfer matrix approach, the two-microphone approach is sensitive to those errors. By examining the algorithm, it was shown that it is preferable that errors accumulate into the upstream wave amplitudes A and B rather than the downstream wave amplitudes C and D, and selecting a downstream microphone as a reference will improve the measurement quality. These conclusions should be qualified by noting that white noise was used for the source sans flow.

The less commonly used scattering matrix approach was also compared to the transfer matrix approach. It was shown that transmission loss curves were especially smooth except for erroneous result at very low frequencies. Results suggest that the scattering matrix approach avoids the issues caused by a microphone location coinciding with a standing wave node, but is more sensitive to errors at low frequency compared to the transfer matrix approach.

Chapter 3 THE MEASUREMENT OF SOURCE STRENGTH AND IMPEDANCE

The knowledge of strength and impedance of the sound source is necessary to predict the overall acoustic performance and radiated noise level of an exhaust or intake system. Different models have been suggested for measuring the source strength and impedance. In this work, the circuit analogy and wave decomposition models are compared and applied to acoustically characterize a diesel engine. To validate the accuracy of both models and measurement, the sound pressure in the exhaust is predicted from the measured source strength and impedance and compared with actual measurement. Good comparison between the prediction and measurement is observed for both models, especially at the first few harmonics of the firing frequency. The source strengths and impedances at different working conditions are measured and compared. In addition to actual measurement, the accuracy of an empirical equation to calculate source strength and impedance of a diesel engine is also checked. It is demonstrated that the empirical equation is only good for the first two harmonics of the firing frequency.

3.1 Introduction

The two commonly used metrics to evaluate the acoustic performance of an exhaust system are insertion and transmission loss (Munjal, 1987). Insertion loss is the attenuation of noise emission due to the muffler element installed in the specific system and is defined as the difference in sound pressure level with

and without the attenuating element in place. It is more straightforward and convenient to measure in experiments than transmission loss.

However, prediction of insertion loss during the design process is difficult because knowledge about source and termination impedances is required. While models for termination impedance are available (Levine and Schwinger, 1948, and Pierce, 1981), acoustic modeling of sources is more challenging. Attempts are sometimes made to predict insertion loss using a constant source impedance (Prasad and Crocker, 1983, Prasad, 1987, Harrison and Davies, 2010, Callow and Peat, 1988) or empirical models (Munjal, 1987, and Munjal and Doige, 1988), but accuracy is suspect. CFD simulations have also been used to determine the source impedance of engines (Fairbrother et al., 2005 and Munjal and Hota, 2010). Though very helpful in the early design stages, the CFD modeling and calculation are time consuming and questionable in accuracy. For convenience, empirical equations to calculate source strength are established for diesel engines based on time-domain numerical simulation and Fourier transform (Hota and Munjal, 1988).

Many research efforts have been dedicated towards experimentally measuring the source impedance of compressors, fans and internal combustion engines. In the current experiment, the source is assumed to be linear and time-invariant. Nonlinear source models are also available (Bodén, 1991, and Rämmal and Bodén, 2007) but are not considered here for simplicity. Such assumption proved acceptable judging from the results. Correspondingly, source properties are

assumed to remain constant regardless of changes in the downstream exhaust system.

Several approaches have been suggested to measure the source impedance. These include a) external source measurement (Prasad and Crocker, 1983), b) the circuit analogy model (Munjal, 1987, Prasad and Crocker, 1983, Prasad and Crocker, 1983, Prasad 1987) and c) a wave decomposition model (Bodén and Åbom, 1995, Rämmal and Åbom, 2007, and Liu and Herrin, 2008). External source measurement is analogous to impedance measurement of acoustic material samples (ASTM, 1998). The impedance at the source is measured by applying a secondary external source that is much higher in amplitude than the primary source. The main drawback is that it can be difficult to procure an external source that is much stronger than the source under test. This is especially true in the case of internal combustion engines because the source strength at low harmonics of the firing frequency is too intense for off-the-shelf sound sources. Another limitation of external source measurement is that the source strength, which is essential to predicting the radiated sound pressure level, cannot be determined. Since a diesel engine is the subject of this experiment, only indirect measurement approaches are considered.

For the circuit analogy model, source strength and particle velocity are analogous to a voltage source and current respectively. The source strength and impedance can be determined if the acoustic load is varied twice. A four-load approach (Prasad, 1987) has also been suggested that permits the measurement of source strength and impedance while avoiding the difficulty of

placing a sensor in the duct where it is exposed to high temperatures and flow. However, the source impedance measured using this approach has been shown to have a negative real part at many frequencies which is not realistic since the real part is the resistive component.

The wave decomposition approach is a similar two-load approach in which the sound pressure is measured at two positions in the pipe and then decomposed into incident and reflected wave amplitudes. The source strength and impedance are then determined from the wave amplitudes. One advantage is that the load impedance need not be determined a priori. This method was first used to determine source strength (Bodén and Åbom, 1995, and Rämmal and Åbom, 2007) but was also shown to be valid for source impedance characterization (Liu and Herrin, 2008). However, this approach had not been applied to a realistic source like a diesel engine.

In this chapter, the source properties of a six-cylinder four-stroke diesel engine are measured using both the circuit analogy and wave decomposition methods. Circuit analogy and wave decomposition models are first reviewed and compared. This is followed by a description of the test set-up. The source properties are determined from multiple acoustic loads and are then used to predict the sound pressure level in the exhaust duct for another load condition. The measurement results are then used to check the time-invariant and linearity assumptions using a linearity index (Rämmal and Bodén, 2007). The accuracy of prediction using source properties calculated by the empirical equation are also

checked. After the accuracy of the measurement methods are validated, the source properties at different RPMs and load conditions are compared.

3.2 Acoustic models and linearity index

3.2.1 Governing equations

Considering the dimensions of common exhaust pipes and that low frequencies are primarily of interest, plane wave propagation can be assumed. For plane waves in a tube with mean flow with visco-thermal loss included, the acoustic pressure can be expressed as

$$p_L = Ae^{-jk_d x} + Be^{jk_u x} \tag{3.1}$$

and the particle velocity distribution is expressed as

$$u_L = \frac{1}{z_c}\left(Ae^{-jk_d x} - Be^{jk_u x}\right) \tag{3.2}$$

where the downstream wavenumber k_d and upstream wavenumber k_u can be determined from temperature, fluid properties and flow rate and the characteristic impedance z_c includes the influence of visco-thermal losses (Mechel, 2002).

3.2.2 Circuit Analogy Model

The diesel engine and attached exhaust system are modeled as a circuit in which the sound source is modeled as a voltage source and a resistor in series (Figure 3.1) or a current source and a resistor in parallel. It is assumed that the particle velocity is continuous at the interface between the source and load, which is analogous to current continuity in a circuit. To use this model, the location of

interface between the sound source and acoustic load must first be defined. This is a somewhat arbitrary choice. The load pressure is the sound pressure at the interface location. From this model, it can be observed that

$$\frac{p_S}{Z_S + Z_L} = \frac{p_L}{Z_L} \tag{3.3}$$

where p_S is source strength and Z_S is normalized source impedance while P_L is load pressure and Z_L is normalized load impedance.

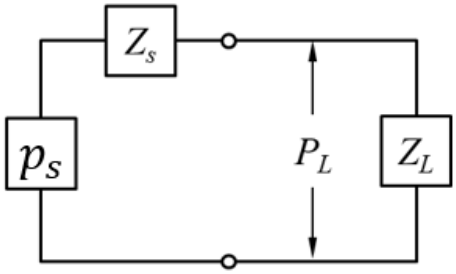

Figure 3.1 Schematic of circuit analogy model.

In the experiment, a sound pressure transducer can be inserted at the interface location to pick up the load pressure signal, while the load impedance Z_L can be predicted via the transfer matrix of the exhaust system and termination impedance (Munjal, 1987, Levine and Schwinger, 1948, and Pierce, 1981). p_L and Z_L can also be determined indirectly from measurement (Rämmal and Bodén, 2007). Using Equations 3.1 and 3.2, the downstream and upstream complex wave amplitudes can be solved from spectra of sound pressure at two locations in the exhaust pipe, then the sound pressure and impedance at the interface can be calculated. With the interface is set to be $x = 0$,

$$p_L = A + B \tag{3.4a}$$

and

$$Z_L = \frac{A + B}{A - B} \tag{3.4b}$$

As there are two unknowns (p_S and Z_S) in Equation 3.3, at least two equations should be obtained from two different working conditions (i.e., acoustic loads) of the system. Common ways of changing loads are changing the length of the exhaust pipe or adding side-branch resonators with different lengths. The set of equations can be represented as

$$\begin{bmatrix} Z_L^{(1)} & -p_L^{(1)} \\ Z_L^{(2)} & -p_L^{(2)} \end{bmatrix} \begin{Bmatrix} p_S \\ Z_S \end{Bmatrix} = \begin{Bmatrix} Z_L^{(1)} p_L^{(1)} \\ Z_L^{(2)} p_L^{(2)} \end{Bmatrix} \tag{3.5}$$

where the superscript indicate the respective load.

For higher accuracy, more than two loads can be used and the source properties can be solved using a least-square method (Bodén, 1988). The overdetermined set of equations can be expressed as

$$\begin{bmatrix} Z_L^{(1)} & -p_L^{(1)} \\ Z_L^{(2)} & -p_L^{(2)} \\ & \vdots \\ Z_L^{(\mathrm{n})} & -p_L^{(\mathrm{n})} \end{bmatrix} \begin{Bmatrix} p_S \\ Z_S \end{Bmatrix} = \begin{Bmatrix} Z_L^{(1)} p_L^{(1)} \\ Z_L^{(2)} p_L^{(2)} \\ \vdots \\ Z_L^{(\mathrm{n})} p_L^{(\mathrm{n})} \end{Bmatrix} \tag{3.6}$$

3.2.3 Wave Decomposition Model

In this model, the complex wave amplitude propagating downstream (A) in the exhaust system is divided into two parts: the direct outgoing wave from the

source (P_{S+}) and reflected wave from the source interface ($B \cdot R_S$). A can be expressed as

$$A = P_{S+} + B \cdot R_S \tag{3.7}$$

where R_S is the reflection coefficient of the source viewed from the load duct. The complex wave amplitudes A and B can be obtained from sound pressures measured at two locations through a wave decomposition calculation.

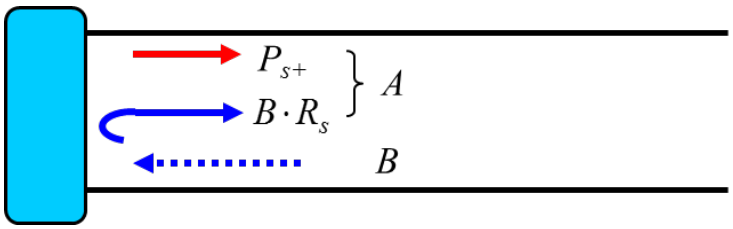

Figure 3.2 Schematic of wave decomposition model.

To solve P_{S+} and R_S in this model, at least two working conditions must be achieved. P_{S+} and R_S can be solved using:

$$\begin{bmatrix} 1 & B^{(1)} \\ 1 & B^{(2)} \end{bmatrix} \begin{Bmatrix} P_{S+} \\ R_S \end{Bmatrix} = \begin{Bmatrix} A^{(1)} \\ A^{(2)} \end{Bmatrix} \tag{3.8}$$

The source strength and source impedance can be further determined from P_{S+} and R_S via (Liu and Herrin, 2008):

$$Z_S = \frac{1 + R_S}{1 - R_S} \tag{3.9a}$$

and

$$p_S = \frac{2}{1 - R_S} P_{S+} \tag{3.9b}$$

Similarly, more than two loads can be used to improve the accuracy.

$$\begin{bmatrix} 1 & B^{(1)} \\ 1 & B^{(2)} \\ & \vdots \\ 1 & B^{(\mathrm{n})} \end{bmatrix} \begin{Bmatrix} P_{S+} \\ R_S \end{Bmatrix} = \begin{Bmatrix} A^{(1)} \\ A^{(2)} \\ \vdots \\ A^{(\mathrm{n})} \end{Bmatrix} \tag{3.10}$$

3.2.4 Linearity Index

It is often under doubt whether the source properties remain constant under different loads as assumed. To check if a linear model is sufficient, Rämmal and Bodén (Rämmal and Bodén, 2007) proposed a linearity index. If m different acoustic loads are used to solve for the source properties (See Equations 3.6 and 3.10), a matrix equation

$$\boldsymbol{A}\boldsymbol{x} = \boldsymbol{b} \tag{3.11}$$

will result, where $\boldsymbol{x}(2 \times 1)$ is a vector consisting of the source properties and $\boldsymbol{A}(m \times 2)$ and $\boldsymbol{b}(m \times 1)$ are a matrix and vector respectively containing measured information. For the over-determined problem where $m > 2$, the linearity index can be defined as

$$\gamma = \boldsymbol{b}^{+}\boldsymbol{A}\boldsymbol{A}^{+}\boldsymbol{b} \tag{3.12}$$

where A^{+} is the pseudo-inverse of A. The linearity index has a value in the interval $0 \leq \gamma \leq 1$, where $\gamma = 1$ indicates a perfectly linear source. To increase the sensitivity of the linearity index, each row of $\boldsymbol{A}$ should be normalized by the corresponding entry in $\boldsymbol{b}$, thus making the right hand side of the equation a unity vector.

3.2.5 Empirical Equation

In order to bypass measurement difficulties or time-domain numerical simulation, empirical equations have been developed from numerical simulations (Hota and Munjal, 1988). The source strengths and impedances of different engine capacities and numbers of cylinders were obtained at discrete RPMs and load conditions based on numerical simulation in the time domain before discrete Fourier transformation was applied. The source properties at other working conditions were then interpolated from these discrete working points.

The generalized equation for source strength level (SSL) is

$$SSL = A_e \times (n_h)^{B_e} \tag{3.13a}$$

where

$$A_e = 173.4 \times (1 - 0.0019AFR) \times (1 + 0.41NS - 0.257NS^2) \times (1 - 0.0023V) \times (1 - 0.021N_{cyl}) \tag{3.13b}$$

and

$$B_e = -0.093 \times (1 + 0.016AFR) \times (1 + 1.24NS - 1.22NS^2) \times (1 - 0.03V) \times (1 - 0.026N_{cyl}) \tag{3.13c}$$

AFR is air fuel ratio, NS is the RPM value normalized by 4000, V is engine capacity and N_{cyl} is number of cylinders.

Due to the difficulties of measurement and simulation, constant source impedance models have been proposed. Harrison and Davies (Harrison and

Davies, 2010) assumed the source had an infinite impedance. Prasad and Crocker (Prasad and Crocker, 1983) proposed the anechoic source approximation ($Z_S = 1$). Callow and Peat (Callow and Peat, 1988) came out with a likely more realistic approximation $Z_S = 0.707 - i * 0.707$ for exhaust system. In current work, values suggested by Callow and Peat are used.

3.3 Test setup

The measurement was made on a six-cylinder four-stroke diesel engine (Figures 3.3 and 3.4). Due to extreme working conditions, two water-cooled pressure transducers (model number: Kulite WCTV-25 and WCTV-100 PSIG type) are used instead of common engineering microphones. The distances between the turbocharger exhaust and microphones are 95.3 cm and 102.9 cm, respectively. The throttle opening percentage was recorded as a reference of the mechanical output load and the torque was measured by a dynamometer. The exhaust mass flow was calculated from the engine control module. Due to the short distance between the turbocharger exhaust and pressure transducers, the temperature gradient is neglected.

To obtain the spectra of sound pressures with phase information, a reference signal independent of the load must be used during measurement. In this measurement, the vibrational acceleration signal on the cylinder head was used as phase reference and measured using an accelerometer.

In actual measurement conditions, the pressure transducers are inevitably subject to turbulence noise. To reduce the noise, a time-domain average should be performed prior to the Fourier transform. If it can be assumed that the

turbulence noise is not coherent with the rotation of the engine cycle, the turbulence noise will be minimized after time-domain averaging over several cycles. In addition, the rotational speed of the diesel engine should be kept constant throughout the measurement, which is not practically feasible. If an ordinary FFT with fixed block size is used, there will be some impact due to leakage and spectral broadening (Bodén, 2014). To perform time-domain averaging, a tachometer signal is required to detect the start and end of each cycle. The time-history of pressure signals is interpolated and resampled at designated time intervals, so that a time-synchronous average can be performed. In this measurement, a tachometer sensor was installed on the flywheel so that it produces one pulse signal each rotation.

Figure 3.3 Exhaust pipe with pressure transducers installed.

Figure 3.4 Simple expansion chamber (Load 2) used in the measurement.

Multiple straight ducts of different length were used in the measurement. As the diameter of the turbocharger exhaust is 10.2 cm, the straight ducts used as loads likewise have diameters of 10.2 cm, except for Load 2, which an expansion chamber (SEC). The detailed specifications of the acoustic loads are recorded in Table 3.1. For each load, three rotational speeds (750 rpm, 1860 rpm and 2400 rpm) were tested and four mechanical load conditions (throttle opening 50%, 75%, 100% and no load) were applied.

Table 3.1 Acoustic loads used in the measuremnet

Load number	Description
1	Duct length: 9.4 m
2	Inlet duct length to SEC: 4.5 m Length of SEC: 76.2 cm Diameter of SEC: 25.4 cm Outlet duct length from SEC: 4.1 m
3	Duct length: 7.2 m
4	Duct length: 8.1 m
5	Duct length: 6.2 m

3.4 Results and discussion

3.4.1 2400 RPM and 100% Throttle Opening Working Condition

In this sub-section, only the result for the 2400 RPM and 100% throttle opening working condition is shown though the conclusions are transferable to other working conditions. The acoustic loads 1-4 were used to determine the source strength and impedance using a least squares approach and the sound pressure was predicted at the transducer location for the fifth acoustic load. The prediction is compared to actual measurement to validate the accuracy of the measurement and processing methods. With the source assumed to be located at the turbocharger exhaust port, the source strength and impedance were calculated

and are shown in Figures 3.5 through 3.7. The horizontal axis in the plots are the orders of harmonics and the resolution is half harmonic. Note that in Figure 3.7, the absolute dB values are not shown. Both the circuit analogy and the wave decomposition models were used to calculate the source properties, and the results are compared against the combination of source strength by empirical equations and constant source impedance.

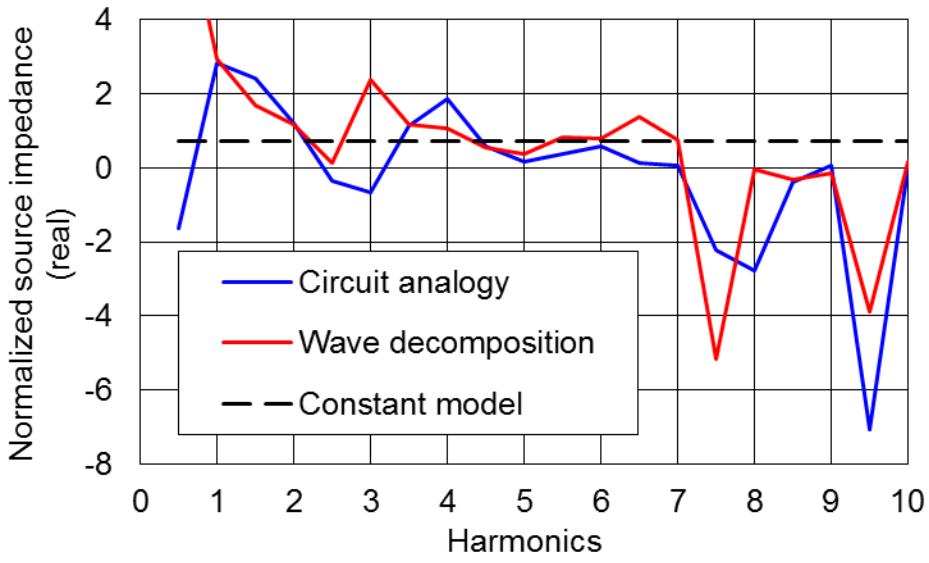

Figure 3.5 Real part of source impedance of tested diesel engine at 2400 RPM and 100% throttle opening working condition.

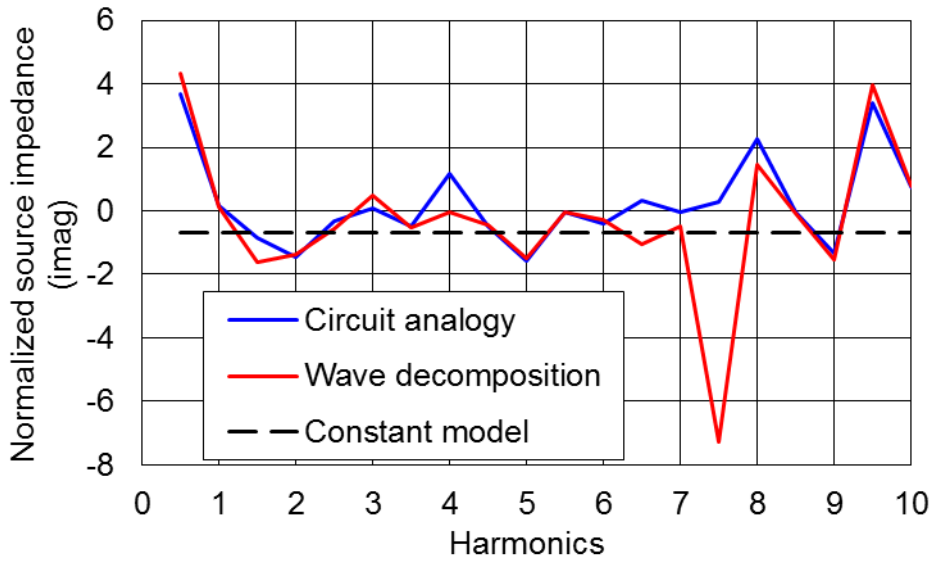

Figure 3.6 Imaginary part of source impedance of tested diesel engine at 2400 RPM and 100% throttle opening working condition.

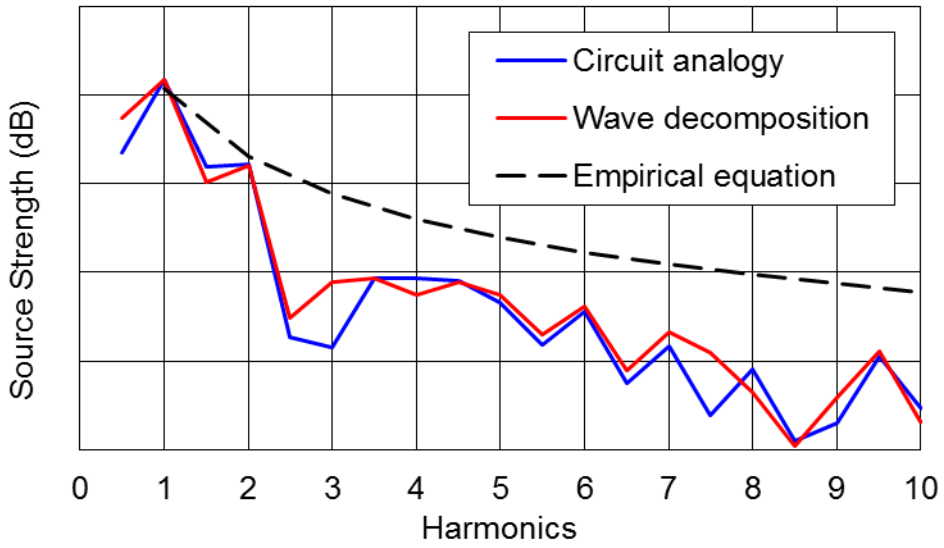

Figure 3.7 Source strength calculated for tested diesel engine at 2400 RPM and 100% throttle opening working condition

For a 6-cylinder 4-stroke diesel engine running at 2400 rpm, the firing frequency is 120 Hz. From the source strength calculated, it is observed that the highest peak appears at the firing frequency and lower peaks at its harmonics, which is

expected. The source strength calculated from the empirical equation is close to the measured source strength at the first two harmonics, but diverges for higher frequencies. For the calculated source impedance, it can be observed at some frequencies that the real part of the impedance is negative. This is common in the case of diesel engines. Possible explanations are provided, including the nonlinearity and time variance of the engine, flow generated noise (Ih and Peat, 2002) and the acoustic load selection (Liu and Herrin, 2009). It is also shown that the constant source impedance assumption of Callow and Peat (Callow and Peat, 1988) approximates the average source impedance for both the real and imaginary parts.

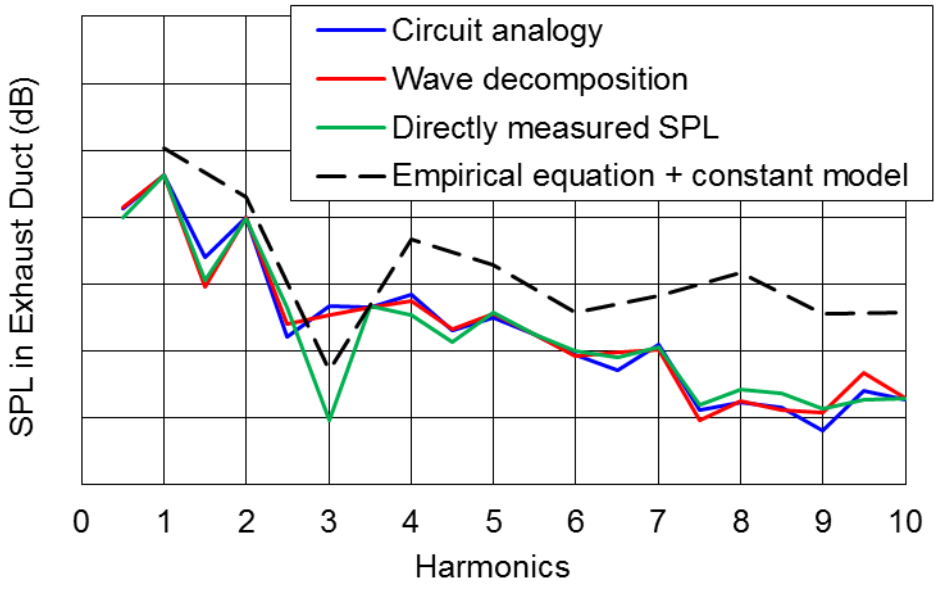

Figure 3.8 Predictions of SPL 95.3 cm downstream from turbo charger exhaust using both models and empirical equations compared against measurement.

The prediction of sound pressure level in the exhaust is compared to actual measurement in Figure 3.8. The sound pressure is predicted accurately for the first two harmonics and approximately for the higher harmonics if either the circuit

analogy or wave decomposition model is used. The overall trend is well predicted and the predicted SPLs for the first 10 harmonics are within the range of the actual measurement. Although the empirical equation predicts source strength very accurately for lower harmonics, there are significant deviations from measurement at higher frequencies. These deviations are a result of the constant source impedance used in calculation.

The linearity index was calculated from Equation 3.12 for both models and is shown in Figure 3.9. For the first two harmonics, the source is nearly linear and time-invariant. At higher harmonics, the linearity index is lower. Aside from the obvious reasons of low signal-noise ratio, the limited resolution for detecting the beginning of a revolution from the tachometer signal might also contribute (Bodén, 2014). It is also shown that the linearity index is very low at the 3x, 4x and 8x firing frequencies. At these frequencies, large discrepancies in the calculated real part of the source impedance and source strength are observed between the two models. The predicted SPL in the exhaust duct also deviates from measurement at these frequencies.

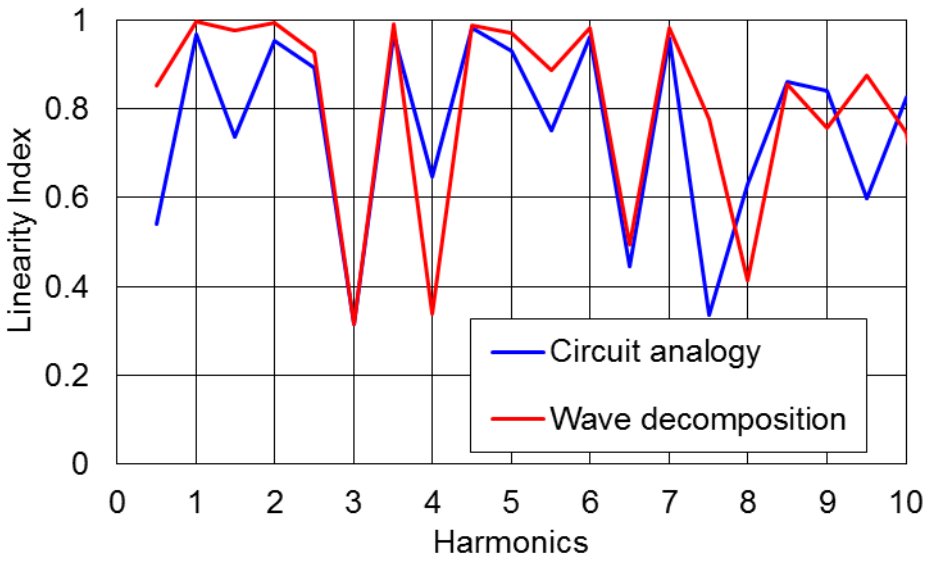

Figure 3.9 Linearity index calculated from both models.

3.4.2 The Effect of mechanical load on Source Properties

To investigate the effect of mechanical load on source properties, 4 different mechanical loads have been applied on the diesel engine successively. The processing method was identical to that used in the previous section. Both the circuit analogy and the wave decomposition models are used to calculate the source properties and similar results were obtained between two models. For simplicity, only the results obtained using the wave decomposition model are shown in this section. The RPMs of the 4 mechanical loads are kept at 2400. The mechanical load applied on the diesel engine was varied by controlling the dynamometer. The output torques for four mechanical loads were approximately 542 N·m, 371 N·m, 256 N·m and close to 0 N·m though small variations were observed between different acoustic loads. The throttle openings were varied from 100%, 75%, 50% and closed due to differing mechanical loads.

The calculated source impedance and source strength are shown in Figure 3.10 through 3.12. No obvious trend is observed for the source impedance results. Large differences are observed between the calculated impedances for different mechanical loads, but the constant estimation still provides decent approximation. The source strengths calculated for different mechanical loads show more similarity between mechanical loads, except for the load with closed throttle. For the first two harmonics of the firing frequency, the source strength decreases with decreasing throttle opening.

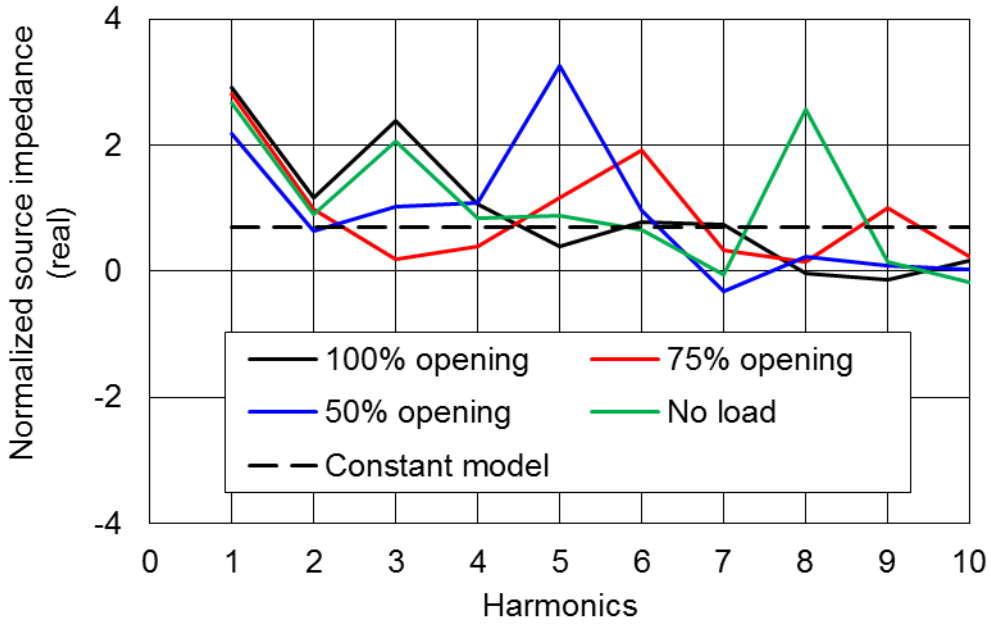

Figure 3.10 Real part of source impedances of tested diesel engine at 2400 RPM and different throttle openings.

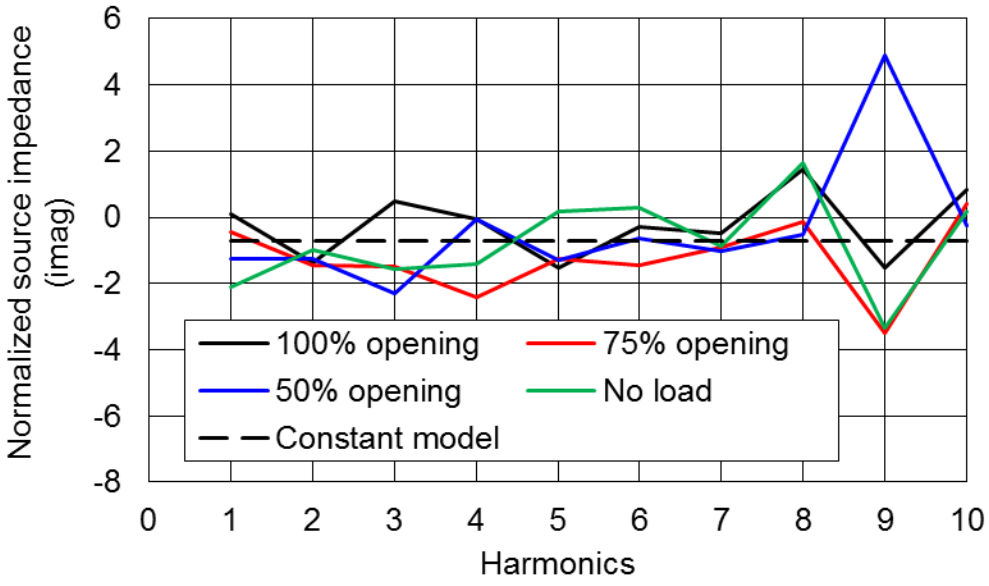

Figure 3.11 Imaginary part of source impedance of tested diesel engine at 2400 RPM and different throttle openings.

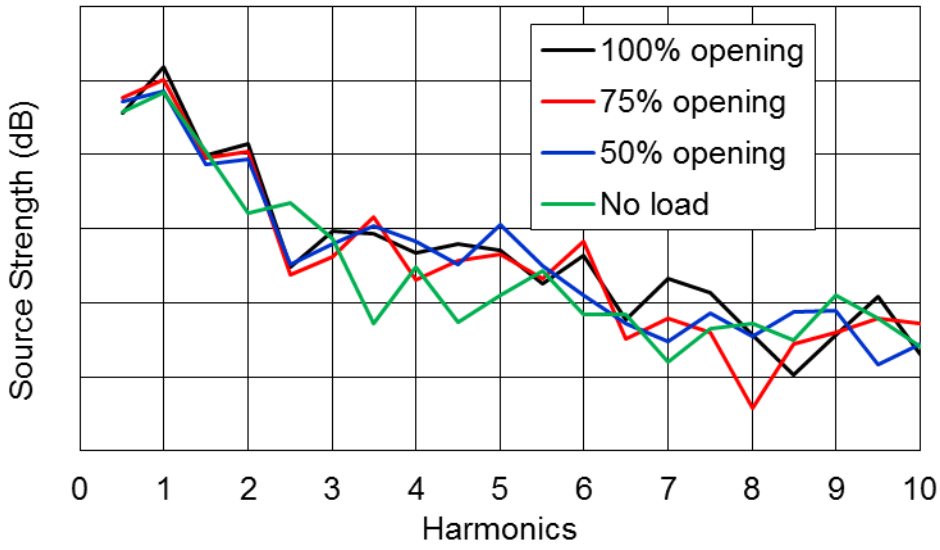

Figure 3.12 Source strength calculated for tested diesel engine at 2400 RPM and different throttle openings.

3.5 CONCLUSIONS

In this chapter, two linear time-invariant models (the circuit analogy model and the wave decomposition model) have been applied for source characterization on

a diesel engine. Practical aspects of the measurement including the test configuration and processing techniques are also discussed. It has been demonstrated that both two models can be used to calculate source strength and impedance that enable prediction of the sound pressure inside of the exhaust system with acceptable accuracy. The empirical equations developed from numerical simulation are also compared against measurement. It is also shown that for the exhaust system of diesel engines, the source strength at lower harmonics can be predicted with acceptable accuracy by using empirical equations, and the constant source impedance model $(0.707 - i * 0.707)$ is a decent approximation for normalized source impedance for diesel engine exhaust. The influence of mechanical load on source properties is also investigated. It is shown that source impedance is significantly influenced by mechanical load at all frequencies, but no obvious pattern is observed for that influence. From our results, the source strength is less dependent on mechanical load, and the influence is restricted to the first two harmonics of firing frequency. The source strength of the first two harmonics of firing frequencies will decrease with reduction of mechanical load.

The characterization of diesel engine is a difficult task with harsh testing environment. Same technique and processing methods are applied on compression drivers in later Chapters and proved to be satisfactorily accurate.

Chapter 4 THE ACOUSTICAL AND STRUCTRAL ANALYSIS OF EXHAUST SYSTEM USING THE MOEBIUS TRANSFORMATION

4.1 Introduction

With the real part plotted as x-axis coordinate and the imaginary part plotted as y-axis coordinate, both the impedance and the dynamic response can be viewed as points in the complex plane. Vincent (Vincent, 1973) and Done and Hughes (Done and Hughes, 1975) showed that the dynamic response will trace a circle in the complex plane if a spring is introduced between two positions in a translational mechanical system, and the stiffness is varied from minus to plus infinity. This principle was termed the Vincent circle by Done and Hughes. Tehrani et al. (Tehrani et al., 2006) observed that the Vincent circle resulted from a complex transformation, the Moebius transformation in particular, and that the principle held for any straight line modification of mechanical impedance between two positions. Hence, the response will trace a circle in the complex plane for a combination of mass, stiffness, or damping modifications so long as the impedance modification traces a straight line in the complex plane.

Following this work, Herrin et al. (Herrin et al., 2009) demonstrated the validity for acoustical impedance modifications. Herrin et al. (Herrin et al., 2009) showed how the principle could be applied to point impedance modifications for vibro-acoustic systems. Additionally, Herrin et al. (Herrin et al., 2009) applied the approach to muffler and silencer systems and showed that it was applicable to series impedances (i.e., source, termination and transfer impedances) as well as parallel impedances (i.e., side branch impedances).

In this chapter, the principle is applied to enclosures, mufflers and mounts. The approach is first illustrated for an enclosure by introducing a short duct to a partition placed inside of an enclosure, and the sound power radiated at the opening is minimized by selecting optimal diameter for the added duct. In addition, it is also observed that the length of an outlet duct extending from an enclosure opening can be tuned to minimize the radiated sound using the principle. It is demonstrated that the principle is particularly useful for determining the range of outlet duct lengths whereby certain noise level requirements are met.

In the case of mufflers, the principle was used to maximize the transmission loss. The term that is inside the logarithm of the transmission loss expression is termed a transmission loss vector and is shown to be in the form of the Moebius transformation if a short duct inside the muffler can be modeled as a transfer impedance. The approach was applied to a variation of the Herschel-Quincke tube (Stewart, 1928) where a short duct is connected between the inlet and outlet ducts of an expansion chamber. It is shown that the transmission loss of an expansion chamber can be greatly improved by in excess of 20 dB at certain frequencies. This improvement was validated experimentally and by analysis.

In a similar manner, the principle is applied to structural mount insertion loss. The equations are nearly identical to those for mufflers, and it is shown that the mount insertion loss can be augmented at target frequencies by adding mass to change the impedance at the foundation side.

4.2 Moebius Transformation

The Moebius transformation can be expressed as

$$Z = \frac{\alpha z + \beta}{\gamma z + \delta} \tag{4.1}$$

where α, β, γ and δ are complex constants such that $\alpha\delta - \beta\gamma \neq 0$. A straight line or circular modification of z will result in a straight line or circle for Z when plotted in the complex plane. The Moebius transformation can be decomposed into the following sequences of simple transformations (Needham, 1998).

$$z \mapsto z + \frac{\delta}{\gamma} \tag{4.2a}$$

$$z \mapsto \left(\frac{1}{z}\right) \tag{4.2b}$$

$$z \mapsto \frac{\beta\gamma - \alpha\delta}{\gamma^2} z \tag{4.2c}$$

$$z \mapsto z + \frac{\alpha}{\gamma} \tag{4.2d}$$

The first and last steps of the transformation are translations. The second is a complex inversion and the third is a dilation and rotation. Of the four transformations, the second is most important to understanding the transformation since a complex inversion creates generalized circles. A generalized circle is either a circle or a straight line, which can be thought of as a circle with an infinite radius. The Moebius transformation will not necessarily map lines to circles. It may also map lines to lines or circles to circles.

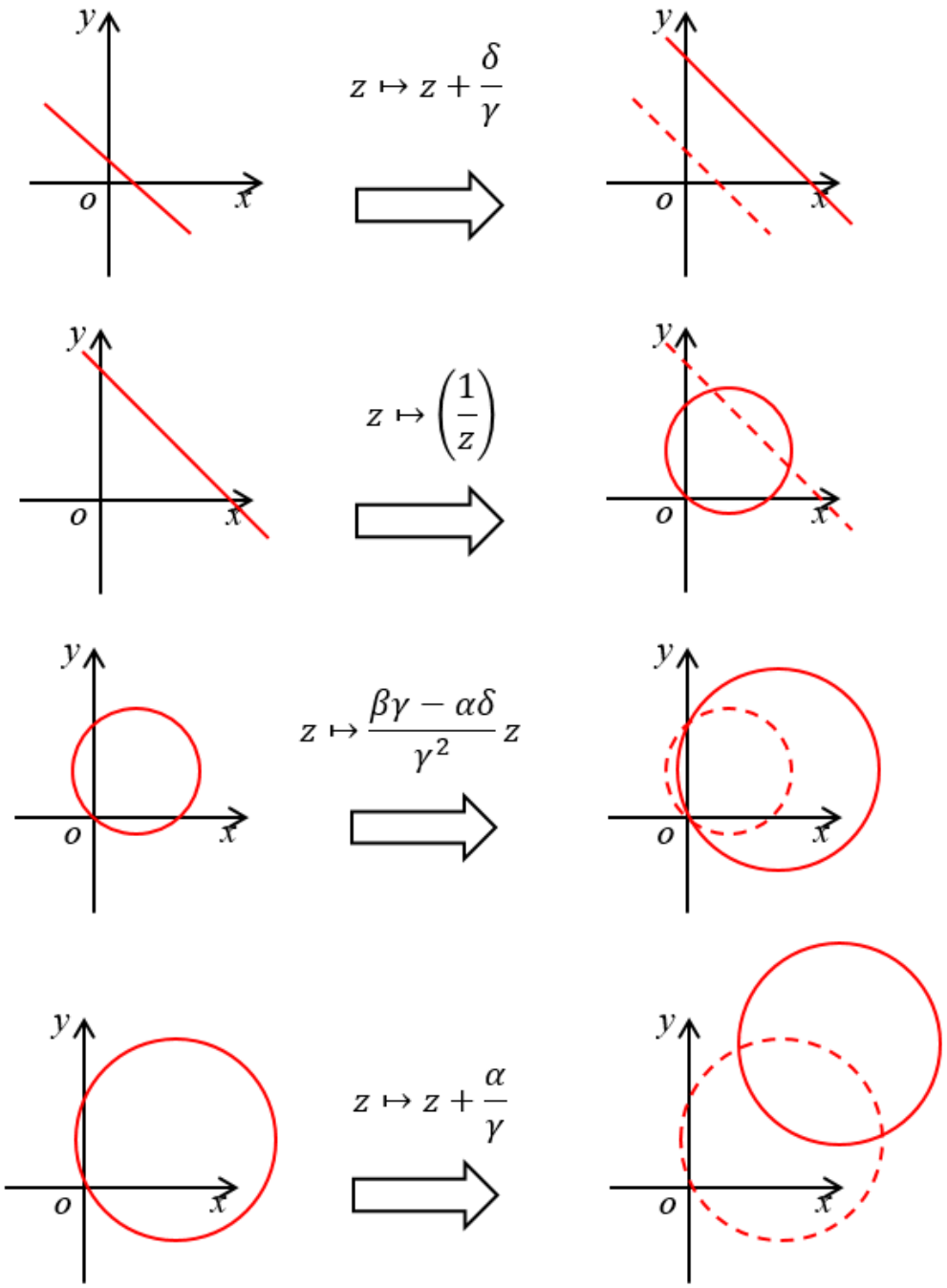

Figure 4.1 Steps of the Moebius transformation for a straight line.

If the original line z and the constants α, β, γ and δ are known, the radius and center location of the mapped circle can be directly calculated. Assuming the function for the original line is:

$$y = fx + g \tag{4.3}$$

where $z = x + iy$. After transformation, the mapped circle can be expressed as:

$$(X - X_C)^2 + (Y - Y_C)^2 = {R_Z}^2 \tag{4.4}$$

where X_C and Y_C are the coordinates of the center and R_Z is the radius of the mapped circle. The center and radius can be calculated via

$$X_C = \frac{\mathrm{Re}\left(\frac{\alpha\delta - \beta\gamma}{\gamma^2}\right) \cdot f - \mathrm{Im}\left(\frac{\alpha\delta - \beta\gamma}{\gamma^2}\right)}{2\left[g + \mathrm{Im}\left(\frac{\delta}{\gamma}\right) - \mathrm{Re}\left(\frac{\delta}{\gamma}\right) \cdot f\right]} + \mathrm{Re}\left(\frac{\alpha}{\gamma}\right) \tag{4.5a}$$

$$Y_C = \frac{\mathrm{Im}\left(\frac{\alpha\delta - \beta\gamma}{\gamma^2}\right) \cdot f + \mathrm{Re}\left(\frac{\alpha\delta - \beta\gamma}{\gamma^2}\right)}{2\left[g + \mathrm{Im}\left(\frac{\delta}{\gamma}\right) - \mathrm{Re}\left(\frac{\delta}{\gamma}\right) \cdot f\right]} + \mathrm{Im}\left(\frac{\alpha}{\gamma}\right) \tag{4.5b}$$

and

$$R_Z = \frac{\sqrt{f^2 + 1} \cdot |\alpha\delta - \beta\gamma|}{2\left|\left[g + \mathrm{Im}\left(\frac{\delta}{\gamma}\right) - \mathrm{Re}\left(\frac{\delta}{\gamma}\right) \cdot f\right]\gamma^2\right|} \tag{4.5c}$$

For optimization purpose, the points that are furthest from and nearest to the origin are often of interest. These two points can be calculated by

$$Z = X_C + iY_C \pm \frac{X_C + iY_C}{\sqrt{X_C^2 + Y_C^2}} \cdot R_Z \tag{4.6}$$

where "+" and "−" give the point furthest and nearest respectively. After the desired Z point is solved, the corresponding z point can be calculated using the inverse Moebius transformation

$$z = \frac{\delta Z - \beta}{-\gamma Z + \alpha} \tag{4.7}$$

Hence, the z which maximizes or minimizes the modulus of Z is obtained.

As an aside, it is well known that the response will trace a circle in the complex plane near a mode as the frequency is modified. Herrin et al. (Herrin et al., 2009) noted that the response is indeed in the form of the Moebius transformation as the frequency is varied close to a modal frequency. In the current effort, the response is plotted as the impedance between two positions is varied.

4.3 Development of the Generalized Vincent Circle

The development that follows is generalized from that shown by Done and Hughes (Done and Hughes, 1975). Figure 4.2 shows a schematic of a structural/acoustic system with a modification of mechanical/acoustical impedance z between points r and s. The system is excited at location p and the response will be computed at location q.

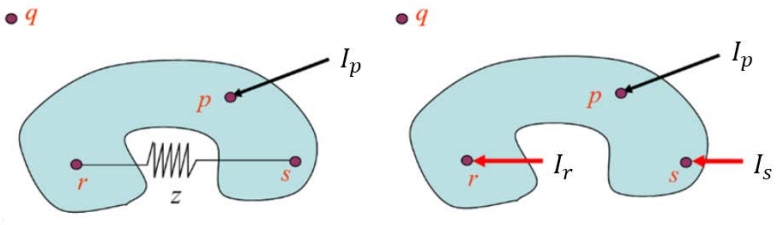

Figure 4.2 Schematic illustrating the development of the Vincent Circle for structural-acoustic applications.

Assume that the mechanical/acoustical impedance is replaced by two inputs I_r and I_s. In that case, the responses at locations q, r and s can be written in terms of the applied inputs I_p, I_r, and I_s. Thus,

$$R_q = H_{qp}I_p + H_{qr}I_r + H_{qs}I_s \tag{4.8a}$$

$$R_r = H_{rp}I_p + H_{rr}I_r + H_{rs}I_s \tag{4.8b}$$

$$R_s = H_{sp}I_p + H_{sr}I_r + H_{ss}I_s \tag{4.8c}$$

where H_{ij} are the unmodified transfer functions between the vibration or acoustic responses at point i and the inputs at point j. The inputs I_r and I_s can be expressed in terms of the impedance z and the responses R_r and R_s as

$$I_r = z(R_s - R_r) = -I_s \tag{4.9}$$

and then substituted into Equation 4.8. Solving for the modified transfer function (R_q/I_p), the following expression is obtained

$$\frac{R_q}{I_p} = \frac{z\left[(H_{rr} + H_{ss} - H_{rs} - H_{sr})H_{qp} + \left(H_{sp} - H_{rp}\right)\left(H_{qr} - H_{qs}\right)\right] + H_{qp}}{z(H_{rr} + H_{ss} - H_{rs} - H_{sr}) + 1} \tag{4.10}$$

Tehrani et al. (Tehrani et al., 2006) observed that Equation 4.10 is a particular case of the Moebius transformation, where α, β, γ and δ are defined as

$$\alpha = (H_{rr} + H_{ss} - H_{rs} - H_{sr})H_{qp} + \left(H_{sp} - H_{rp}\right)\left(H_{qr} - H_{qs}\right) \tag{4.11a}$$

$$\beta = H_{qp} \tag{4.11b}$$

$$\gamma = H_{rr} + H_{ss} - H_{rs} - H_{sr} \tag{4.11c}$$

$$\delta = 1 \tag{4.11d}$$

When the modification of z traces a known straight line in the complex plane, the center and radius of the mapped circle of the response can be calculated. The optimal value of R_q/I_p in Equation 4.10, which corresponds to the possible maximum suppression of the response, should be the point on the circle closest to the origin of the complex plane. Hence, the approach is ideal for selecting an optimal impedance minimizing the vibrational or acoustic response for a passive control mechanism at a particular frequency.

The Moebius transformation can straightforwardly be extended to cases having multiple excitations in the following manner. Assuming N inputs are applied on the structure, the partial response at point q due to input n can be expressed as

$$R_q^{(n)} = \frac{z\left[(H_{rr} + H_{ss} - H_{rs} - H_{sr})H_{qn} + (H_{sn} - H_{rn})\left(H_{qr} - H_{qs}\right)\right]I_n + H_{qn}I_n}{z(H_{rr} + H_{ss} - H_{rs} - H_{sr}) + 1} \tag{4.12}$$

where I_n is an input at point $n(n = 1,2, \dots, N)$. The complete response R_q is the summation of the partial responses which can be expressed as

$$\begin{aligned} R_q &= \sum_{n=1}^{N} R_q^{(n)} \\ &= \frac{z\sum_{n=1}^{N}\left\{\left[(H_{rr} + H_{ss} - H_{rs} - H_{sr})H_{qn} + (H_{sn} - H_{rn})\left(H_{qr} - H_{qs}\right)\right]I_n\right\} + \sum_{n=1}^{N} H_{qn}I_n}{z(H_{rr} + H_{ss} - H_{rs} - H_{sr}) + 1} \end{aligned} \tag{4.13}$$

Observe that Equations 4.13 can be written in the form of the Moebius transformation with

$$\alpha = \sum_{n=1}^{N} \{[(H_{rr} + H_{ss} - H_{rs} - H_{sr})H_{qn} + (H_{sn} - H_{rn})(H_{qr} - H_{qs})]I_n\} \tag{4.14a}$$

$$\beta = \sum_{n=1}^{N} H_{qn} I_n \tag{4.14b}$$

$$\gamma = H_{rr} + H_{ss} - H_{rs} - H_{sr} \tag{4.14c}$$

$$\delta = 1 \tag{4.14d}$$

Though Equation 4.13 and 4.14 require a large number of transfer functions to determine α, β, γ and δ, transfer functions can be determined quickly using simulation. More importantly, it can be observed that the ratios between complex constants α, β, γ and δ can be solved by making three known modifications z to a system and measuring each resultant response Z (i.e., the response circle can be determined if three points on the circle are known). A three unknown linear system of equations can be solved so that Equation 4.1 can be used directly in the place of Equation 4.13.

4.4 Application to Vibro-Acoustical Optimization

The Moebius transformation is first applied to acoustic impedance modifications between two locations. The acoustic impedance modification could be either a series or parallel impedance. In practice, a parallel impedance would correspond to a resonator or side branch. A series impedance is less trivial and of greater interest in this discussion. For example, a short duct may be approximated as a

transfer impedance. The transfer matrix for a duct is expressed as (Munjal, 1987)

$$\begin{Bmatrix} p_1 \\ u_1 \end{Bmatrix} = \begin{bmatrix} \cos(kl) & \frac{i\rho_0 c}{s}\sin(kl) \\ \frac{is}{\rho_0 c}\sin(kl) & \cos(kl) \end{bmatrix} \begin{Bmatrix} p_2 \\ u_2 \end{Bmatrix} \tag{4.15}$$

where s is the cross-sectional area of the duct, l is the length, k is the wavenumber, and ρ_0 and c are the density of the fluid and speed of sound respectively. For convenience, note that volume velocity is used in Equation 4.15. If l is assumed to be small,

$$\begin{Bmatrix} p_1 \\ u_1 \end{Bmatrix} = \begin{bmatrix} 1 & \frac{i\rho_0 c}{s}kl \\ 0 & 1 \end{bmatrix} \begin{Bmatrix} p_2 \\ u_2 \end{Bmatrix} \tag{4.16}$$

This approximation is accurate to within a 10% tolerance if $kl < 0.45$. In case of room temperature and no flow, the assumption is valid at low frequencies (<200Hz) for a duct with length of 0.1 m or less. By examining the form of the simplified transfer matrix in Equation 4.16, it is evident that the small duct can be modeled as a transfer or series impedance which depends on the ratio between the length and cross-sectional area and can be expressed as

$$z \approx \frac{i\rho_0 c}{s}kl \tag{4.17}$$

It follows that z will trace a straight line on the imaginary axis (i.e., a vertical straight line) for a modification to either the length or cross-sectional area. For a

vertical straight line modification (i.e., $f = \infty$ in Equation 4.3), Equation 4.5 can be simplified as

$$X_C = \frac{\mathrm{Re}\left(\frac{\beta\gamma - \alpha\delta}{\gamma^2}\right)}{2\mathrm{Re}\left(\frac{\delta}{\gamma}\right)} + \mathrm{Re}\left(\frac{\alpha}{\gamma}\right) \tag{4.18a}$$

$$Y_C = \frac{\mathrm{Im}\left(\frac{\beta\gamma - \alpha\delta}{\gamma^2}\right)}{2\mathrm{Re}\left(\frac{\delta}{\gamma}\right)} + \mathrm{Im}\left(\frac{\alpha}{\gamma}\right) \tag{4.18b}$$

and

$$R_Z = \left| \frac{\beta\gamma - \alpha\delta}{2\gamma^2 \cdot \mathrm{Re}\left(\frac{\delta}{\gamma}\right)} \right| \tag{4.18c}$$

The design which minimizes or maximizes the response can be determined using Equations 4.6 and 4.7.

4.4.1 Application to Enclosures

The concept is demonstrated using a short duct in an enclosure. As shown in Figure 4.3, a panel is located so that there is no straight line of sight between the acoustic monopole source and the outlet. An unflanged termination impedance Z_{rad} (Levine and Schwinger, 1948 and Pierce, 1981) is assumed at the outlet. The radiated sound power (P_{rad}) can be calculated as

$$P_{rad} = \frac{1}{2}\mathrm{Re}(p_3 v_3^*) \cdot S = \frac{|p_3|^2 S}{2\mathrm{Re}(Z_{rad})} \tag{4.19}$$

where v_3^* is the conjugate of particle velocity and S is the cross-sectional area of the outlet. The insertion loss of the enclosure is defined as the difference between the sound power of the source (P_{inp}) and that radiated (P_{rad}) from the opening of the enclosure in dB which can be expressed as

$$IL = 10log_{10}\left(\frac{P_{inp}}{P_{rad}}\right) = 10log_{10}\left(\frac{2P_{inp}\cdot \mathrm{Re}(Z_{rad})}{S}\right) - 20log_{10}|p_3| \qquad (4.20)$$

For maximum sound attenuation, the modulus of radiated sound pressure (p_3) should be minimized.

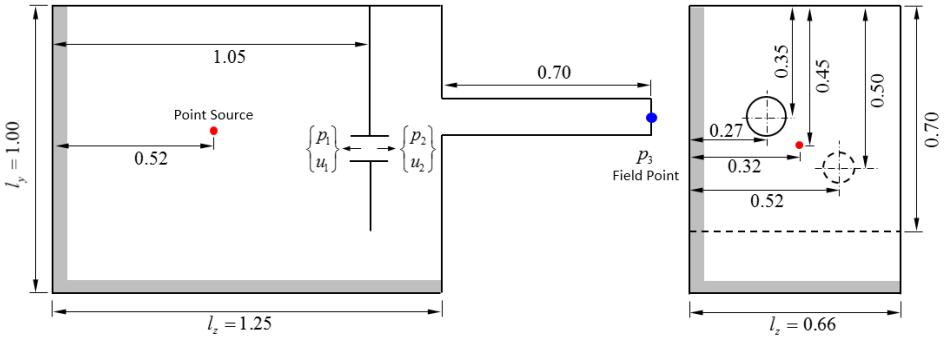

Figure 4.3 Enclosure model layout (Unit: m).

A small bypass duct was added at a random location on the panel as shown in Figure 4.3, and plane wave propagation was assumed in the bypass and outlet ducts since their diameters were small compared to an acoustic wavelength. Equations 4.10 and 4.11 were used to determine the ratio p_3/Q_{inp} where Q_{inp} is the volume velocity of the source. Location 3 corresponds to the response q and positions 1 and 2 correspond to r and s respectively. The transfer functions (H_{ij}) that relate sound pressure and volume velocity were determined using boundary element simulation in LMS Virtual.Lab (LMS, 2011). The element

length for most elements was approximately 50 millimeters, resulting in 3583 elements and 3590 nodes. 2.5 cm thick foam with a flow-resistivity of 15,000 rayls/m was assumed on three adjacent faces inside of the enclosure to attenuate acoustic resonances as shown in grey shading in Figure 4.3. The surface impedance of the foam was found using the model of Wu (Wu, 1988).

The diameter of the bypass duct was modified while length was fixed. It was assumed that the transfer functions will not vary with the cross-sectional area of the bypass duct. Since p_3/Q_{inp} is in the form of the Moebius transformation, the sound pressure will trace a circle in the complex plane as the diameter is varied. Modifications were made to improve the insertion loss at the first resonant frequency ($kl_Z = 3.7$ in Figure 4.5). This analysis assumes that the source amplitude peak coincides with that particular frequency. With all the transformation constants known, sound pressure at the outlet can be computed analytically using Equation 4.1 and plotted for the bypass duct diameter varying from 0.002 m to 0.100 m with a step size of 0.002 m (Figure 4.4).

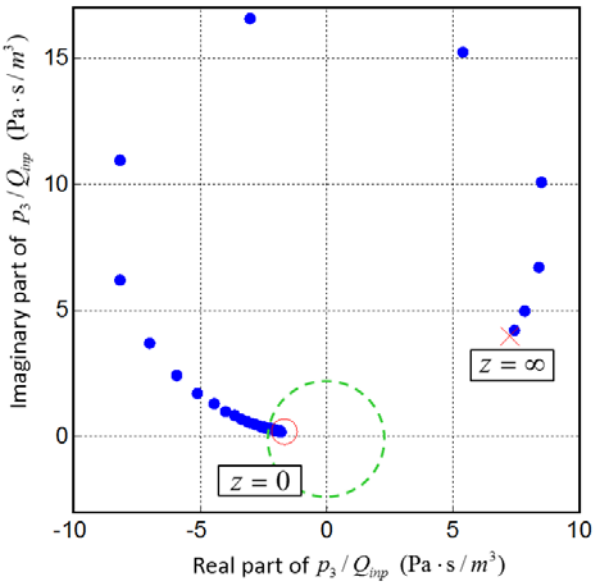

Figure 4.4 p_3 with bypass ducts of different diameters (Unit: mm).

If there is no bypass duct on the panel, this case can be considered as a bypass duct with diameter of zero. In that case, the transfer impedance of the bypass duct is infinite (Equation 4.17) and the transformed complex value is determined by the ratio of α and γ.

$$\lim_{|z|\to\infty} Z = \lim_{|z|\to\infty} \left(\frac{\alpha z + \beta}{\gamma z + \delta}\right) = \frac{\alpha}{\gamma} \tag{4.21}$$

On the other hand, when the diameter is relatively large (but still small compared to the acoustic wavelength at that particular frequency), the transfer impedance is very small and the transformed value is determined by the ratio of β and δ.

$$\lim_{|z|\to 0} Z = \lim_{|z|\to 0} \left(\frac{\alpha z + \beta}{\gamma z + \delta}\right) = \frac{\beta}{\delta} \tag{4.22}$$

The values of p_3/Q_{inp} in these two extreme situations are indicated by the cross and circle in Figure 4.4 respectively. At these two ends of the arc, the density of

the dots is higher, suggesting that the outlet pressure converges to the limits α/γ and β/δ.

For this case, the objective was to achieve a specified insertion loss performance. In that case, the modulus of p_3/Q_{inp} needs to be smaller than a set allowable value. Viewed in the complex plane, the allowable value is a circle centered at the origin, and the circle of p_3/Q_{inp}will intersect the allowable circle at two points if the following conditions are met

$$R_z + R_A > \sqrt{X_c^2 + Y_c^2} \text{ and } |R_z - R_A| < \sqrt{X_c^2 + Y_c^2} \tag{4.23}$$

where R_A is the radius of the allowable circle and X_C, Y_C and R_Z are center coordinates and radius of the mapped circle. The intersection points are given as

$$\partial = \frac{1}{4}\sqrt{-[X_c^2 + Y_c^2 - (R_z + R_A)^2][X_c^2 + Y_c^2 - (R_z - R_A)^2]} \tag{4.24a}$$

$$x_{1,2} = \frac{X_C}{2} - \frac{X_C(R_Z^2 - R_A^2)}{2(X_c^2 + Y_c^2)} \pm 2\frac{Y_C}{X_c^2 + Y_c^2}\partial \tag{4.24b}$$

$$y_{1,2} = \frac{Y_C}{2} - \frac{Y_C(R_Z^2 - R_A^2)}{2(X_c^2 + Y_c^2)} \mp 2\frac{X_C}{X_c^2 + Y_c^2}\partial \tag{4.24c}$$

The arc between the two intersection points inside of the allowable circle brackets the designs that satisfy the insertion loss requirement.

At the first resonant frequency, the original insertion loss without the bypass duct is -16 dB. The targeted insertion loss value after modification is set to 0 dB, resulting in an allowable circle with radius of 2.3 Pa·s/m^3 in complex plane, which is shown in the dashed line. There are two intersection points between the

mapped circle and allowable circle, but one of them is not feasible (negative diameter value). Another intersection point corresponds to a diameter of 0.050 m. With this diameter, the modified geometry was constructed and the insertion loss calculated and compared with that of the original enclosure. Both the original and modified enclosures were analyzed using boundary element analysis (Figure 4.5). The insertion loss at $kl_Z = 3.7$ is increased by 15 dB and is close to the targeted improvement.

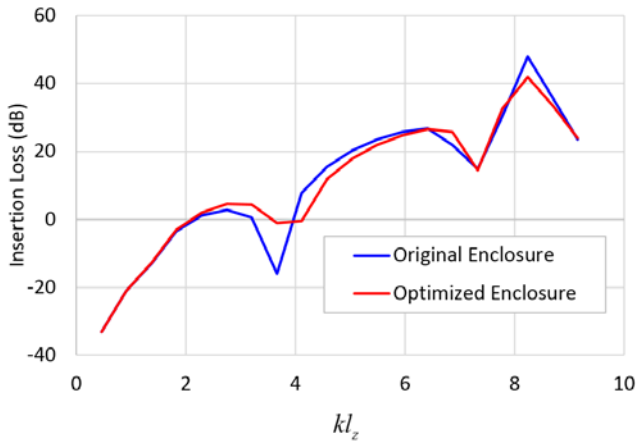

Figure 4.5 Comparison of insertion loss between original and optimized enclosure (l_z: longest dimension of enclosure).

A second test case examined the effect of changing the outlet duct length on a simple box enclosure. The box enclosure evaluated is shown in Figure 4.7. For the analysis that follows, the outlet duct is assumed to have a short length l and cross-sectional area s so that the outlet pipe can be modeled as a transfer impedance. Due to the short length of attached duct l, the termination situation can be considered as flanged and a flanged termination impedance Z_{rad} (Levine and Schwinger, 1948 and Pierce, 1981) is applied at the outlet. Sound pressure and volume velocity at different locations are defined as shown.

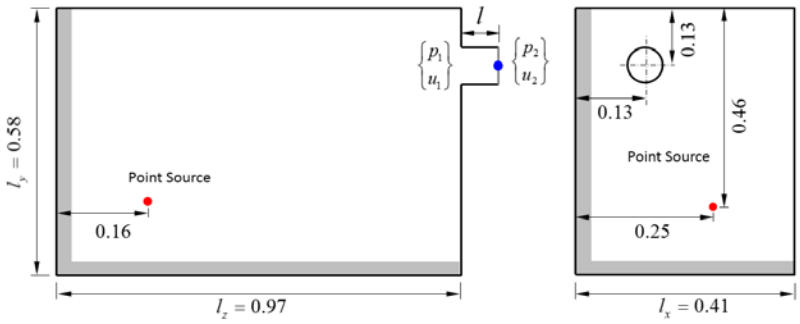

Figure 4.6 Enclosure model layout (Unit: m).

The insertion loss can be defined and calculated in the same way as Equation 4.20. Comparing the system to that shown in Figure 4.2 and described by Equation 4.8, response q and point r are coincident and correspond to Location 2 in Figure 4.6. Location 1 corresponds to point s.

The transfer functions (H_{ij}) were determined using boundary element simulation in LMS Virtual.Lab (LMS, 2011). The element length for most elements was approximately 30 millimeters, resulting in 4103 elements and 4100 nodes. A 2.5 cm thick foam with flow-resistivity of 15,000 rayls/m was assumed on three adjacent faces inside of the enclosure. The empirical model by Wu (Wu, 1988) was again used to characterize the surface impedance.

After all the transfer functions are determined, the transfer function p_2/Q_{inp} can be calculated and the center and radius are obtained using Equation 4.11 and 4.18. Since the enclosure performance at the resonant frequency of the enclosure is often problematic, the second resonance ($kl_z = 3$ in Figure 8) is set as the target frequency. As anticipated, p_3/Q_{inp} will trace a circle in the complex plane as the length is varied provided that it is small compared to an acoustic wavelength ($kl \ll 1$).

For this case, the objective was to achieve a specified insertion loss performance at the second resonance. Without an outlet pipe, the insertion loss at this frequency is -32.1 dB. If an insertion loss of -15 dB is targeted, the radius of the allowable circle will be 30 Pa·s/m^3 in the complex plane. Using Equation 4.7 and 4.24, lengths of outlet pipe that provide -15 dB insertion loss are -0.07 m and 0.05 m. The first value is not feasible.

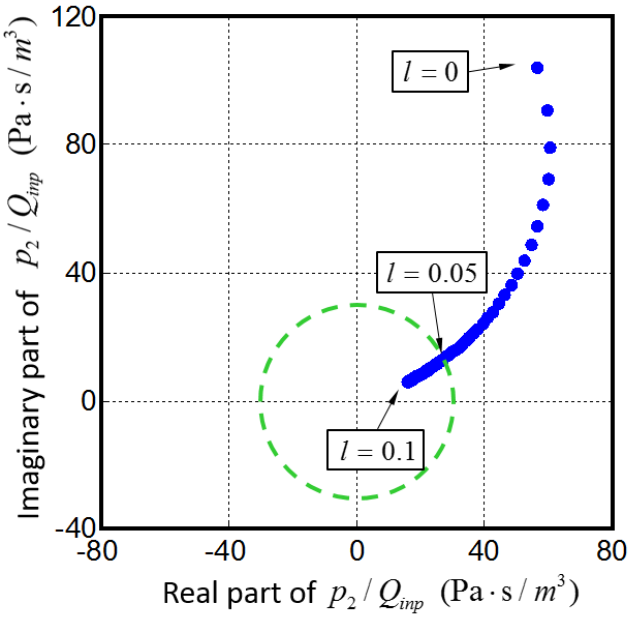

Figure 4.7 Sound pressure with different outlet length (Unit: m).

In Figure 4.7, the outlet pressure at the target frequency is plotted with outlet length varying from 0 to 0.1 m with step of 0.002 m using Equation 4.1. The allowable response circle is shown as a dashed line. As the length of the outlet increases, the points enter the circle at $l = 0.05$ m. There is a higher density of responses as l approaches 0.1 m, suggesting that the outlet pressure converges to a constant value. The insertion loss curves for two cases with different outlet lengths are determined from boundary element simulation and plotted in Figure

4.8. At the target frequency, the insertion loss is approximately the targeted value.

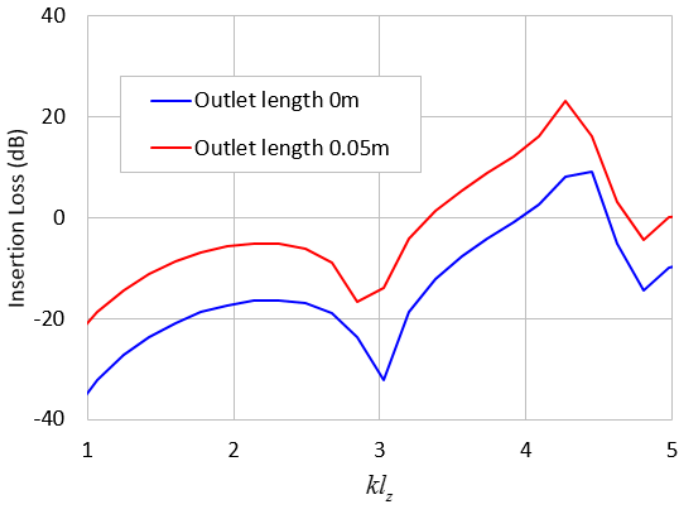

Figure 4.8 Insertion loss comparison with different outlet length (l_z: longest dimension of enclosure).

4.4.2 Application to Mufflers

The Herschel-Quincke tube has been investigated by a number of researchers (Stewart, 1928, Selamet et al., 1994, Selamet and Easwaran, 1997, and Karlsson et al., 2008). The attenuation mechanism is cancellation at the intersection of the two branches. In industry, it has been observed that adding short bypass ducts or intentional leaks which are variations of the Herschel-Quincke tube into a muffler or silencer can sometimes prove beneficial to the performance. For example, Karlsson and Glav (Karlsson and Glav, 2007) improved the performance of an expansion chamber using a variation of the Herschel-Quincke tube. It will be shown that the Moebius transformation is beneficial for optimizing the dimensions of short bypass ducts.

A silencer was designed and modeled using the transfer matrices. Then, an impedance modification between the inlet and outlet is introduced by adding a bypass duct similar to the Herschel-Quincke tube. When the bypass duct is short, the selection of length (l) and cross-sectional area (s) is equivalent to finding an optimal impedance, which can be found using the approach described previously. The Herschel-Quincke tube considered here is different than the typical Herschel-Quincke tube since it is attached in parallel to an expansion chamber similar to Karlsson and Glav's work (Karlsson and Glav, 2007) rather than a straight duct. The muffler with and without a bypass duct is shown in Figure 4.9. If the muffler is constructed with the inlet and outlet ports parallel to one another, the bypass duct can be very short.

Figure 4.9 The experimental muffler with and without bypass duct.

With the parameters of the transfer matrix of the muffler (A_T, B_T, C_T and D_T) known, the transmission loss can then be calculated as (Munjal, 1987)

$$TL = 20log\left|\frac{1}{2}\left(A_T + \frac{S}{\rho_0 c}B_T + \frac{\rho_0 c}{S}C_T + D_T\right)\right| \quad (4.25)$$

if both the inlet and outlet ducts have the same cross-sectional area S. To take advantage of the Moebius transformation, a complex vector of the transmission loss (S_{TL}) can be defined as

$$S_{TL} = A_T + \frac{S}{\rho_0 c} B_T + \frac{\rho_0 c}{S} C_T + D_T \tag{4.26}$$

which can be expressed in the form of the Moebius transformation as

$$S_{TL} = \frac{\alpha z + \beta}{z + \delta} \tag{4.27}$$

where

$$z = \frac{i\rho_0 c}{s} kl \tag{4.28a}$$

$$\alpha = A_1 + \frac{S}{\rho_0 c} B_1 + \frac{\rho_0 c}{S} C_1 + D_1 \tag{4.28b}$$

$$\beta = 2B_1 + \frac{\rho_0 c}{S} (A_1 + D_1 - 2) \tag{4.28c}$$

$$\delta = B_1 \tag{4.28d}$$

where A_1, B_1, C_1 and D_1 are the transfer matrix parameters for the mainstream element, which is parallel to the bypass duct.

If the short bypass duct is added to a straight duct (with length l_1 and cross-sectional area s_1), which is the mainstream element of a traditional Herschel-Quincke tube, δ/γ in Equation 4.18c is purely imaginary and the radius of the mapped circle is infinity (i.e., a straight line is mapped in the complex plane). If

this is the case, it is possible for the modulus of S_{TL} to reach infinity, when the denominator is zero (Equation 4.27). This yields the optimal solution $z = -\delta$. Plugging in $z = i\rho_0 c(kl)/s$ and $\delta = i\rho_0 c \cdot \sin(kl_1)/s_1$, the optimal kl/s can be expressed as

$$\frac{kl}{s} = -\frac{\sin(kl_1)}{s_1} \tag{4.29}$$

which is identical to that suggested by Selamet and Easwaren (Selamet and Easwaren, 1997).

The muffler experimented on is a cuboid with a panel in the middle as a partial partition (as shown in Figure 4.10). The muffler is divided into 6 parts where parts 1 and 6 are straight ducts and parts 2 through 5 are approximated as cones. The transfer matrices and the model validation are available in references (Munjal, 1987 and Mechel, 2002). Some end corrections are made to the dimensions of the elements to better fit the transmission loss curve from the plane wave model to that from the 2-load measurement (ASTM, 2009). It can be seen in Figure 4.12 that the transmission loss curves from the plane wave model and 2-load measurement compare well.

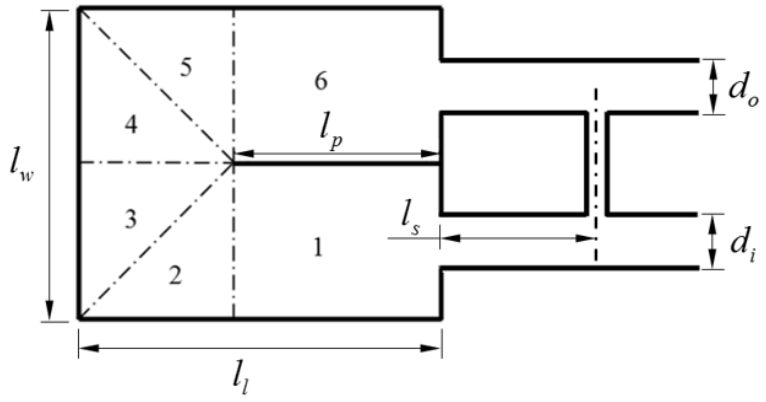

Figure 4.10 Muffler dimensions: l_w=0.3m, l_l=0.3m, l_p=0.2m, l_s=0.17m, d_i = d_o =0.05m, with height of $0.15m$.

In this example, 150 Hz was selected as the target frequency for optimization to enhance the transmission loss. The mapped circle with varying bypass duct dimensions is determined analytically using Equation 4.1 and plotted in Figure 4.11. The point on the mapped circle and farthest from the origin is of interest (large dot in Figure 4.11). Following the method discussed above, the optimal ratio between l and s was determined. The optimized muffler was built and transmission loss curves from measurement and plane wave model are both shown in Figure 4.12. The results indicate that the performance is improved in excess of 20 dB at low frequencies.

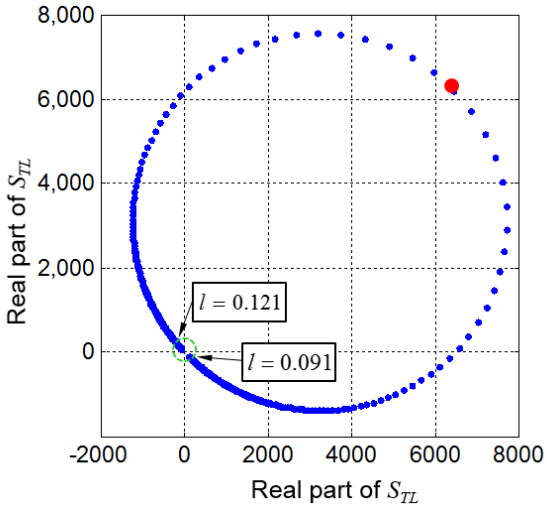

Figure 4.11 Effect of changing length of bypass duct of the on S_{TL}. (Blue: S_{TL} values of different lengths; Red: optimal solution).

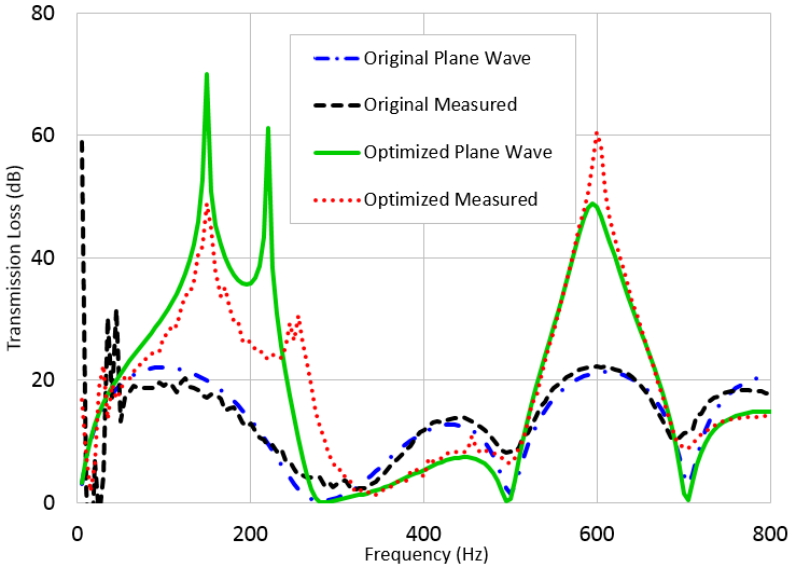

Figure 4.12 TL curves of original and optimized muffler.

The range of lengths to meet a requirement of 40 dB transmission loss at 150 Hz was also identified. This requirement results in an allowable circle with radius of 200 in the complex plane. With the diameter of the bypass duct fixed (0.016 m), the S_{TL} circle intersects the allowable circle for duct lengths of 0.091 m and 0.121 m, respectively. The two intersection points bracket the designs that satisfy the

requirement. Thus, a length between 0.091 m and 0.121 m will ensure a transmission loss above 40 dB at the targeted frequency. Transmission loss curves calculated using the plane wave model with these two lengths are plotted in Figure 4.13.

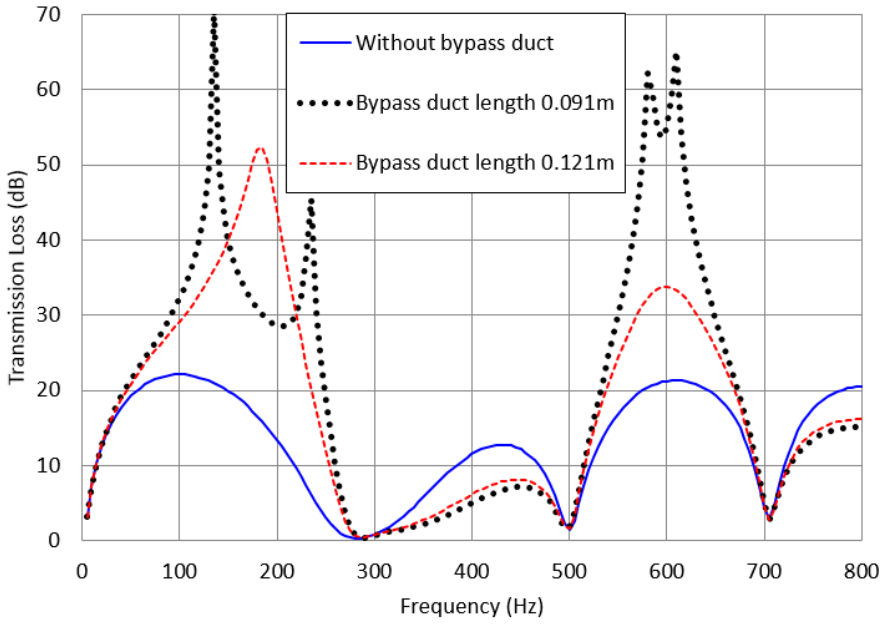

Figure 4.13 Adding bypass duct with length of limit values of feasible range.

4.4.3 Application to Isolation Mounts

The Moebius transformation can also be applied to isolation mounts. A number of authors (Wallin et al., 2012, Izak, 1993, Norwood and Dickens, 1998) have suggested the isolator effectiveness as a performance metric. The primary advantage is that the impedances of both the machine (Z_S) and foundation (Z_F) are included in the assessment. The isolator can be modeled using transfer matrix theory which is analogous to that for muffler elements. In this case, the force and vibrational velocity on one side are related to those on the other side via the transfer matrix

$$\begin{Bmatrix} F_1 \\ v_1 \end{Bmatrix} = \begin{bmatrix} A & B \\ C & D \end{bmatrix} \begin{Bmatrix} F_2 \\ v_2 \end{Bmatrix} \tag{4.30}$$

where F_1 and F_2 are the forces and v_1 and v_2 are the velocities on either side of the mount (Izak, 1993). The mount insertion loss (Wallin et al., 2012, Izak, 1993, Norwood and Dickens, 1998) or isolator effectiveness is defined as the difference of vibrational velocities in decibels between a hard contact case (no isolation) and isolated case at the foundation side. It is expressed mathematically as

$$IL = 20log_{10}\left|\frac{AZ_F + B + CZ_FZ_S + DZ_S}{Z_S + Z_F}\right| \tag{4.31}$$

where Z_S and Z_F are the impedances on the source and foundation side respectively.

If the isolator is modeled as a spring, mass, and damper, the transfer matrix can be expressed as (Izak, 1993)

$$\begin{Bmatrix} F_1 \\ v_1 \end{Bmatrix} = \begin{bmatrix} 1 + \dfrac{i\omega M}{K/i\omega + R} & i\omega M \\ \dfrac{1}{K/i\omega + R} & 1 \end{bmatrix} \begin{Bmatrix} F_2 \\ v_2 \end{Bmatrix} \tag{4.32}$$

where K, M and R are the respective stiffness, mass, and damping. For the example considered here, the isolator was assumed to have a mass (M) of 40 grams, stiffness (K) of 10 kN/m and a damping (R) of 20 N·s/m.

For the sake of illustration, an isolator is assumed to be positioned in between two simply supported rectangular plates. The driving point impedances (Z_S and Z_F) at point (p, q) can be determined using (Soedel, 2004)

$$Z = \frac{\rho hab}{4i\omega \sum_{m=1}^{\infty}\sum_{n=1}^{\infty} \frac{sin^2\left(\frac{m\pi p}{a}\right) sin^2\left(\frac{n\pi q}{b}\right)}{\omega_{mn}^2 - \omega^2 + 2i\zeta_{mn}\omega_{mn}\omega}} \tag{4.33a}$$

$$\omega_{mn} = \pi^2\left(\frac{m^2}{a^2} + \frac{n^2}{b^2}\right)\sqrt{\frac{Eh^2}{12\rho(1-\mu^2)}} \tag{4.33b}$$

where ω_{mn} is the natural frequency of mode (m, n), ρ is the density of plate material, E is the Young's modulus, μ is the Poisson's ratio, ζ_{mn} is the damping coefficient and other dimension parameters are shown in Figure 4.14. In practice, Z_S and Z_F can be measured with an impact hammer and an accelerometer. In this paper, the imaginary part of Z_F is modified by adding mass to the position where the isolator is attached. Adding a mass of m_{ad} will increase the impedance by $i\omega m_{ad}$ at a frequency of ω. Viewed in the complex plane, this will modify the impedance along a vertical straight line.

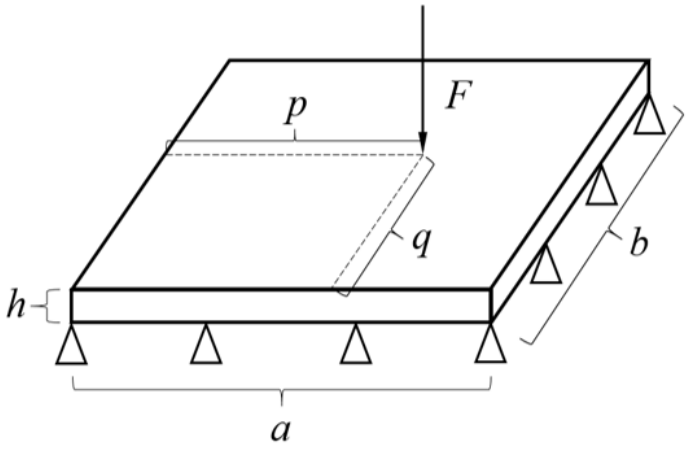

Figure 4.14 Driving point impedance calculation at point (p, q).

Based on Equation 4.31, we define an insertion loss vector (S_{IL}) as

$$S_{IL} = \frac{AZ_F + B + CZ_F Z_S + DZ_S}{Z_S + Z_F} \tag{4.34}$$

By inspection, S_{IL} is in the form of the Moebius transformation for both modifications to Z_S and Z_F. When the modulus of S_{IL} is a maximum, the insertion loss is maximized at that particular frequency. For demonstration, driving point impedances of two simply-supported steel plates of dimension of 0.15m×0.15m×0.003m at point (p_1, q_1) = (0.07, 0.07) and (p_2, q_2) = (0.1, 0.1) are used for Z_S and Z_F, respectively. The material constants used in the simulation are ρ=7850 kg/m^3, E=200 GPa, μ=0.303, and ζ_{mn}=0.01.

In this case, the analysis was targeted at the first resonant frequency of the system. Figure 4.15 shows the effect of changing the imaginary part Z_S on the insertion loss vector (S_{IL}). Figure 4.16 compares the insertion loss before and after optimization. Notice that the insertion loss is substantially increased in the frequency range around the target frequency by adding the mass (0.06 kg) selected using the Moebius transformation.

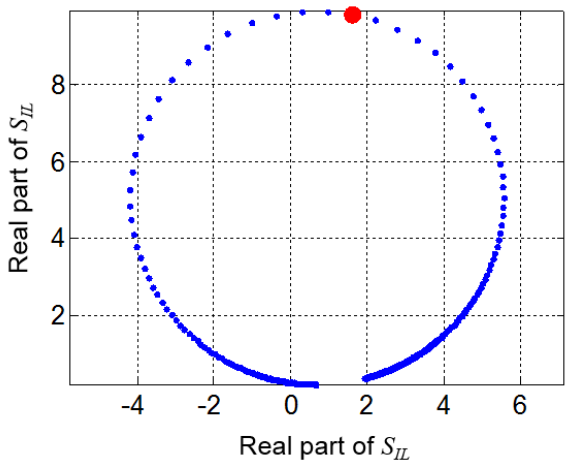

Figure 4.15 Effect of changing the imaginary part of the foundation impedance on S_{IL}. (Blue: S_{IL} values of different modifications; Red: optimal solution).

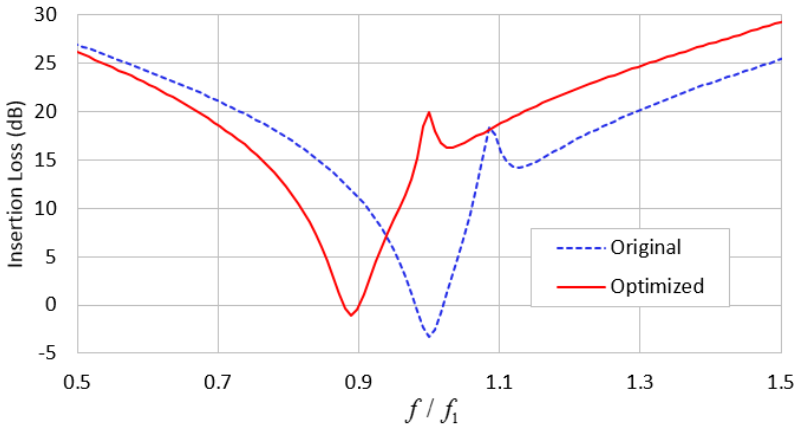

Figure 4.16 IL comparison between before and after optimization (f_1: first resonant frequency of original system).

4.5 Conclusion

It has been shown that the transmission and insertion loss vectors are in the form of the Moebius transformation for vibro-acoustic systems. The strategy can deal with both series and parallel impedance modifications. Moreover, the methods that have been described can be integrated into more sophisticated optimization strategies and may improve their efficiency.

It was shown that a short bypass duct can be utilized in an enclosure to improve the insertion loss at a selected frequency. In addition, the length of the outlet duct can be tuned to achieve optimal performance at a selected target frequency. Similarly, it was shown that a short bypass duct could be integrated into a muffler or silencer which will improve the transmission loss without increasing the size. This amounts to a variation of the Herschel-Quincke Tube. It was shown to be especially advantageous to place a bypass duct in parallel with an expansion chamber. The feasibility of using the approach was also demonstrated for

isolation mounts attached in between two plates. The method can be used to optimize the impedance of the machine or foundation attachment point, which maximizes the insertion loss at a selected frequency.

Chapter 5 SENSITIVITY ANALYSIS USING THE MOEBIUS TRANSFORMATION

5.1 Introduction

As stated in Section 2.1, the performance of exhaust system is not only dependent on the system itself, but also on the boundary conditions, which are the impedances at the inlet and outlet. For many cases, the exact value of these impedances are not known or easily measured. It is of interest to see the range of performance variation given the range of possible values of impedance. An exhaustive method to determine the response variation is computationally expensive. However, it was noted in Section 4.2 that the relationship between source impedance and response is in the form of the Moebius transformation, which is a conformal transformation. Taking advantage of this property, the computation can be much reduced. It is also shown that the sensitivity of this dependence can be studied visually using the Moebius transformation.

5.2 Conformal transformation

In vibro-acoustic problems, the exact values of boundary impedance are sometimes unavailable. An estimated value with specified deviation range can be provided for the uncertain impedance. With the real part plotted as x-axis coordinate and the imaginary part plotted as y-axis coordinate, the estimation range can be represented by an area in complex plane. Since the impedance modification can be bounded by geometric or functional requirements, the feasible range of impedance will be a closed domain in the complex plane.

The Moebius transformation is a conformal transformation (Needham, 1998), which preserves the angles of curves during transformation. It can be further proved that the Moebius transformation maps an oriented circle C to an oriented circle $\tilde{C}$ in such a way that the region to the left of C is mapped to the region to the left of $\tilde{C}$.

It can be made easier to understand by looking at the separate steps of the Moebius transformation. Among the four steps of the Moebius transformation, translation, rotation and dilation all preserve the orientation of C and map the interior of C to the interior of the image $\tilde{C}$. However, the effect of complex inversion on C depends on whether or not C contains the origin. After the first step, if C does contain the origin then $\tilde{C}$ has the opposite orientation and the interior of C is mapped to the exterior of $\tilde{C}$. If C does not contain the origin then $\tilde{C}$ has the same orientation and the interior of C is mapped to the interior of $\tilde{C}$. If C passes through the origin then its interior is mapped to the half-plane lying to the left of the oriented straight line $\tilde{C}$.

The vibro-acoustic problem for exhaust system can be viewed as source acting on a passive system, if no active control mechanism is considered. For a passive system, the real part of the impedance, which may be a transfer, source or surface impedance, should be positive, as long as there is some damping. Viewed in complex plane, a realist impedance range should always be in right half plane.

From Equation 4.2 and 4.11, the first translation step before complex inversion is defined as

$$z \mapsto z + \frac{\delta}{\gamma} \tag{5.1a}$$

$$\gamma = H_{rr} + H_{ss} - H_{rs} - H_{sr} \tag{5.1b}$$

$$\delta = 1 \tag{5.1c}$$

Assume there are two inputs to the system, at points r and s, respectively. The resultant velocities at points r and s can be calculated as the summation of responses due to each input. This may be expressed as

$$v_r = H_{rr}F_r + H_{rs}F_s \tag{5.2a}$$

$$v_s = H_{sr}F_r + H_{ss}F_s \tag{5.2b}$$

The input power is

$$\begin{aligned} P_{input} &= real(v_r F_r^* + v_s F_s^*) \\ &= (H_{rr}F_r^* + H_{rs}F_s^*)F_r^* + (H_{sr}F_r^* + H_{ss}F_s^*)F_s^* \end{aligned} \tag{5.3}$$

If the input forces are $F_r = 1, F_s = -1$ (force is applied in the direction opposite to the direction in which transfer function is defined), the input power can be expressed as

$$P_{input} = real(H_{rr} + H_{ss} - H_{rs} - H_{sr}) \tag{5.4}$$

which should be equal to the dissipation within the system. For realist system, the dissipation due to damping should be positive and thus

$$real(H_{rr} + H_{ss} - H_{rs} - H_{sr}) > 0 \tag{5.5}$$

Since $\delta = 1$ and $real(\gamma) > 0$, the first translation step shifts the feasible range to the right hand side in the complex plane. Since the feasible range is in the right hand side of the complex plane after the first translation step, the feasible range will not contain the origin prior to the complex inversion step. It can be concluded that for a realist system with feasible range of impedance, the mapped response space is always a closed domain in complex plane, and the boundary after transformation is mapped from the boundary of the feasible range. It can also be confirmed that the adjacent points will be adjacent after transformation. The immediate points to the optimal response are mapped from the immediate points to the optimal design.

5.3 Influence of boundary conditions on isolator effectiveness

5.3.1 Mapping of feasible range

To validate the previous statement, an example on isolator effectiveness is used. Equation 4.34 is in the form of the Moebius transformation for both Z_F and Z_S. If variations of Z_F are considered, the Equation 4.34 can be rearranged so that it is in the form of the Moebius transformation with

$$\alpha = CZ_S + A \tag{5.6a}$$

$$\beta = DZ_S + B \tag{5.6b}$$

$$\gamma = 1 \tag{5.6c}$$

$$\delta = Z_S \tag{5.6d}$$

As $real(Z_S) > 0$, it can be confirmed that the first step of translation is to shift rightward and the mapped domain is also closed, and its boundary is mapped from the boundary of the feasible range of Z_F.

For demonstration, the same parameters are used as in Section 4.4.3. Driving point impedance of a simply-supported steel plate is used for the original values of both Z_F and Z_S. The plate has an area of 0.15m×0.15m and a thickness of 0.003m. The material constants used for the steel plate is the same as in Section 4.4.3. In this analysis, the target frequency is set at the first resonant frequency of the system. A driving point impedance at point (p_1, q_1) = (0.07, 0.07) is used for Z_S, and the driving point impedance at point (p_2, q_2) = (0.1, 0.1) is used for Z_F.

At the target frequency, the original Z_F is calculated to be (10.4-87.6i) N·s/m. The real part can be increased by adding damping and the imaginary part can be increased by adding mass. The feasible range of Z_F is assumed to be a rectangular from (20,-80i) to (220,200i). The feasible range of Z_F is shown in Figure 5.1 and is discretized evenly. Discrete points are shown by vertices of rectangles. The transformation of these selected points are calculated and shown in Figure 5.2.

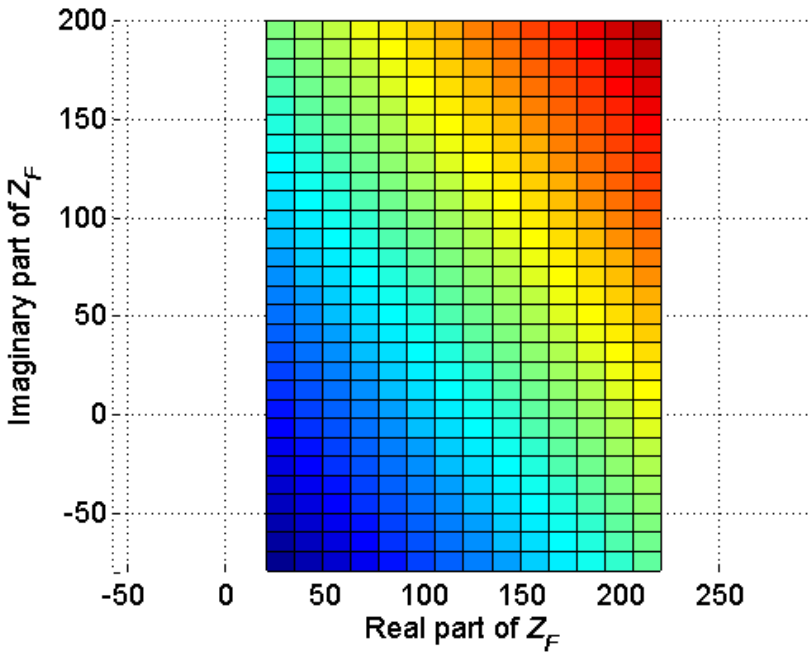

Figure 5.1 Feasible range of Z_F

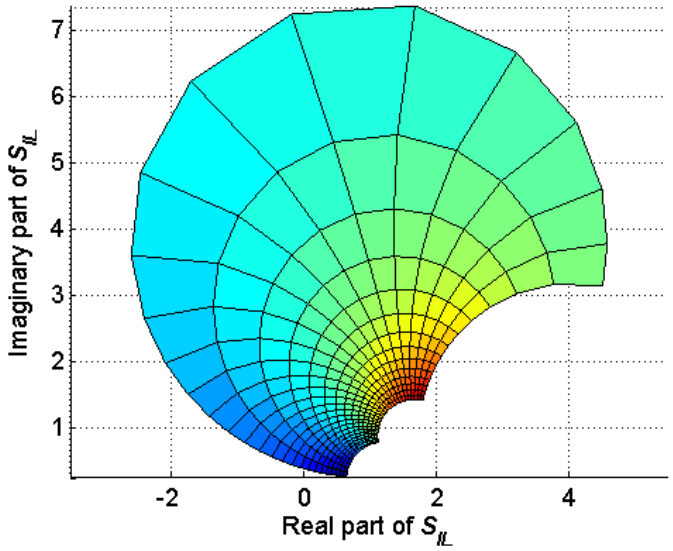

Figure 5.2 Response range of S_{IL}

5.3.2 Determining optimum for a feasible range

The boundary of the response range is the Moebius transformation of the boundary of the feasible range of impedance. The optimal response, which has the maximum modulus in this isolator insertion loss example, will be on the

boundary of the response area, and is mapped from a point on the boundary of the feasible range. As a result, to find the optimal design in a given feasible range, one only needs to find the optimal design along the boundary of the feasible range.

For a feasible range which has a boundary composed of straight lines and arcs, the optimal design can be quickly determined by following steps:

1. Three points are selected for each straight line and arc on the boundary of the feasible range. The three points should include the start and end points of the straight line or arc, so that the central angle of mapped arcs can be determined.
2. The transformations of the selected points are calculated.
3. Based on the transformations of the three selected points, the center, radius and central angle of the transformed arc can be obtained.
4. The point with maximum modulus on each mapped arc can be found before it is found for the whole boundary.
5. The optimal design can be then obtained using the inverse transformation (Equation 4.7).

The isolator example is used to demonstrate this method. the feasible range from (20,-80i) to (220,200i) for Z_F is selected as shown in Figure 5.3. The selected points are indicated by circles of different colors on the boundary lines. The sequence of selected points is indicated by the diameters of the circles (from

smaller to larger). The sequence is chosen so that the feasible range is on the left side of the boundary.

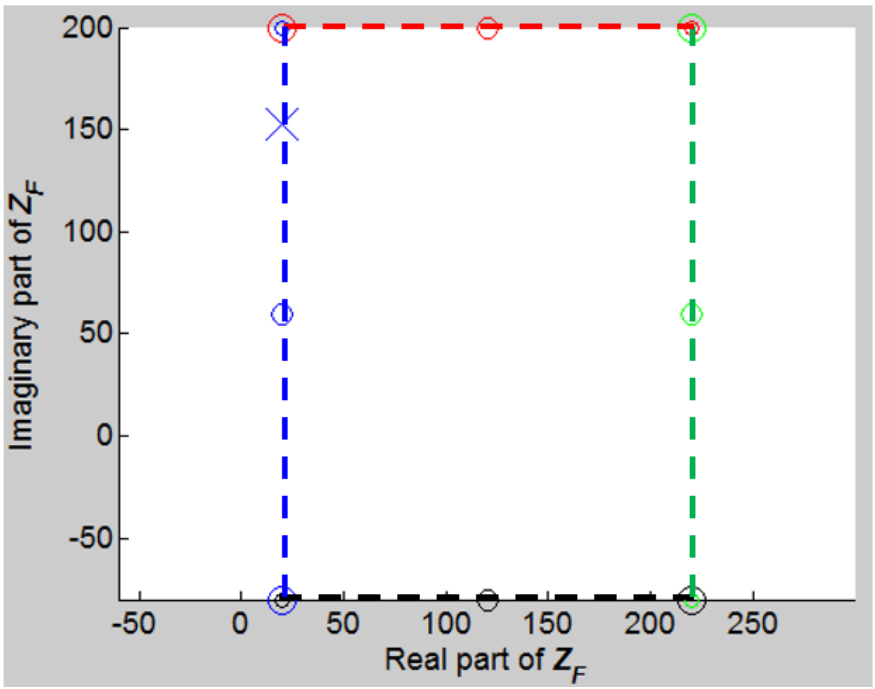

Figure 5.3 Feasible range Z_F and selected points.

There are 8 total points selected on 4 edges of the rectangular area, with three points on each edge. The transformation of these 8 points are first calculated. Then for each edge, the mapped arc is determined following the method described previously. The optimal point, which has the largest modulus, can be found for each edge. In Figure 5.4, the optimal points are indicated by crosses. It is obvious that the overall best point is on the blue arc, which is mapped from the left edge of the feasible range rectangle. After the overall optimal point is obtained, the optimal design from which the optimal point is mapped can be calculated using Equation 4.7. The best design is also plotted in Figure 5.3 and is indicated by a blue cross.

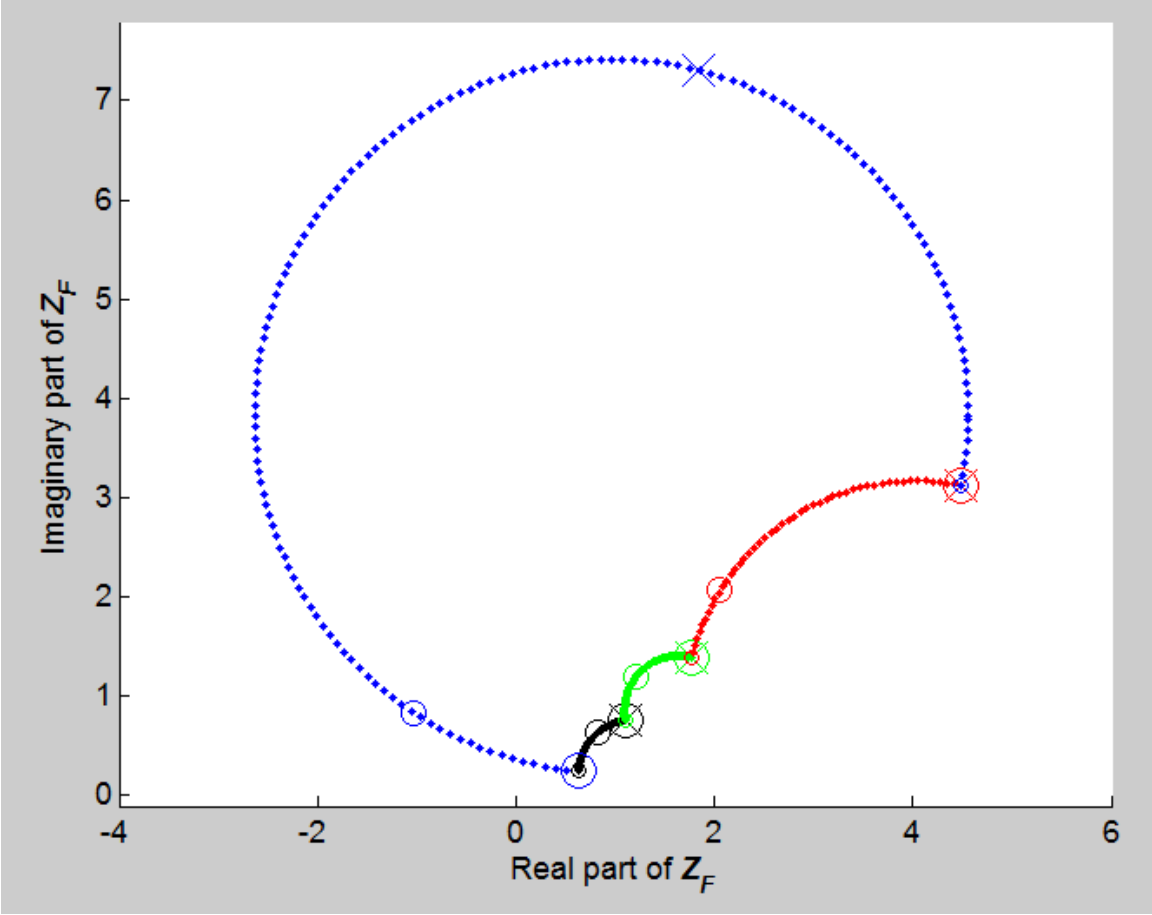

Figure 5.4 Mapped boundary of feasible range and optimal points on each edge.

5.4 Influence of source impedance on muffler insertion loss

For many mufflers, the source impedance and termination strongly influence the attenuation. The source and termination characteristics change the modal frequencies of the upstream and downstream ducting. Though acceptable models have been developed for termination impedance for many standard duct outlet geometries, such models do not exist for source impedance. In the design stages, constant source impedances have been assumed by some authors, but that is an obvious approximation and large deviations can be expected. In the

discussion which follows, the range of muffler insertion loss is determined using the Moebius transformation approach.

5.4.1 Calculation of muffler insertion loss

Insertion loss is the reduction of noise emission due to a muffler element being installed in the system and is defined as the difference in sound pressure level at a point downstream the outlet of the silencer with and without the attenuating element in place. With source impedance known as Z_S and termination impedance as Z_T, the insertion loss of a muffler can be calculated as

$$IL = 20log_{10}\left|\frac{T_{11}Z_T + T_{12} + T_{21}Z_SZ_T + T_{22}Z_S}{T_{11}^tZ_T + T_{12}^t + T_{21}^tZ_SZ_T + T_{22}^tZ_S}\right| \tag{5.7}$$

where T_{11}, T_{12}, T_{21} and T_{22} are transfer matrix entries of the muffler and T_{11}^t, T_{12}^t, $T_{21}^t$and T_{22}^t are transfer matrix entries of a straight pipe with same diameter as the source, which is used for comparison purposes.

An insertion loss complex vector can be defined as

$$S_{IL} = \frac{T_{11}Z_T + T_{12} + T_{21}Z_SZ_T + T_{22}Z_S}{T_{11}^tZ_T + T_{12}^t + T_{21}^tZ_SZ_T + T_{22}^tZ_S} \tag{5.8}$$

By observation it is found that S_{IL} is in the form of the Moebius transformation of Z_S, with the coefficients defined as follows

$$\alpha = CZ_T + D \tag{5.9a}$$

$$\beta = AZ_T + B \tag{5.9b}$$

$$\gamma = C_0 Z_T + D_0 \tag{5.9c}$$

$$\delta = A_0 Z_T + B_0 \tag{5.9d}$$

It can be seen that for the first step of translation, the shifting vector is

$$\frac{\delta}{\gamma} = \frac{A_0 Z_T + B_0}{C_0 Z_T + D_0} \tag{5.10}$$

It is the input impedance into a straight pipe, with termination impedance Z_T applied at the end. It is obvious that the real part of δ/γ should be non-negative. It can be confirmed that the feasible range will be in the right half plane in complex plane after the first step, and the mapped response range is a closed domain.

5.4.2 Feasible range of Z_S

To get a more reasonable estimation of feasible range of Z_S, the constant models (Prasad and Crocker, 1983, and Callow and Peat, 1988) and measured source impedance for the first 10 harmonics on a diesel engine in Chapter 3 are plotted in the complex plane. The source impedance should have a positive real part. Accordingly, any measured data with a negative real part should be omitted. The reason for the negative real part may be the nonlinearity and time variance of the engine, flow generated noise and the acoustic load selection. In total, there were 16 points satisfying this requirement. The modulus and angle of each of these 16 points are calculated. 99% confidence intervals for modulus and angle are calculated respectively based on these 16 samples. There is a 99% chance that the true mean value of the modulus and angle will be contained in the calculated

intervals.The resulted 98.01% confidence interval for source impedance can be determined by the individual confidence intervals for modulus and angle. The resultant feasible range is an annular sector and is shown in Figure 5.5.

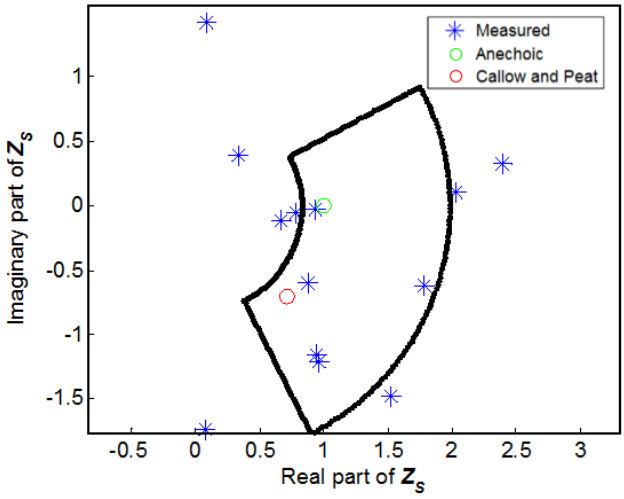

Figure 5.5 Source impedance models and feasible range of Z_F.

5.4.3 Insertion loss variation due to source impedance

A similar approach is adopted for determining the feasible insertion loss range. The feasible range of source impedance is enclosed by two straight lines and two arcs. The mapped response range will be enclosed by four arcs. To demonstrate different sensitivities due to source impedance with different mufflers, the following muffler designs have been used.

Muffler A is a simple expansion chamber. The length of the chamber is 25.4 cm and diameter is 7.6 cm. Muffler B is a simple expansion chamber with extended inlet and outlet. The overall dimension is the same as Muffler A. The extension lengths are 12.7 cm and 6.4 cm, respectively. Muffler C is more complex than the first two designs. It is a cross-flow muffler with three chambers and perforated

tubes inside. Cross-flow takes place twice across the perforated tubes and the friction against the holes induces considerable damping. To reduce the resonances within the inlet and outlet ducts, the inlet and outlet ducts are kept same on all three mufflers, with diameters of 3.5 cm in and lengths of 20.3 cm. The transmission loss curves for these three mufflers are shown in Figure 5.9 (SIDLAB, 2011).

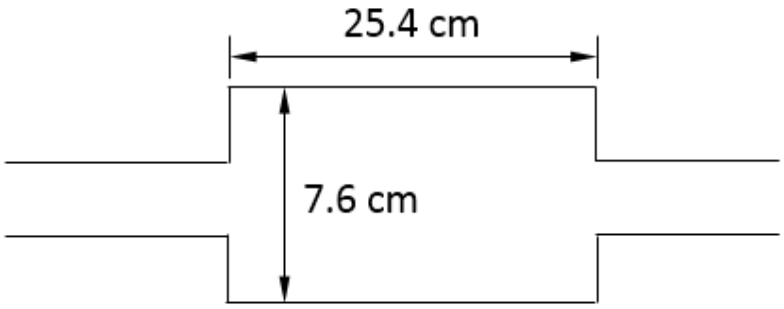

Figure 5.6 Schematic of Design 1.

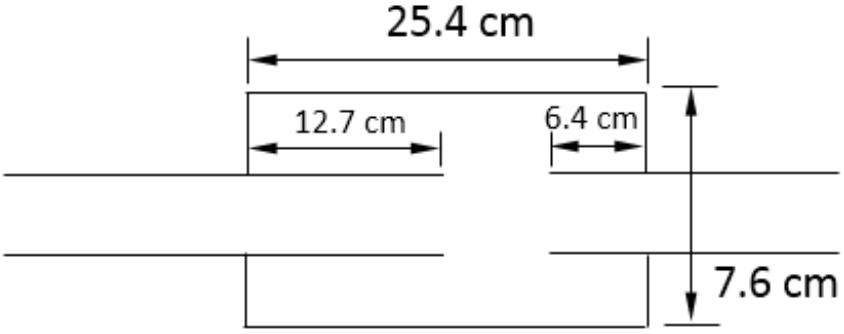

Figure 5.7 Schematic of Design 2.

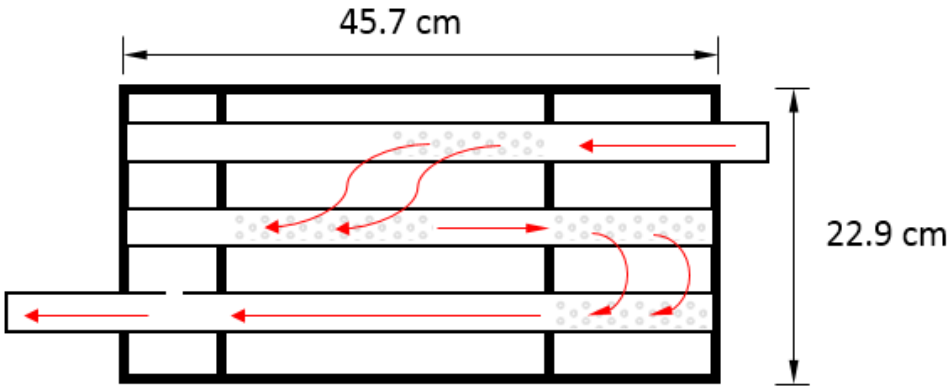

Figure 5.8 Schematic of Design 3.

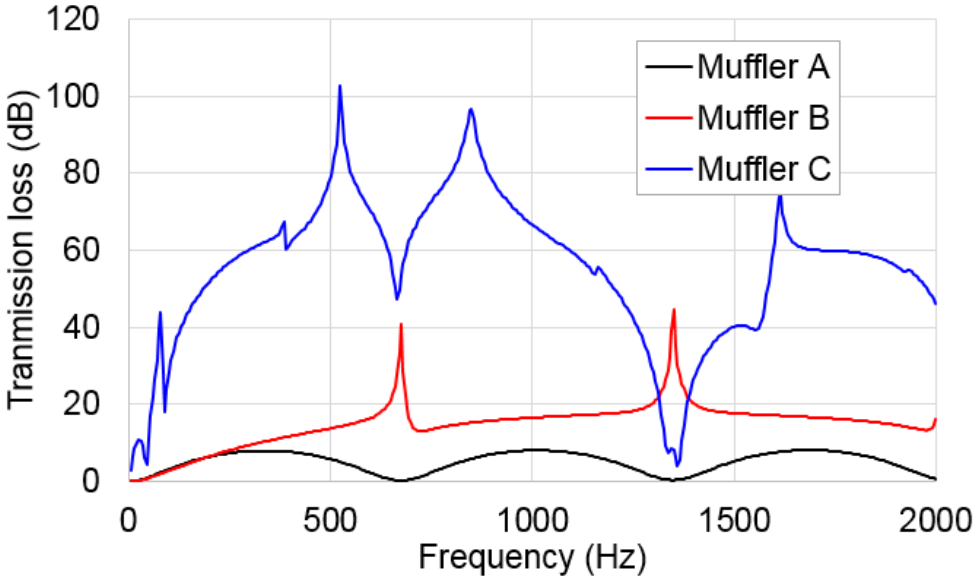

Figure 5.9 Transmission loss comparison between three designs.

With source impedance given within a certain range, the maximum and minimum insertion loss at each frequency can be obtained. The variation of insertion loss versus frequency is plotted in Figure 5.10, 5.11 and 5.12 for Design 1, 2, and 3 respectively. For comparison purpose, the transmission loss of each muffler is also plotted.

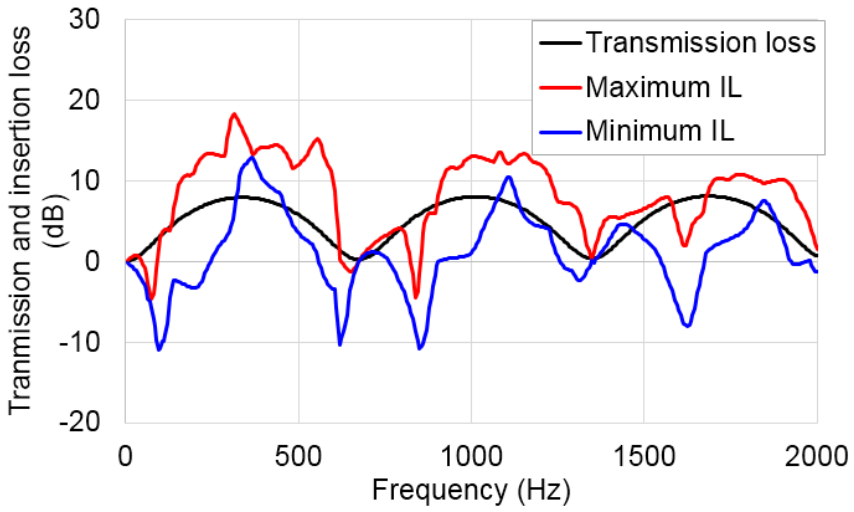

Figure 5.10 Transmission loss and insertion loss variation for Design 1.

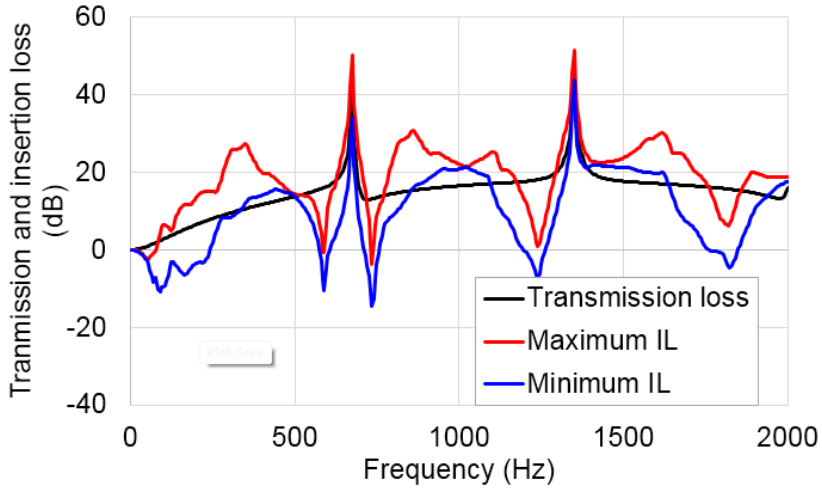

Figure 5.11 Transmission loss and insertion loss variation for Design 2.

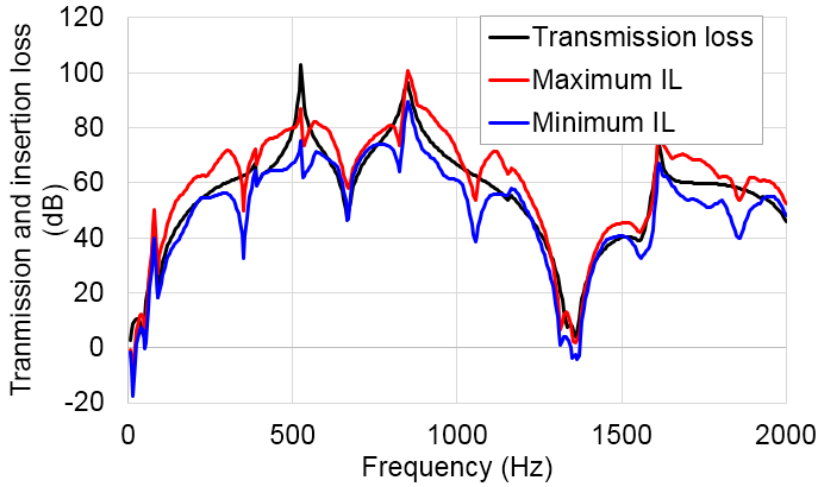

Figure 5.12 Transmission loss and insertion loss variation for Design 3.

A metric SIS (source impedance sensitivity) can be defined to evaluate the sensitivity due to source impedance for each muffler. It is the ratio of insertion loss variation to the transmission loss value at each frequency averaged over the frequency range of interest and can be expressed as

$$SIS = ave[(IL_{max} - IL_{min})/TL] \tag{5.11}$$

The calculated SIS for Muffler A is 1.93. For Muffler B it is 0.86 and For Muffler C it is 0.21. It is in accordance with our experience that a muffler with high broadband transmission loss is usually less sensitive due to source impedance variation. It can be noted from the Figures 5.10 through 5.12 that at the frequencies of the peaks of transmission loss, the variation of insertion loss is usually smaller. Also it is demonstrated that the Moebius transformation can be used to predict the extremes for a given range of impedance variation.

5.5 Conclusions

If the feasible range of source impedance can be assumed, the Moebius transformation can be used to efficiently obtain the extreme values of the response. This approach provides a significant computation advantage to sampling the response over the entire feasible range of source impedances. The minimum and maximum response values can be determined by mapping the boundary of the impedance variation to the corresponding response range. The response range will be bounded by connected arcs or straight lines and maximum and minimum values will lie on the mapped arcs and straight lines. Then, maximum and minimum values can be determined quickly. This method has two advantages. 1) the location of optimal solution is proved to be always on the boundary of feasible range, and 2) the mapped boundaries will be either arcs or straight lines provided the boundaries of feasible range of impedance modification are consist of arcs and straight lines. These two advantages enables great reduction of computation cost compared to exhaustive method. The effectiveness of this approach is demonstrated on examples of calculating insertion loss variation due to boundary impedance variation for isolators and mufflers.

Chapter 6 THE ANALYSIS OF MULTI-INLET MULTI-OUTLET MUFFLER

6.1 Introduction

Most prior muffler research has been dedicated to the single-inlet and single-outlet (SISO) muffler case. However, often multi-inlet and multi-outlet (MIMO) configurations are used in practice. There has been limited work in these cases. In general, two approaches have been used to investigate MIMO mufflers. Selamet and Ji (Selamet and Ji, 2000) and Denia et al. (Denia et al., 2003) investigated the transmission loss of circular expansion chambers using a mode-matching approach and developed analytical solutions for pre-defined configurations. The solutions from mode-matching approach are for certain configurations only and cannot be easily extended to the general case. Another approach by Jiang et al. (Jiang et al., 2005) and Mimani and Munjal (Mimani and Munjal, 2012) is based on an impedance matrix, which is obtained by either plane wave analysis or the boundary or finite element method. In both approaches, it is noted that transmission loss and insertion loss for MIMO mufflers are dependent on the amplitude and phase relationship between the sources, which can be dealt with by using complex ratios between each source and a reference source.

In the work by Xin (Hua et al., 2014), the transmission and insertion loss for a two-inlet one-outlet muffler is defined using a different approach based on transfer matrix theory and superposition. In this chapter, the definitions for transmission and insertion loss are extended to the MIMO case. A MIMO muffler is considered as combination of several SISO mufflers, and transfer matrix theory

is used to characterize each. The approach is validated using an experimental 2-inlet 2-outlet muffler.

Like the SISO muffler, the effect of source impedance on the response is again investigated by taking advantage of the Moebius transformation. It is demonstrated that the Moebius transformation is useful for analyzing MIMO methods and is more efficient than an exhaustive analysis through the complete range of source impedances.

6.2 Performance metrics for MIMO muffler

6.2.1 Source model

For MIMO mufflers, the amplitude and phase relationship between sources and the source impedance must be taken into consideration when defining transmission and insertion loss. In this work, a circuit analogy model (Munjal, 1987, Prasad and Crocker, 1983, Prasad and Crocker, 1983, Prasad 1987) is used to describe the sources. The sound source is modeled as a pressure source (p_S) (analogous to a voltage source) and source impedance (z_S) in series with the acoustic load impedance (z_L) (Figure 6.1). It is assumed that the particle velocity (analogous to electrical current) is continuous at the source-load interface.

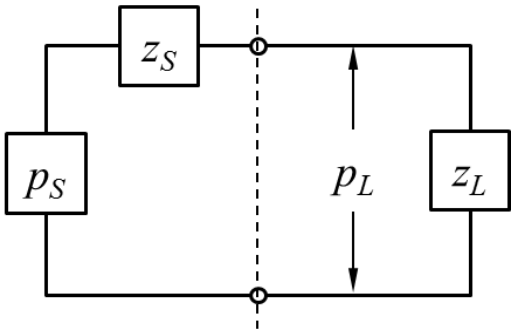

Figure 6.1 Schematic showing circuit analogy for acoustic sources.

From this model, it can be observed that

$$\frac{p_S}{z_s + z_L} = \frac{p_L}{z_L} \tag{6.1}$$

where p_S and z_S are the source strength and source impedance respectively. p_L and z_L are the respective load sound pressure and impedance. To use this model, the interface between the sound source and load must be assumed. p_L and z_L can be determined indirectly from measurement by performing wave decomposition downstream of the source using the two-microphone method (Rämmal and Bodén, 2007). Methods described in Chapter 3 have been applied to acoustically characterize the sources used in this chapter. Four different acoustic loads (an expansion chamber, a divergent cone, an open tube and an absorptive foam) have been attached to the source. Wave decomposition model has been applied to calculate the source strengths and impedances of the sound source used in this chapter.

6.2.2 Transmission loss for MIMO muffler

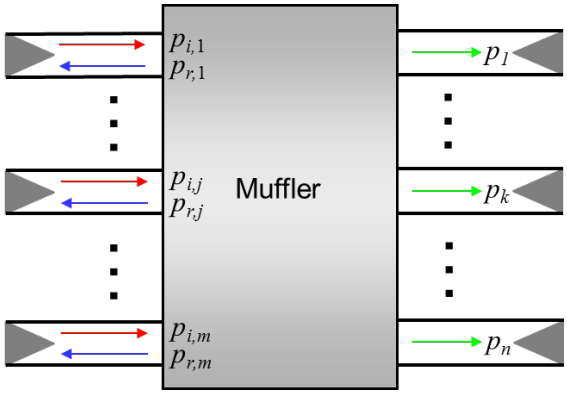

Figure 6.2 m-inlet n-inlet muffler with anechoic sources and terminations.

The definition of transmission loss for MIMO mufflers is a straightforward extension from the SISO case. As Figure 6.2 shows, the sound pressures inside Inlet j are decomposed into incident and reflected waves $p_{i,j}$ and $p_{r,j}$ respectively. Under the assumption that all the sources and terminations are anechoic, the transmission loss is defined as the ratio between the summation of incident sound power in the inlets and the summation of transmitted sound power in the outlets where s_j and s_k are cross-sectional areas of inlets and outlets respectively. Accordingly,

$$TL = 10log_{10}\frac{\sum_{j=1}^{m} W_{j,incident}}{\sum_{k=1}^{n} W_{k,transimitted}} = 10log_{10}\frac{\sum_{j=1}^{m}\left|p_{i,j}\right|^2 s_j}{\sum_{k=1}^{n}|p_k|^2 s_k} \tag{6.2}$$

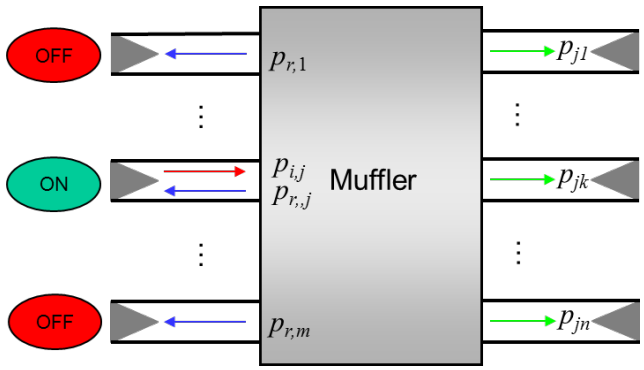

Figure 6.3 Superposition model for transmission loss calculation.

To calculate $p_{i,j}$ and p_k, a superposition model can be used. First assume only one source (j) is active (Figure 6.3), the transmitted sound pressure at Outlet k can be calculated using transfer matrix between Inlet j and Outlet k and the circuit analogy source model. Hence,

$$\begin{Bmatrix} p_{L,j} \\ v_{L,j} \end{Bmatrix} = \begin{bmatrix} A_{jk}^a & B_{jk}^a \\ C_{jk}^a & D_{jk}^a \end{bmatrix} \begin{Bmatrix} p_{jk} \\ v_{jk} \end{Bmatrix} \tag{6.3}$$

The load sound pressure and particle velocity can be expressed as

$$p_{L,j} = p_{i,j} + p_{r,j} \tag{6.4}$$

and

$$v_{L,j} = \frac{p_{i,j} - p_{r,j}}{\rho_0 c} \tag{6.5}$$

where the superscript a indicates the transfer matrix is obtained with anechoic boundary conditions applied to all inlets and outlets other than Inlet j and Outlet k. From the circuit analogy in Figure 6.1,

$$v_{L,j} = \frac{p_{S,j} - p_{L,j}}{\rho_0 c} \tag{6.6}$$

Since outlets are assumed anechoic,

$$v_{jk} = \frac{p_{jk}}{\rho_0 c} \tag{6.7}$$

The transfer function between the transmitted sound pressure at Outlet k and Source Strength j can be calculated from Equations 6.3-6.7. Hence,

$$H_{jk}^{a} = \frac{p_{jk}}{p_{S,j}} = \frac{1}{A_{jk}^{a} + \frac{B_{jk}^{a}}{\rho_0 c} + \rho_0 c C_{jk}^{a} + D_{jk}^{a}} \tag{6.8}$$

and

$$p_{i,j} = \frac{1}{2} p_{S,j} \tag{6.9}$$

With all sources active, the sound pressure at each outlet can be calculated by summing the contribution from each source. The amplitude and phase relationship between sources can be described using complex ratios α_j. In this work, the reference source is chosen to be the source at Inlet 1.

$$\alpha_j = \frac{p_{S,j}}{p_{S,1}} \tag{6.10}$$

Plugging in Equations 6.8-6.10, Equation 6.2 can be simplified as

$$TL = 10log_{10} \frac{\sum_j \left|\alpha_j \frac{1}{2} p_{S,j}\right|^2 s_j}{\sum_k \left|\sum_j \left(H_{jk}^{a} \alpha_j p_{S,1}\right)\right|^2 s_k} = 10log_{10} \frac{\sum_j \frac{1}{4} \left|\alpha_j\right|^2 s_j}{\sum_k \left|\sum_j \left(H_{jk}^{a} \alpha_j\right)\right|^2 s_k} \tag{6.11}$$

6.2.3 Insertion Loss for MIMO muffler

The insertion loss of a MIMO muffler is defined as the ratio between the summation of transmitted sound power in each outlet and the summation of transmitted power if all sources are connected to straight tubes of a certain length. This can be expressed as

$$IL = 10log_{10}\frac{\sum_{j=1}^{m}|p_j^t|^2 s_j}{\sum_{k=1}^{n}|p_k|^2 s_k} \tag{6.12}$$

A similar superposition method to that used to determine transmission loss can be used to calculate p_k and p_j^t. p_k is the sound pressure in the outlet pipes for the case with muffler (Figure 6.4) and p_j^t is the sound pressure at the outlet for a straight pipe (Figure 6.5). The difference in this calculation is that realistic source and termination impedances are applied as boundary conditions. Then,

$$\begin{Bmatrix} p_{L,j} \\ v_{L,j} \end{Bmatrix} = \begin{bmatrix} A_{jk}^Z & B_{jk}^Z \\ C_{jk}^Z & D_{jk}^Z \end{bmatrix} \begin{Bmatrix} p_{jk} \\ v_{jk} \end{Bmatrix} \tag{6.13}$$

where the superscript Z indicates the transfer matrix is obtained with realistic impedance boundary conditions applied on all inlets and outlets other than Inlet j and Outlet k. The source and termination impedances can be expressed as

$$z_{S,j} = \frac{p_{S,j} - p_{L,j}}{v_{L,j}} \tag{6.14}$$

and

$$z_{T,k} = \frac{p_{jk}}{v_{jk}} \tag{6.15}$$

respectively.

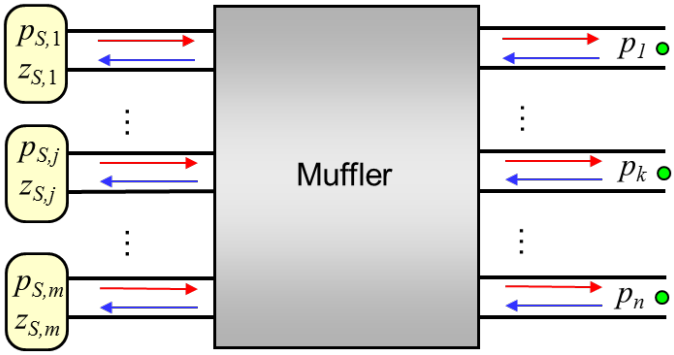

Figure 6.4 *m*-inlet *n*-inlet muffler with realistic sources and terminations.

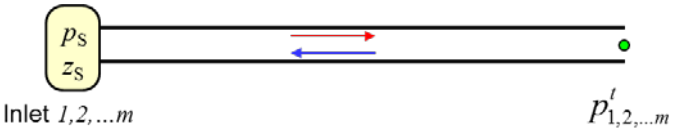

Figure 6.5 Source connected to a straight tube.

The transfer function between transmitted sound pressure at Outlet k and Source j can be calculated from Equations 6.13-6.15 and is written as

$$H^Z_{jk} = \frac{p_{jk}}{p_{S,j}} = \frac{z_{T,k}}{A^Z_{jk} z_{T,k} + B^Z_{jk} + C^Z_{jk} z_{T,k} z_{S,j} + D^Z_{jk} z_{S,j}} \tag{6.16}$$

The transfer functions for straight tube connections can be derived in the same way and are expressed as

$$H^Z_{j,tube} = \frac{z_{T,k}}{A_t z_{T,k} + B_t + C_t z_{T,k} z_{S,j} + D_t z_{S,j}} \tag{6.17}$$

where the subscript t indicates the transfer matrix entries are for a straight tube. Plugging in Equations 6.16-6.17, Equation 6.12 can be simplified as

$$IL = 10log_{10}\frac{\sum_j \left|H^z_{j,tube}\alpha_j p_{S,j}\right|^2 s_j}{\sum_k \left|\sum_j \left(H^z_{jk}\alpha_j p_{S,1}\right)\right|^2 s_k} = 10log_{10}\frac{\sum_j \left|H^z_{j,tube}\alpha_j\right|^2 s_j}{\sum_k \left|\sum_j \left(H^z_{jk}\alpha_j\right)\right|^2 s_k} \quad (6.18)$$

6.3 Experimental validation for superposition model

6.3.1 2-inlet 2-outlet muffler

To validate the superposition method, a 2-inlet 2-outlet muffler is built (Figure 6.6). The muffler cylinder has a length of 50.8 cm and diameter of 25.4 cm. Plates of lengths 25.4 cm and 20.3 cm are inserted to add complexity and avoid symmetry. The test setup is shown in Figure 6.7. Two compression drivers (JBL 2447H and 2426H) are used as sources. The compression drivers are connected to the inlets using Spectronics impedance tubes. To conveniently control the phase difference between these two sources, sine waves are used as driving signals. The central frequencies of octave bands from 125 Hz to 4000 Hz are used in this experiment. At each frequency, the phase delay between Source 1 and Source 2 is changed from 0 to 180 degrees, with step sizes of 45 degrees. The sound pressure at each outlet is measured and compared against the prediction determined using the superposition model.

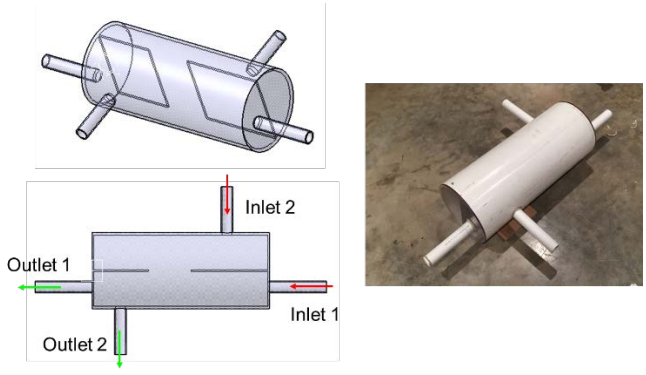

Figure 6.6 2-inlet 2-outlet muffler built using PVC.

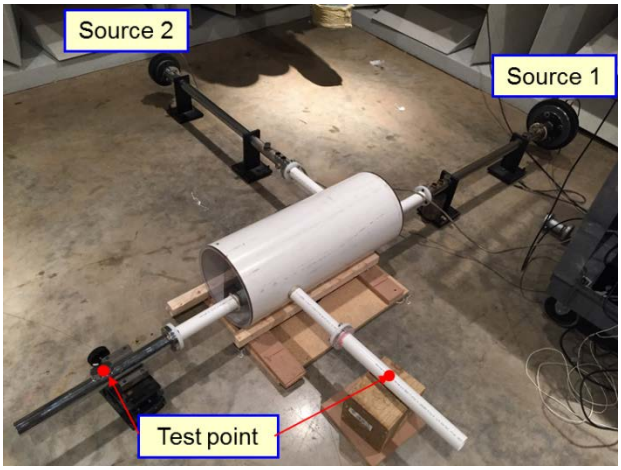

Figure 6.7 Test setup for experimental validation.

6.3.2 Source properties

The source strengths and source impedances of both compression drivers are measured at specified frequencies using the multi-load method (Liu and Herrin, 2009). The four loads used in determining the source properties are a simple expansion chamber, straight tube, divergent cone, and foam termination. The measured source strengths are phase-referenced to the input signal. The measured source strengths and source impedances for both compression drivers are shown in Figures 6.8 and 6.9.

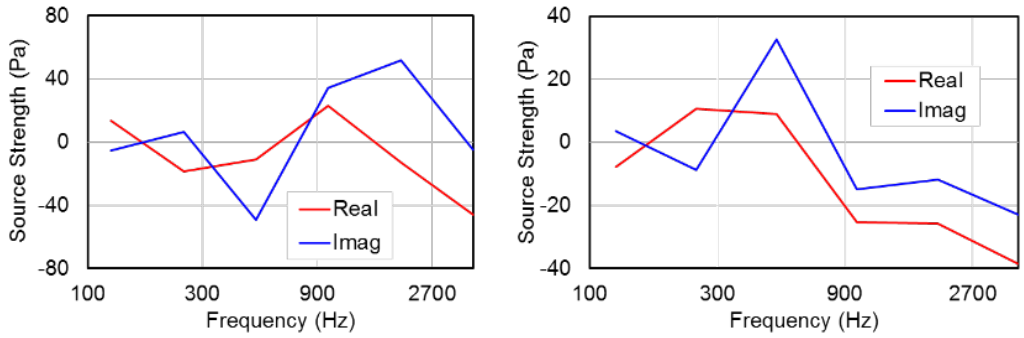

Figure 6.8 Measured source strengths for both compression drivers (left: Source 1: JBL 2447H; right: Source 2: JBL 2426H).

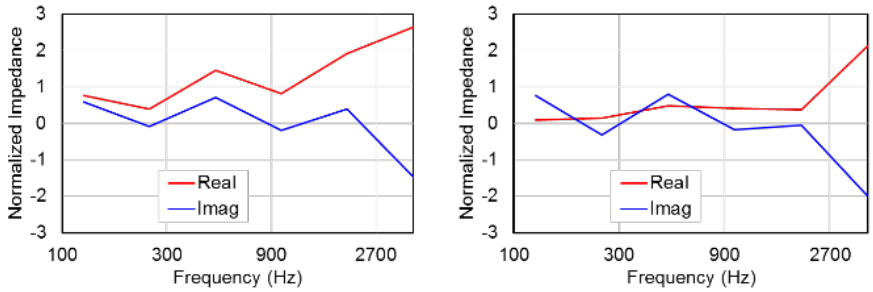

Figure 6.9 Measured source impedances for both compression drivers (left: Source 1: JBL 2447H; right: Source 2: JBL 2426H).

6.3.3 Termination impedance

Additionally, termination impedance is needed to predict the sound pressure at the outlets. The test point is selected to be 20.3 cm from the opening of the outlets. The impedance at this point towards the opening is measured using ASTM-E1050 (ASTM, 1998), and the measured termination impedance is shown in Figure 6.10.

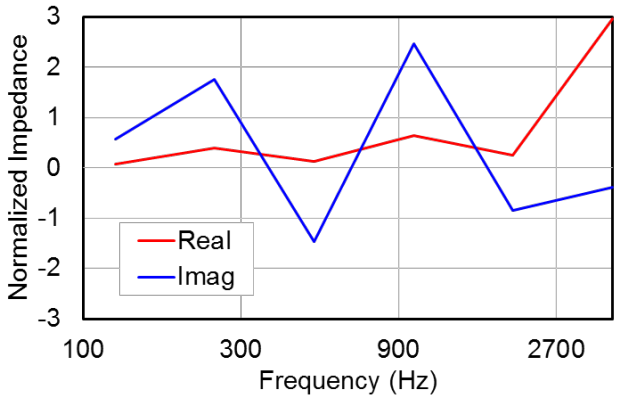

Figure 6.10 Measured termination impedance.

6.3.4 Transfer matrix

To predict the sound pressure at the outlets, the transfer matrices between inlets and outlets must be measured with realistic boundary conditions applied at the

ports. The transfer matrices are measured using ASTM-E2611 (ASTM, 2009). To keep the boundary conditions unchanged at inlets, when measuring transfer matrix between one inlet and one outlet, the compression driver at the other inlet is still active but with a driving signal about 1/100 of the normal amplitude. This small amplitude has been shown to excite the compression driver to a minimal source strength and preserve the source impedance (Hua et al., 2014).

6.3.5 Results and Discussion

The sound pressures at the outlets, both directly measured and predicted using the superposition model, are shown in Figures 6.11 and 6.12. From the comparisons, it can be seen that the prediction using the superposition method is very accurate for a varying phase delays.

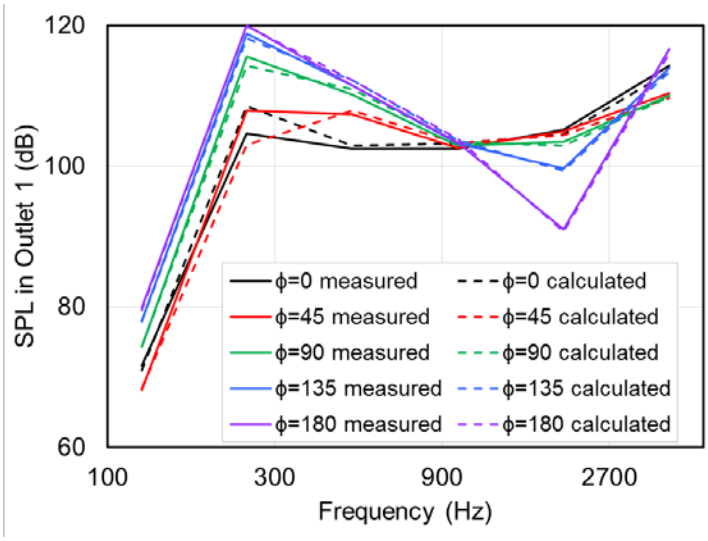

Figure 6.11 Comparison between direct measurement and prediction of sound pressure at Outlet 1.

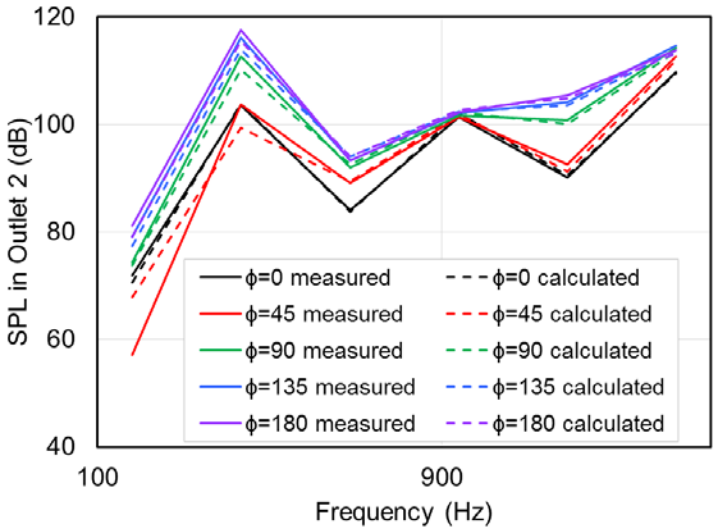

Figure 6.12 Comparison between direct measurement and prediction of sound pressure at Outlet 2.

After the superposition model was validated, the transmission loss and insertion loss of the muffler can be calculated for different phase delays between the sources. To calculate transmission loss, transfer matrices with all other ports anechoic are required. These transfer matrices can be obtained using simulation or approximated using measurement. In the current work, a measurement method is used. When transfer matrices are measured, the unused ports are closed with foam with thickness of 25.4 cm (Figure 6.13), which can be considered approximately anechoic. The test setup and absorption coefficients of these two foams are shown in Figure 6.14. The calculated insertion loss and transmission loss are shown in Figure 6.15 and 6.16 respectively.

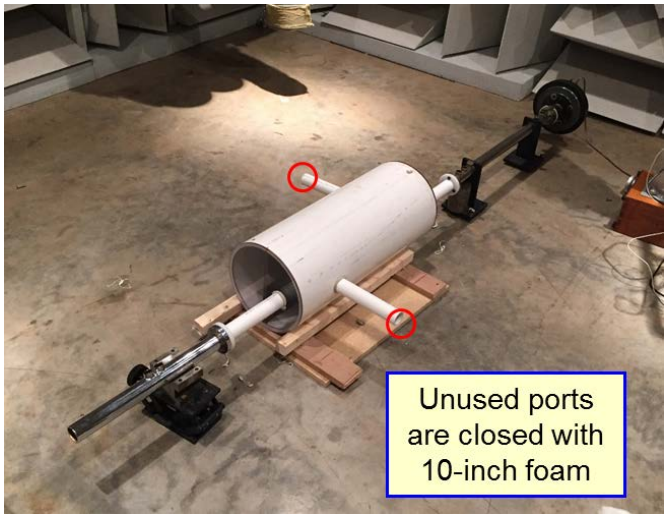

Figure 6.13 Test setup to measure transfer matrices with other ports anechoic.

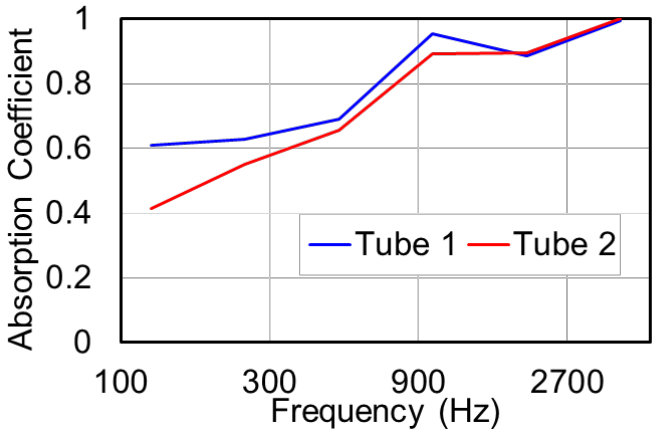

Figure 6.14 Sound absorption of the terminations for each tube.

The trend of insertion loss variation with phase delay correlates well with the results of outlet sound pressure. From Figure 6.11 and 6.12, it can be seen that below 1000 Hz, the sound pressures at both outlets increase with phase delay increases. In this frequency range, the insertion loss decreases with increasing phase delay. At 1000 Hz, the influence of phase on the outlet sound pressure is negligible for both outlets, and insertion loss remains constant with varying phase delay. At the frequency of 2000 Hz, with phase delay increases, the sound

pressure decreases at Outlet 1 while increasing at Outlet 2. The insertion loss remains constant suggesting that the corresponding increase and decrease of outlet sound pressure counteract one another.

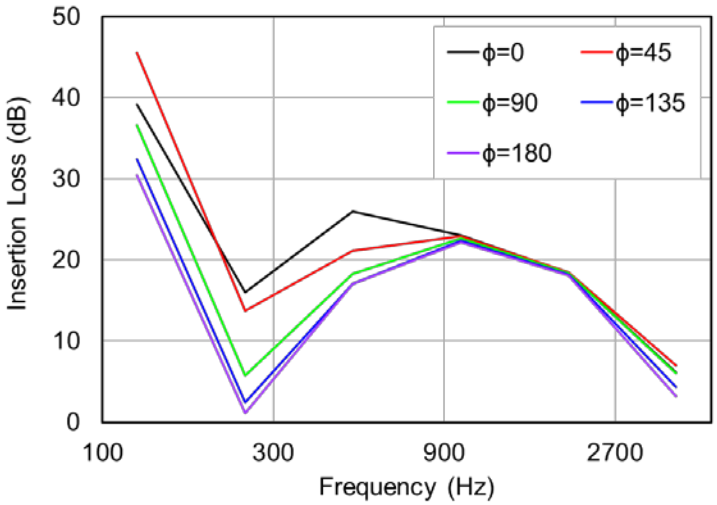

Figure 6.15 Insertion loss calculated for different phase delay between the sources.

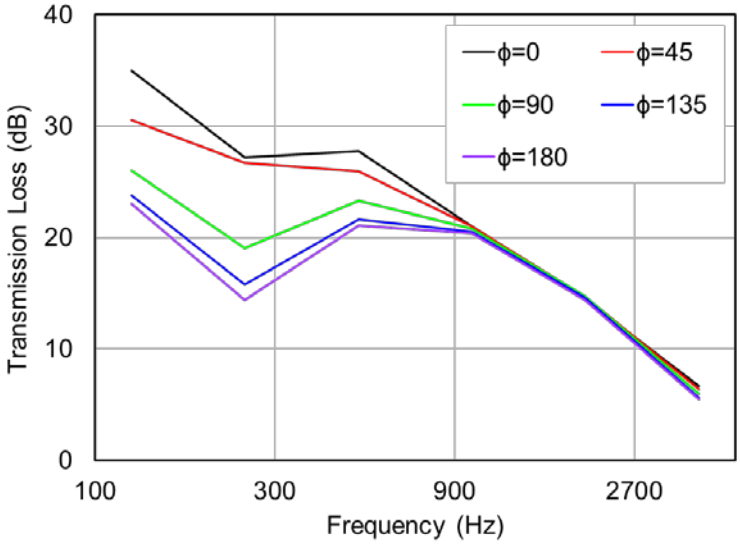

Figure 6.16 Transmission loss calculated for different phase delay between the sources.

The transmission loss calculated using the superposition model also shows a very similar trend compared to insertion loss. It demonstrates that without knowledge of source and termination impedance, transmission loss provides an estimate of the actual performance for this muffler. It is shown that phase delay plays a more important role in the lower frequency range than at higher frequencies for this 2-inlet 2-outlet muffler. Though only one example is shown in this paper, similar conclusions were also seen for a more practical muffler (Hua et al., 2014).

6.4 Source impedance sensitivity analysis on MIMO muffler

In Chapter 5, the sensitivity of SISO muffler performance due to source impedance was examined using the Moebius transformation. In this chapter, a similar analysis is performed on a MIMO muffler.

For this analysis, the transfer matrix is not suitable since the transfer matrix between specific inlet and outlet pair is dependent on boundary conditions at other inlet and outlet ports. To take boundary conditions at all inlet and outlet ports into consideration at the same time, the impedance matrix approach is more appropriate.

6.4.1 Impedance matrix

The impedance matrix relates sound pressure at all inlets and outlets to particle velocity at all inlets and outlets. The impedance matrix approach is particularly convenient for MIMO case and for use with numerical simulation procedures like boundary and finite element methods though it can be determined using transfer

matrix theory as well (Mimani and Munjal, 2012).The development below follows Jiang's work (Jiang et al., 2005). For a muffler having two inlets and one outlet as shown in Figure 6.17, with velocity direction defined inward, the impedance matrix is defined as

$$\begin{Bmatrix} p_1 \\ p_2 \\ p_3 \end{Bmatrix} = \begin{bmatrix} z_{11} & z_{12} & z_{13} \\ z_{21} & z_{22} & z_{23} \\ z_{31} & z_{32} & z_{33} \end{bmatrix} \begin{Bmatrix} v_1 \\ v_2 \\ v_3 \end{Bmatrix} \tag{6.19}$$

where subscripts 1,2 and 3 denote the first inlet, second inlet and outlet location respectively. The impedance matrix can be obtained using the boundary element method (BEM) by setting a velocity boundary condition $v = 1$ alternately at locations 1, 2 and 3. For example, the entries in the first column of the matrix are obtained by setting $v_1 = 1$ and $v_2 = v_3 = 0$. Although three different BEM runs are needed to create the impedance matrix, they share the same BEM matrix, which need only be solved once. The three different boundary condition sets correspond to three trivial back substitutions.

Figure 6.17 Two-inlet and one-outlet muffler

To the author's knowledge, there has been no work with respect to measurement of the impedance matrix of a MIMO muffler. In a nearly identical manner to the simulation method, the impedance matrix can be obtained from transfer matrices between each two ports among all inlets and outlets, which can be measured or simulated. In the 2-inlet 1-outlet case shown in Figure 6.17, the impedance matrix can be solved in following steps. With Port 3 blocked ($v_3 = 0$) and velocities defined using common convention (velocity at Port 1 defined inward and outward at Port 2), the transfer matrix between Ports 1 and 2 can be expressed as

$$\begin{Bmatrix} p_1 \\ v_1 \end{Bmatrix} = \begin{bmatrix} A_{12}^b & B_{12}^b \\ C_{12}^b & D_{12}^b \end{bmatrix} \begin{Bmatrix} p_2 \\ v_2 \end{Bmatrix} \tag{6.20}$$

where the superscript b denotes that the transfer matrix is obtained with the other port blocked. Similar equations can be written relating Ports 1 and 3 (with Port 2 blocked) and Ports 2 and 3 (with Port 1 blocked)

$$\begin{Bmatrix} p_1 \\ v_1 \end{Bmatrix} = \begin{bmatrix} A_{13}^b & B_{13}^b \\ C_{13}^b & D_{13}^b \end{bmatrix} \begin{Bmatrix} p_3 \\ v_3 \end{Bmatrix} \tag{6.21a}$$

$$\begin{Bmatrix} p_2 \\ v_2 \end{Bmatrix} = \begin{bmatrix} A_{23}^b & B_{23}^b \\ C_{23}^b & D_{23}^b \end{bmatrix} \begin{Bmatrix} p_3 \\ v_3 \end{Bmatrix} \tag{6.21b}$$

To convert these transfer matrices into impedance matrices, the direction of velocity must be changed accordingly. Equations 6.17 and 6.18 can be reformed into

$$\begin{Bmatrix} p_1 \\ v_1 \end{Bmatrix} = \begin{bmatrix} A_{12}^b & -B_{12}^b \\ C_{12}^b & -D_{12}^b \end{bmatrix} \begin{Bmatrix} p_2 \\ v_2 \end{Bmatrix} \tag{6.22a}$$

$$\begin{Bmatrix} p_1 \\ v_1 \end{Bmatrix} = \begin{bmatrix} A_{13}^b & -B_{13}^b \\ C_{13}^b & -D_{13}^b \end{bmatrix} \begin{Bmatrix} p_3 \\ v_3 \end{Bmatrix} \tag{6.22b}$$

$$\begin{Bmatrix} p_2 \\ v_2 \end{Bmatrix} = \begin{bmatrix} A_{23}^b & -B_{23}^b \\ C_{23}^b & -D_{23}^b \end{bmatrix} \begin{Bmatrix} p_3 \\ v_3 \end{Bmatrix} \tag{6.22c}$$

The first column of the impedance matrix can be obtained by setting $v_1 = 1$ and $v_2 = v_3 = 0$ in Equations 6.19. The second and third columns can be determined similarly. The impedance matrix can then be constructed as

$$\begin{Bmatrix} p_1 \\ p_2 \\ p_3 \end{Bmatrix} = \begin{bmatrix} \frac{A_{13}^b}{C_{13}^b} & -B_{12}^b + \frac{A_{12}^b D_{12}^b}{C_{12}^b} & -B_{13}^b + \frac{A_{13}^b D_{13}^b}{C_{13}^b} \\ \frac{1}{C_{12}^b} & \frac{A_{23}^b}{C_{23}^b} & -B_{23}^b + \frac{A_{23}^b D_{23}^b}{C_{23}^b} \\ \frac{1}{C_{13}^b} & \frac{1}{C_{23}^b} & \frac{D_{13}^b}{C_{13}^b} \end{bmatrix} \begin{Bmatrix} v_1 \\ v_2 \\ v_3 \end{Bmatrix} \tag{6.23}$$

6.4.2 Source impedance relationship

If the impedance matrix of a multi-inlet multi-outlet muffler is known, the transfer function between source and outlet sound pressure can be calculated, with the influence of source impedance taken into consideration. For a two-inlet one-outlet muffler, the transfer function between the source at Inlet 1 and the Outlet can be obtained via the following steps. With velocities at Inlet 2 and the Outlet defined pointing outward, the impedance matrix in Equation 6.19 can be rearranged into

$$\begin{Bmatrix} p_1 \\ p_2 \\ p_3 \end{Bmatrix} = \begin{bmatrix} z_{11} & -z_{12} & -z_{13} \\ z_{21} & -z_{22} & -z_{23} \\ z_{31} & -z_{32} & -z_{33} \end{bmatrix} \begin{Bmatrix} v_1 \\ v_2 \\ v_3 \end{Bmatrix} \tag{6.24}$$

When calculating the contribution from the source at Inlet 1, the source at Inlet 2 can be considered as passive. The source impedance of the source at Inlet 2 can be applied as

$$\frac{p_2}{v_2} = Z_{S2} \tag{6.25}$$

Plugging Equation 6.25 into Equation 6.24, the transfer matrix between Inlet 1 and the Outlet can be obtained after rearrangement. The entries of the transfer matrix are

$$A_{13} = \frac{z_{11}(Z_{S2} + z_{22}) - z_{12}z_{21}}{z_{31}(Z_{S2} + z_{22}) - z_{32}z_{21}} \tag{6.26a}$$

$$B_{13} = \frac{(z_{11}z_{33} - z_{13}z_{31})(Z_{S2} + z_{22}) + (z_{12}z_{23}z_{31} + z_{13}z_{32}z_{21} - z_{11}z_{32}z_{23} - z_{12}z_{21}z_{33})}{z_{31}(Z_{S2} + z_{22}) - z_{32}z_{21}} \tag{6.26b}$$

$$C_{13} = \frac{Z_{S2} + z_{22}}{z_{31}(Z_{S2} + z_{22}) - z_{32}z_{21}} \tag{6.26c}$$

$$D_{13} = \frac{z_{33}(Z_{S2} + z_{22}) - z_{32}z_{23}}{z_{31}(Z_{S2} + z_{22}) - z_{32}z_{21}} \tag{6.26d}$$

Using the same steps, the transfer matrix entries between Inlet 2 and the Outlet can be calculated as

$$A_{23} = \frac{z_{22}(Z_{S1} + z_{11}) - z_{21}z_{12}}{z_{32}(Z_{S1} + z_{11}) - z_{31}z_{12}} \tag{6.27a}$$

$$B_{23} = \frac{(z_{22}z_{33} - z_{23}z_{32})(Z_{S1} + z_{11}) + (z_{21}z_{13}z_{32} + z_{23}z_{31}z_{12} - z_{22}z_{31}z_{13} - z_{21}z_{12}z_{33})}{z_{32}(Z_{S1} + z_{11}) - z_{31}z_{12}} \tag{6.27b}$$

$$C_{23} = \frac{Z_{S1} + z_{11}}{z_{32}(Z_{S1} + z_{11}) - z_{31}z_{12}} \tag{6.27c}$$

$$D_{23} = \frac{z_{33}(Z_{S1} + z_{11}) - z_{31}z_{13}}{z_{32}(Z_{S1} + z_{11}) - z_{31}z_{12}} \tag{6.27d}$$

The transfer matrix between Inlet 2 and the Outlet can also be obtained by interchanging the 1 and 2 in the subscripts in Equation 6.26. The transfer function between Inlets 1 and 2 and the Outlet can then be calculated as

$$H_{13}^{Z} = \frac{Z_{T,3}}{A_{13}Z_{T,3} + B_{13} + C_{13}Z_{T,3}z_{S1} + D_{13}z_{S1}} \tag{6.28a}$$

$$H_{23}^{Z} = \frac{Z_{T,3}}{A_{23}Z_{T,3} + B_{23} + C_{23}Z_{T,3}z_{S2} + D_{23}z_{S2}} \tag{6.28b}$$

The outlet sound pressure is then calculated as

$$p_3 = p_{S1}H_{13}^{Z} + p_{S2}H_{23}^{Z} \tag{6.29}$$

Plugging Equations 6.22-6.24 into Equation 6.25, the expression for outlet sound pressure is

$$p_3 = \frac{Z_{T,3}z_{31}p_{S1}Z_{S2} + Z_{T,3}z_{32}\alpha_2 p_{S1}Z_{S1} + Z_{T,3}[(z_{32}z_{11} - z_{31}z_{12})\alpha_2 + (z_{31}z_{22} - z_{32}z_{21})]p_{S1}}{(Z_{T,3} + z_{33})Z_{S1}Z_{S2} + (z_{22}z_{33} - z_{23}z_{32} + Z_{T,3}z_{22})Z_{S1} + (z_{11}z_{33} - z_{13}z_{31} + Z_{T,3}z_{11})Z_{S2} + (z_{11}z_{22} - z_{12}z_{21})Z_{T,3} + |Z|} \tag{6.30}$$

where $|Z|$ is the determinant of the impedance matrix. It can be seen that Equation 6.30 is in the form of the Moebius transformation for both Z_{S1} and Z_{S2}. It can be assumed that the feasible range for source impedance in Chapter 5.4 also applies for MIMO muffler case. The following paragraph is to prove that in the complex plane, the boundary of p_3 is mapped from the boundaries of Z_{S1} and Z_{S2}.

Assume p_3^*, which is one point on the boundary of p_3, is mapped from Z_{S1}^* and Z_{S2}^*, and Z_{S1}^* is not on the boundary of its feasible range. In this case, if the value of Z_{S2} is fixed to Z_{S2}^*, then p_3 is in the form of the Moebius transformation of Z_{S1}, and the boundary of p_3 should be mapped from the boundary of Z_{S1}, which is contradictory to the assumption that Z_{S1}^* is not on the boundary. So that it can be proved that for the Moebius transformation of two variables, the boundary of target function value will be mapped from the boundaries of feasible ranges of each variable.

6.4.3 Example

A two-inlet single-outlet simple expansion chamber was used to demonstrate the influence of source impedances on outlet sound pressure. The dimensions are shown in Figure 6.18. The length and the diameter of the expansion chamber are 0.5 m and 0.31 m, respectively. The diameters of the two inlets are 0.03 m and 0.04 m, and the diameter of the outlet is 0.05 m. The diameters of the inlets and outlet are set to different values to avoid symmetry. The transmission loss of the muffler can be calculated using the superposition method described in Chapter 6.3. In Figure 6.19, the transmission loss curves for in-phase and out-of-phase sources are plotted.

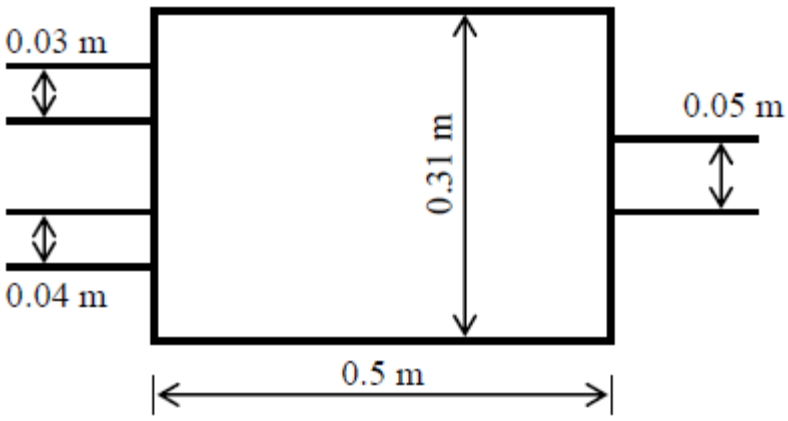

Figure 6.18 Dimensions of a two-inlet muffler

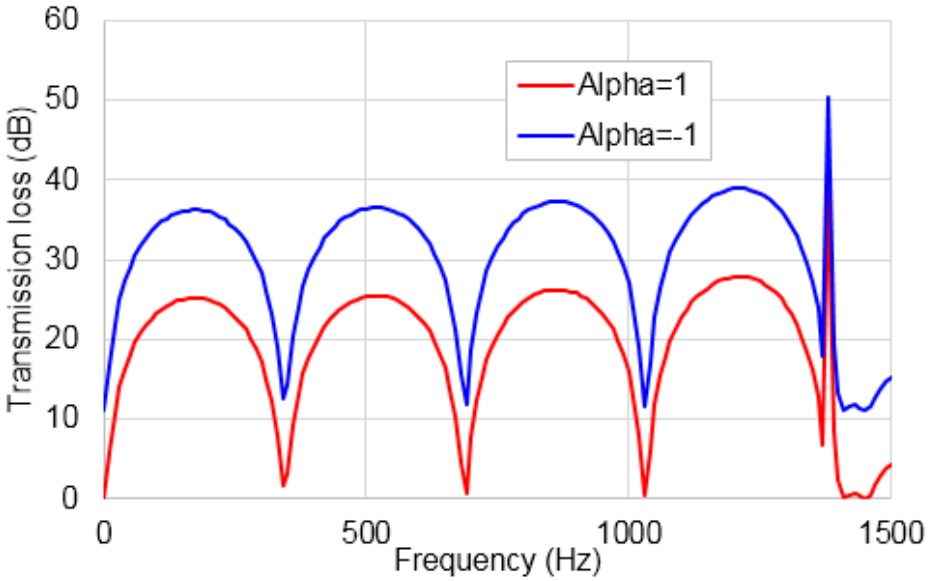

Figure 6.19 Transmission loss of a 2-inlet 1-outlet muffler

The impedance matrix of the muffler can be established following the steps described in Section 6.4.1. The transfer functions between sources and outlet sound pressure can be obtained via the steps laid out in Section 6.2.3. The feasible ranges of Z_{S1} and Z_{S2} are evenly discretized to 100 points with 10 steps in central angles and 10 steps in the radial direction. For each combination of Z_{S1} and Z_{S2}, a resultant p_3 can be calculated using Equation 6.26. The discretized

values of source impedance are shown in Figure 6.20 and the resultant outlet sound pressures are shown in Figure 6.21. This process in analogous to application of the exhaustive method to find the extreme values of outlet sound pressure due to different combinations of source impedances and requires calculation of 10^4 calculations.

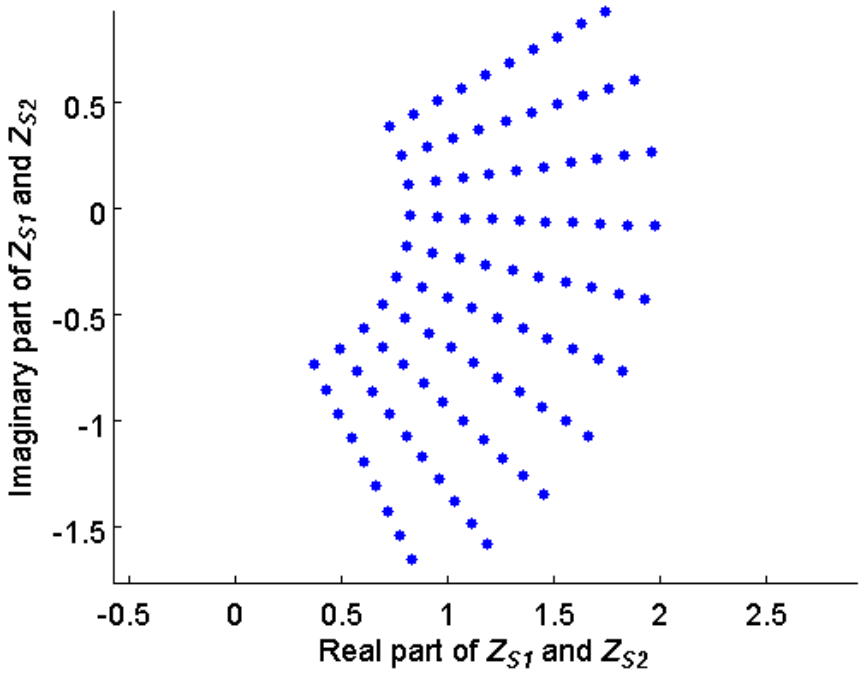

Figure 6.20 Discretized points of feasible ranges of source impedance.

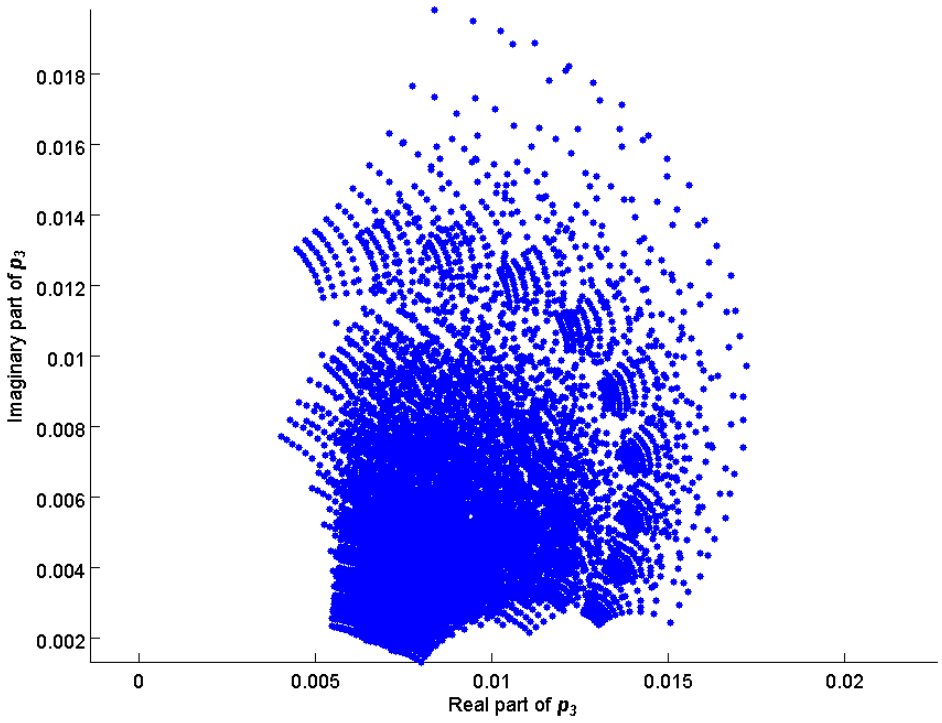

Figure 6.21 Resultant sound pressure due to varying source impedances.

This process can be greatly simplified by applying the Moebius transformation. As stated previously, the boundary of p_3 will be mapped from the combination of the boundaries of Z_{S1} and Z_{S2}. To get the extreme values, only the combination of values on the boundary needs to be calculated. To demonstrate the usage of the Moebius transformation, the boundary of Z_{S1} is discretized into 40 points, with 10 on each edge. This discretization resolution is the same as the previous discretization. For each point of Z_{S1} , p_3 is in the form of the Moebius transformation of Z_{S2}, and the boundary of the mapped area of the feasible range of Z_{S2} can be calculated using the same technique described in Chapter 5. For each point of Z_{S1}, only 8 points on the boundary of Z_{S2} need to be included in the calculation to obtain the boundary of p_3 for that Z_{S1} value. In total 320

calculations need to be performed, which constitutes a 97% reduced compared to the exhaustive method. To show the effect of variation of source impedance, different colors are assigned to different Z_{S1} points and the resultant boundary of p_3, as shown in Figure 6.22 and 6.23, respectively. It can be seen that the boundaries in Figure 6.23 are consistent with the envelope of the points in Figure 6.21, which were calculated by exhaustive method.

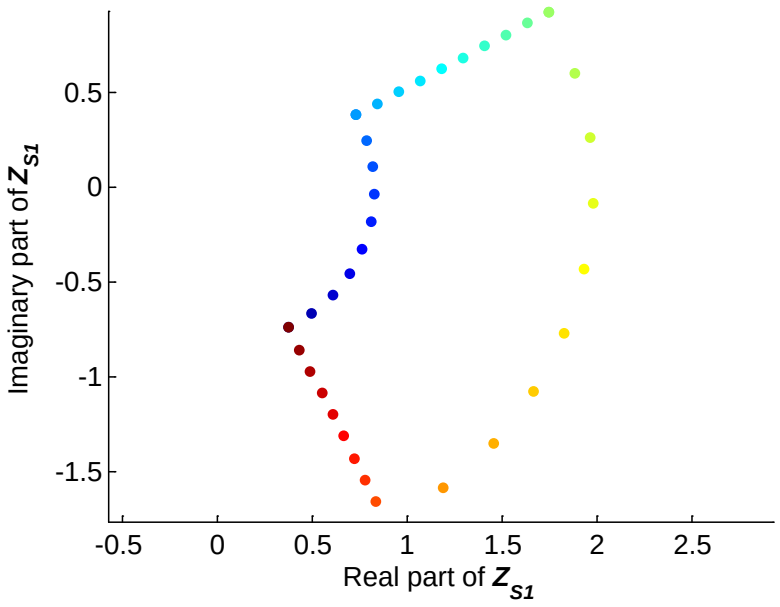

Figure 6.22 Discretization of boundary of source impedance.

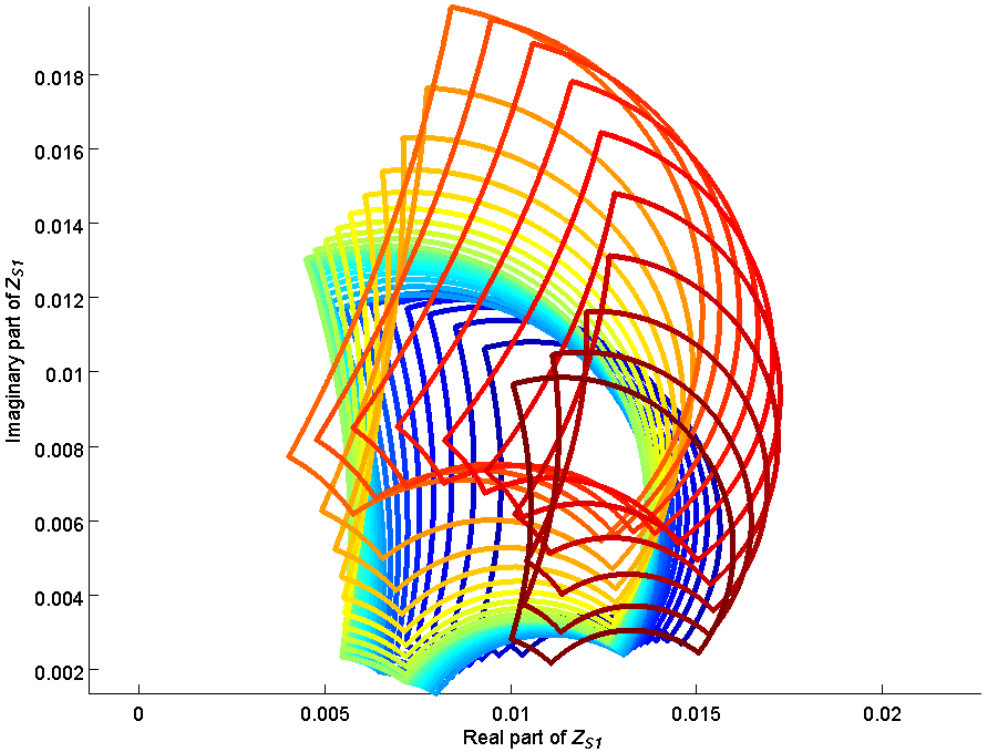

Figure 6.23 Outlet pressure range calculated using the Moebius transformation.

6.5 Conclusion

Compared to the analytical mode-matching and impedance matrix approaches, the advantage of the superposition approach is that the measurement and simulation techniques to obtain transfer matrices are very well developed, and the concept of superposition is mathematically straightforward to understand.

In this chapter, definitions of transmission loss and insertion loss are given for MIMO mufflers based on the superposition method. The approach was validated experimentally using a 2-inlet 2-outlet muffler. It is observed that low frequency

performance of a muffler is more sensitive to the phase difference between sources.

The source impedances will influence the performance of a MIMO muffler, and the sensitivity due to source impedance may be examined using the Moebius transformation. It is demonstrated that using the Moebius transformation, the calculation cost can be greatly reduced.

Chapter 7 CONCLUSIONS AND RECOMMENDATION

This dissertation is comprised of five chapters dealing with different aspects in research of acoustic performance of exhaust system. A high level summary of the major conclusion from each chapter is included in the discussion which follows.

7.1 Measurement of muffler performance

This chapter focuses on the measurement of transmission loss measurement of single-inlet single-outlet muffler using impedance tube. It is found that the standing wave node can introduce error to the measurement and the error can be minimized by choosing the right reference microphone and taking the measurement simultaneously.

Impedance tube measurement is often considered highly repeatable and noise-free, but for two-load measurements where a reflective load is often inevitable, the coincidence of standing wave node with reference microphone is often problematic. Similar behavior is observed in the measurement of thin membrane. Like stated in Chapter 2, when the attenuation of tested muffler is not strong enough, the error introduced by reflection is more pronounced. Thin membrane structures usually contain very limited resistance. As a result, the measurement of thin membrane can be challenging and the best practice when measuring thin membranes should be looked into for the next steps. It is also found that scattering matrix approach is more sensitivity to error at very low frequencies. The different sensitivities at low frequencies between scattering and transfer matrix approach also needs more investigation.

7.2 Measurement of source strength and impedance

This chapter addresses the measurement of source properties on a diesel engine, which is an extreme experimental environment. Same experimental practices and processing technique have been applied on characterization of loudspeakers with good accuracy in Chapter 6.

This measurement is easy to perform and accuracy is good in terms of prediction of downstream sound pressure. In the future, the following questions should be answered to standardize the procedures.

1. The choice of spacing of microphones. The existence of high temperature and turbulence have influence on wavelength and signal-noise-ratio. Good selection of microphone spacing can ensure accuracy within frequency range of interest and suppression of turbulence noise. In current work, two pressure sensors have been used but multiple sensors can be used to expand frequency range.
2. Time-synchronized average has been used to reduce noise, but the effect of time-synchronized average hasn't been fully examined due to lack of recording length. It should be noted that the required length is dependent on number of averaged and engine RPM.
3. Choice of terminations. Idea terminations should have largely different termination impedance and similar flow resistance. Simple expansion chambers, side branches and other duct systems have been used but no comparison or recommendation is made.

7.3 Analysis of exhaust system using the Moebius transformation

Chapter 4 and 5 use the Moebius transformation to optimize the structure of exhaust system and examine the sensitivity due to impedance variation. It is shown that based on properties of the Moebius transformation, the range of objective function can be effectively obtained if the feasible range of impedance variation is well-defined.

1. The connection between BEM and the Moebius transformation should be researched in the future as next step. The entries of matrix generated by BEM are in closed form of impedance and if a connection can be made, the Moebius transformation can make a more powerful optimization tool.
2. Due to the geometrical limitation, the value of transfer impedance of MPP is restricted to a certain range. As a result, the absorption performance of MPP absorber is limited. With the Moebius transformation, the optimal geometrical parameters for MPP-based absorber might be found in an analytical way.

7.4 Analysis of multi-inlet multi-outlet muffler

Chapter 6 proposes definition of transmission loss and insertion loss for MIMO mufflers based on transfer matrix. The connection between transfer matrix and impedance matrix is also established to analyze the sensitivity due to source impedance. In the future, several improvements can be made.

1. Simultaneous measurement. Theoretically, transfer matrices between different ports can be measured simultaneously by correctly choosing

excitation signals and processing technique. This will greatly expedite the process of characterization of MIMO muffler.

2. Pseudo-random excitation. To better control the phase of source strengths of the loudspeakers, sine wave is used in Chapter 6. However, this requires multiple runs which are time-consuming. One possible way to simplify the process is to apply phase delay to a recording of random signal of certain length and feed the original signal and delayed signal to each loudspeaker.

3. Measurement of impedance matrix. Impedance matrix is powerful in analysis of MIMO muffler and is convenient to obtain using simulation tools like FEM and BEM. However, there is no effort made to obtain impedance matrix experimentally.

REFERENCE

M. Åbom, (1990). “Derivation of the Four-pole Parameters Including Higher Order Mode Effects for Expansion Chamber Mufflers with Extended Inlet and Outlet,” Journal of Sound and Vibration, **137**(3), 403-418.

M. Åbom, (1991). “Measurement of the scattering-matrix of acoustical two-ports,” Mechanical Systems and Signal Processing, **5**(2), 89-104.

M. Åbom, (1992). “A Note on the Experimental Determination of Acoustical Two-port Matrices,” Journal of Sound and Vibration, **155**(1), 185-188.

ASTM Standard E1050, (1998). "Standard Test Method for Impedance and Absorption of Acoustical Material Using a Tube, Two Microphones and a Digital Frequency Analysis System." Philadelphia: American Society of Testing and Material.

ASTM Standard E2611, (2009). "Standard Test Method for Measurement of Normal Incidence Sound Transmission of Acoustical Materials Based on the Transfer Matrix Method." Philadelphia: American Society of Testing and Material.

H. Bodén, (1988). "Error analysis for the two-load method used to measure the source characteristics of fluid machines", Journal of Sound and Vibration, **126**(1), 173-177.

H. Bodén, (1991). "The multiple load method for measuring the source characteristics of time-variant sources", Journal of Sound and Vibration, **148**(3).

H. Bodén and M. Åbom, (1995). "Modelling of Fluid Machines as Sources of Sound in Duct and Pipe Systems", Acta acustica, **3**(6), 549-560.

H. Bodén, (2014). “The effect of speed variation on in-duct source data determination”, the 21st International Congress on Sound and Vibration, 13-17 July, Beijing, China.

G.D. Callow and K.S. Peat, (1988). “Insertion Loss of engine inflow and exhaust silencers”, I Mech. E C19/88, 39046.

F.D. Denia, L. Baeza, J. Albelda and F.J. Fuenmayor, (2003). "Acoustic behavior of elliptical mufflers with single-inlet and double-outlet." In Proceedings of the Tenth International Congress on Sound and Vibration, **6**, 3287-3294.

G.T.S. Done and A.D. Hughes, (1975). "The response of a vibrating structure as a function of structural parameters", Journal of Sound and Vibration, **38**(2), 255-266.

T. Elnady, (2007). “A Platform to Measure Transmission Loss of Muffler with Flow,” Inter-Noise 28-31 August 2007, Istanbul, Turkey.

R. Fairbrother, H. Bodén, and R. Glav, (2005). “Linear acoustic exhaust system simulation using source data from non linear simulation”, No. 2005-01-2358, SAE Technical Paper.

F. Fahy, (2001). Foundation of Engineering Acoustics, London: Elsevier Academic Press.

M.F. Harrison, and P.O.A.L. Davies, (2010). "Rapid Prediction of Vehicle Intake/Exhaust Radiated Noise", Proceedings of the Institution of Mechanical Engineers, C487/019/94, 183-190.

D.W. Herrin, Y. Zhang, P. Wang, T.W. Wu and T. Elnady, (2014). "Notes on the Muffler Design Process", INTER-NOISE and NOISE-CON Congress and Conference Proceedings.

D.W. Herrin, J. Liu and G. Sampath, (2009). "The applicability of the Moebius transformation to mechanical and acoustic impedance modifications", Journal of Sound and Vibration, **328**(4), 382-395.

R.N. Hota and M.L. Munjal, (1988). "Approximate empirical expressions for the aeroacoustic source strength level of the exhaust system of compression ignition engines", International Journal of Aeroacoustics, **7**(3-4).

X. Hua, C. Jiang, D.W. Herrin and T.W. Wu, (2014). "Determination of transmission and insertion loss for multi-inlet mufflers using impedance matrix and superposition approaches with comparisons." Journal of Sound and Vibration, **333**(22), 5680-5692.

J.G. Ih and K.S. Peat, (2002). "On the causes of negative source impedance in the measurement of intake and exhaust noise sources", Applied Acoustics, **63**(2), 153-171.

G. D. Izak, (1993). Noise and Vibration Control in Vehicles, eds. M.J. Crocker and N.I. Ivanov, Politekhnika, St. Petersurg.

C. Jiang, T.W. Wu and C.Y.R. Cheng, (2005). "Evaluation of transmission loss using the boundary element method for mufflers with two inlets." The Journal of the Acoustical Society of America, **118**(3), 1919.

M. Karlsson, R. Glav and M. Åbom, (2008). "The Herschel–Quincke tube: The attenuation conditions and their sensitivity to mean flow", The Journal of the Acoustical Society of America, **124**(2), 723-732.

M. Karlsson and R. Glav, (2007). "The Flow Reversal Resonator", SAE Technical Paper 2007-01-2203, doi:10.4271/2007-01-2203.

H. Levine, and J. Schwinger, (1948). “On the Radiation of Sound from an Unflanged Circular Pipe”, Physical Review, **73**(4).

J. Liu, and D.W. Herrin, (2008). "A Simplified Two-Load Method for Measuring Source Impedance", INTER-NOISE and NOISE-CON Congress and Conference Proceedings.

J. Liu, and D.W. Herrin, (2009). “Load effect on source impedance measurement accuracy”, No. 2009-01-2041, SAE Technical Paper.

LMS, (2011). LMS Virtual Lab Rev 10-SL1 BEM Acoustic Manual.

T.Y. Lung and A.G. Doige, (1983). “A Time-averaging Transient Testing Method for Acoustic Properties of Piping System and Mufflers,” Journal of the Acoustical Society of America, **73**(3), 867-876.

D.Y. Maa, (1998). "Potential of Microperforated Panel Absorber," Journal of the Acoustical Society of America, **104**(5), 2861-2866.

F.P. Mechel, (2002). Formulas of acoustics, Springer Science & Business Media.

A. Mimani and M.L. Munjal, (2012). "Acoustical analysis of a generaln of multi-port elements—an impedance matrix approach." International Journal of Acoustics and Vibration, **17**(1), 23.

M.L. Munjal and A.G. Doige, (1990). “Theory of a Two Source-location Method for Direct Experimental Evaluation of the Four-pole Parameters of an Aeroacoustic Element,” Journal of Sound and Vibration, **141**(2), 323-333.

M.L. Munjal, (1987). Acoustic of Duct and Mufflers, John Wiley & Sons, New York.

M.L. Munjal and A. G. Doige, (1988). "On uniqueness, transfer and combination of acoustic sources in one-dimensional systems", Journal of Sound and Vibration, **121**(1).

M.L. Munjal, and R.N. Hota, (2010) "Acoustic source characteristics of the exhaust and intake systems of a spark ignition engine", INTER-NOISE and NOISE-CON Congress and Conference Proceedings, **2010**(11).

T. Needham, (1998). Visual Complex Analysis, Oxford University Press.

C. J. Norwood and J. D. Dickens, (1998). "The effect of vibration isolator properties and structural stiffness on isolator performance", Journal of Vibration and Control, **4**(3), 253-275.

A.D. Pierce, (1981). Acoustics, An Introduction to Its Physical Principles and Applications, McGraw-Hill.

M.G. Prasad and M.J. Crocker, (1983). "Acoustical Source Characterization Studies on a Multi-cylinder Engine Exhaust System", Journal of Sound and Vibration, **90**(4), 479-490.

M.G. Prasad and M.J. Crocker, (1983). "Studies of Acoustical Performance of a Multi-cylinder Engine Exhaust Muffler System", Journal of Sound and Vibration, **90**(4), 491-508.

M.G. Prasad, (1987). "A Four Load Method for Evaluation of Acoustical Source Impedance in a Duct", Journal of Sound and Vibration, **114**(2), 347-356.

H. Rämmal, and M. Åbom, (2007). "Characterization of Air Terminal Device Noise Using Acoustic 1-port Source Models", Journal of Sound and Vibration, **300**(3), 727-743.

H. Rämmal, and H. Bodén. (2007). "Modified multi-load method for nonlinear source characterization", Journal of sound and vibration, **299**(4), 1094-1113.

A. Selamet, N. S. Dickey and J. M. Novak, (1994). "The Herschel–Quincke tube: a theoretical, computational, and experimental investigation", The Journal of the Acoustical Society of America, **96**(5), 3177-3185.

A.F. Seybert and D.F. Ross, (1977). "Experimental Determination of Acoustic Properties using a Two-Microphone Random-Excitation Technique," Journal of the Acoustical Society of America, **61**(5), 1362-1370.

A.F. Seybert and B. Sornarko, (1981). “Error Analysis of Spectral Estimates with Application to the Measurement of Acoustic Parameters using Random Sound Field in Ducts,” Journal of Acoustical Society of America, **69**(4), 1190-1199.

A. Selamet and V. Easwaran, (1997). "Modified Herschel–Quincke tube: Attenuation and resonance for n-duct configuration", The Journal of the Acoustical Society of America, **102**(1), 164-169.

A. Selamet and Z.L. Ji, (2000). "Acoustic attenuation performance of circular expansion chambers with single-inlet and double-outlet." Journal of sound and vibration, **229**(1), 3-19.

SIDLAB, (2011). SIDLAB Acoustics User’s Manual, Version 2.6.

W. Soedel, (2004). Vibrations of shells and plates, CRC Press.

B.H. Song and J.S. Bolton, (2000). “A Transfer-Matrix Approach for Estimating the Characteristic Impedance and Wave Numbers of Limp and Rigid Porous Materials,” Journal of Acoustical of Society of America, **107**(3), 1131–1152.

G. W. Stewart, (1928). "The theory of the Herschel-Quincke tube", Physical Review, **31**(4), 696.

Z. Tao and A.F. Seybert, (2003). “A Review of Current Techniques for Measuring Muffler Transmission Loss,” SAE Technical Paper No. 2003-01-1653.

M. G. Tehrani, W. Wang, C. Mares and J. E. Mottershead, (2006). "The generalized Vincent circle in vibration suppression", Journal of sound and vibration, **292**(3), 661-675.

C.W.S. To and A.G. Doige, (1979). "A Transient Testing Technique for the Determination of Matrix Parameters of Acoustic Systems, 1: Theory and Principles," Journal of Sound and Vibration, **62**(2), 207-222.

C.W.S. To and A.G. Doige, (1979). "A Transient Testing Technique for the Determination of Matrix Parameters of Acoustic Systems, 2: Experimental Procedures and Results," Journal of Sound and Vibration, **62**(2), 223-233.

I.L. Ver and L.L. Beranek, (2006). Noise and Vibration Control Engineering Principles and Applications, John Wiley & Sons, Hoboken, New Jersey.

A.H. Vincent, (1973). "A note on the properties of the variation of structural response with respect to a single structural parameter when plotted in the complex plane", Dynamics Department Report GEN/DYN/RES/010R, Westland Helicopters Ltd.

H.P. Wallin, U. Carlsson, M. Åbom, H. Bodén, and R. Glav, (2012). Sound and Vibration, Marcus Wallenburg Laboratoriet.

Q. Wu, (1988). “Empirical Relations between Acoustical Properties and Flow Resistivity of Porous Plastic Open-Cell Foam,” Applied Acoustics, **25**(3), 141-148.

Y. Zhang, D. W. Herrin and T. W. Wu, (2013). "Adding bypass ducts to enhance muffler performance without increasing size", SAE Int. J. Passeng. Cars - Mech. Syst. **6**(2):1102-1107.

VITA

Yitian Zhang was born in Anhui, China in 1989. He received the degree of Bachelor of Science in Automotive Engineering from Hefei University of Technology in 2011. In August 2011, he enrolled in the PhD program in Mechanical Engineering at the University of Kentucky. His research involves engineering acoustics and noise and vibration control. During his five years in the PhD program, he published 4 journal papers and 5 conference papers. He was rewarded Student Paper Award and Michiko So Finegold Award in Noise-Con 2013 in Denver, Colorado. In the year of 2015, he received Leo Beranek Student medal for Excellence in the Study of Noise Control from Institution of Noise Control Engineering. In the same year he also received Hallberg Foundation Travel Award and Best Student Paper Award in Inter-Noise 2015 in San Francisco, California.